NASA CONTRACTOR REPORT 189597

FINITE ELEMENT ANALYSIS OF THE STIFFNESS OF FABRIC REINFORCED COMPOSITES

R. L. Foye

Lockheed Engineering and Sciences Company
Hampton, VA 23666

February 1992

NASA

National Aeronautics and
Space Administration

LANGLEY RESEARCH CENTER
Hampton, Virginia 23665-5225

TABLE OF CONTENTS

LIST OF SYMBOLS

a,b,c	Subcell side lengths
A,B,C,	Unit cell side lengths
[B]	Strain/displacement matrix
CW,CCW	Clockwise, counterclockwise
D, [D], D_{ij}	Stress-strain stiffness coefficients
d(vol)	Increment of volume
E, E_{ij}	Young's modulus
Ep	Epoxy
{F}	Force vector
Gr	Graphite
G, G_{ij}	Shear modulus
[H], [J]	Coefficient matrix
[k], [K]	Stiffness matrix
NX,NY,NZ	Number of node points on coordinate axes
psi, msi	Pounds/square inch, 10^6 pounds/square inch
S, [S], S_{ij}	Stress-strain flexibility matrix
T	Matrix transpose
N.A.	Not available/not applicable
U,V,W,U_i,V_i,W_i	Displacements in coordinate directions
$x,y,z,\bar{x},\bar{y},\bar{z}$	Rectangular coordinates
X,Y,Z,X_i,Y_i,Z_i	Forces in coordinate directions
γ, $\bar{\gamma}$, γ_{ij}, $\bar{\gamma}_{ij}$	Shear strain
{δ}	Displacement vector
ε, $\bar{\varepsilon}$, ε_{ij}, $\bar{\varepsilon}_{ij}$	Normal strain
η_{ij}, k	Coefficients of mutual influence
ν, ν_{ij}	Poisson's ratio
σ, $\bar{\sigma}$, σ_{ij}, $\bar{\sigma}_{ij}$	Normal stress
τ, $\bar{\tau}$, τ_{ij}, $\bar{\tau}_{ij}$	Shear stress
υ, υ_i	Volume fraction
ϕ, ϕ_i	Fiber orientation angle
2-D	Two dimensional
3-D	Three dimensional

ABSTRACT

This report concerns the prediction of elastic moduli for fabric reinforced composites. Many analysis methods previously applied to this problem are not general enough for use with the more complex reinforcing geometries that have been suggested for suppressing impact damage and general delamination. The proposed analysis places no restrictions on fabric microgeometry except that it be determinate within some repeating rectangular pattern. No assumptions are made regarding fiber cross-sectional shapes or fiber paths.

The analysis is based on a mechanical model that consists of a single rectangular unit cell which typically contains one repeating pattern of the fabric design. Every unit cell is assumed to be surrounded on six sides by identical unit cells, similarly oriented, with all common surfaces perfectly bonded. Elastic analysis of one such cell element yields all 3-D moduli of the composite.

For analysis purposes the unit cell is assumed to be divisible into small rectangular subcells in which the reinforcing geometries are easier to visualize, define, and analyze. Details of micromodeling and the use of single, finite element hexahedra to mathematically represent each subcell are described in this report. The analysis is applied to a variety of woven, braided, and knitted fabric reinforcements in epoxy matrix. A special purpose computer program based on this analysis is also described. Moduli predictions from this program are compared to fabric reinforced composite test data. A program listing with sample input and output is included in the Appendices.

PRECEDING PAGE BLANK NOT FILMED   PAGE __ⅳ__ INTENTIONALLY BLANK

1. INTRODUCTION

Complex fibrous preforms (made from weaves, braids, knits, XYZ construction, etc.) are under consideration for use as composite reinforcing materials. As reinforcers, these preforms should increase impact resistance, reduce lay up time, and generally improve interlaminar properties. Use of these textile structures introduces a variety of both new and old manufacturing processes into the fabrication cycle and creates an intermediate material stage. This stage consists of an array of systematically interlaced fiber bundles (yarns or tows) surrounded and impregnated by a matrix material. The basic repeating structural element in this array has characteristic dimensions that are much larger than a single fiber diameter, but are on the order of the structural plate or shell wall thickness (Figure 1). From an analyst's point of view this stage creates a gap between micro-mechanics and laminate analysis, and requires a new level of mechanics analysis. The term "fabric mechanics" seems appropriate for categorizing this level of composite mechanics. However, use of this terminology may confuse textile engineers who normally associate fabric mechanics with unimpregnated fabric behavior. The goals of fabric mechanics is to predict material properties at the fabric reinforced composite level from knowledge of unidirectional composite and bulk matrix material properties. This level of analysis is necessary to reduce dependence on testing and to assist in data extrapolation and interpretation. The influence of factors such as fiber curvature, misalignment, and ply nesting are not conveniently assessed by either micro-mechanics or laminate analysis. Fabric mechanics' role in the scheme of composite mechanics is shown in Figure 1. For laminates made from unidirectional material, fabric mechanics is not required because micro-mechanics provides all the necessary information for laminate analysis.

Although methods of fabric analysis are not firmly established, its goals are identical to those of all mechanics analyses; namely, to predict stresses and deformations within a deterministic structure as a result of prescribed external loads or deformations. From these predictions (plus suitable failure criteria) composite static properties of stiffness and strength can be estimated. The limited objective of this report is to develop adequate capability (and a computer code) to predict static stiffness of various fabric reinforced composites proposed for minimizing impact damage. Several methods for predicting these properties have been proposed, but they are built on many assumptions, and do not enjoy widespread use or confidence.

The principal barrier to improved analyses is the geometric complexity of most fabric microstructures. The proposed analysis crosses this barrier via two stages of mechanical modeling. For example, consider the rib weave fabric microstructure shown in Figure 2. This fabric geometry can be subdivided into small block substructures or subcells (as shown in the same Figure). Simpler reinforcing fiber geometry within each different subcell can be modeled by finite element hexahedra. After reassembling the subcells the boundary conditions required to simulate the six independent unit strain cases of 3-D elasticity may be enforced (as in micro-mechanics). The resulting elastic solutions yield all necessary information for computation of the 6 X 6 stiffness or flexibility matrix of the composite. The approach is well-suited to computer analysis. A special propose code has been written that predicts the stiffness of fabric reinforced composites on the foregoing basis. A laminate analysis must be performed if several different fabrics are combined into a thick, laminated structure. This approach has the added advantage of lying within the range of experience of most structural analysts.

One of the long range objectives of this work is to develop the capability of estimating all of the 3-D static material property inputs required of transient dynamic impact codes that analyze the response of composite target plates to spherical impactors (Ref. 1). This capability will permit rational selection of woven, braided, and stitched fabric parameters to best meet impact damage requirements with the least penalty to the basic static design properties.

2. REINFORCING GEOMETRY

In the textile sense, the term "fabric" is applicable to any network of bonded or unbonded fibers which results in an essentially planar structure that is flexible yet cohesive beyond the point of being self-supporting. The fabrics can be categorized as having either a random distribution of fiber (as in a felt or bonded flock) or an orderly distribution (as in weaves, braids or knits). Hybrids of both are possible and some elements of order and disorder are always present in both. Yarns or tows can also be continuous or discontinuous or a hybrid of both (as in cut pile carpets). In this report, only fabrics made from continuous tows arranged in identifiable and repetitious patterns of entanglement will be considered. It is also assumed that this repetitious pattern has finite dimensions and can be contained exclusively within the volume of a rectangular prism. This prism is termed a "unit cell" of the fabric. Reproduction of this unit cell, rigid transformation of it, and attachment to compatible surfaces of other unit cells, allows any large planar area to be covered by this fabric, with areal contours closely approximated by outer boundaries of units cells. Also unit cells can by layered to fill any closed volume, even where minimum dimensions of that volume are several orders of magnitude larger than unit cell dimensions. It is assumed in this process that all common boundaries between unit cells are perfectly bonded to each other.

This 3-D unit cell often visually relates to the 2-D fabric design plan that, along with the harness draft and the chain draft, is typically used to describe a weave pattern and to set up a shuttle loom to make that weave. The design plan is a coded representation of a weave, whereas the unit cell is a true scale model of the weave, albeit a somewhat idealized one. A design plan is usually drawn on 8 X 8 design paper. Columns represent warp yarns; rows represent fill yarns. Each

small square represents an intersection of one warp and one fill yarn. A shaded square indicates that the fill yarn crosses over the warp yarn at that intersection.

One unit cell representation of a plain weave is shown in Figure 3A. The corresponding fabric design plan is shown in Figure 3B. But, neither the unit cell nor the design plan are unique. Another very different unit cell of the same weave is shown in Figure 3C.

Since unit cells are not unique, the question arises as to which unit cell should form the basis for fabric analysis. The answer is that unit cell which is simplest to analyze. Often, the simplest cell is presumed to be the smallest cell. However, the smallest unit cell is frequently difficult to analyze, particularly when it has complex boundaries, for example the twill weave (Figure 4). Boundaries of the smallest twill weave unit cell do not form a rectangular prism. Hence, mechanical analysis of this weave can be difficult. The larger unit cell of Figure 4C does not pose this problem.

Several rectangular unit cells for common weaves, knits and braids are shown in Figure 5. For some complex fabrics, it is difficult to identify a rectangular unit cell. For woven fabrics, one repeat of the design plan often resembles an out-of-scale projection of a unit cell surface. But with knits or braids there is no corresponding 2-D design plan. However, rectangular unit cells generally can be established, although some liberties with the tow geometry may be required. For example, some tow geometries like satin weaves (with large, complex, rectangular, unit cells) contain smaller, simpler, trapezoidal, unit cells. Slightly distorting the boundary of the smaller unit cell can make it rectangular but this process entails some violation of the true microgeometry.

3. HISTORICAL DEVELOPMENT

Woven fiberglass cloth was the first reinforcing material with enough strength and stiffness for general use on aircraft structures. However, relatively few fabric weave styles saw extensive application. These fabrics were experimentally characterized using epoxy and polyester resins and were treated like new orthotropic materials with little consideration of fabric microstructural analysis. Although it was known at that time that fabric microgeometry had a significant effect on moduli and was one of the determining factors in stress failure of this material, a convincing mechanical analysis of this problem was beyond computational capabilities. The advent of filament winding and unidirectional prepregging, along with increased capability in computing, soon made such an analysis possible at the unidirectional level. It was assumed that a wide range of fiber volume fractions and fiber cross-sectional shapes would necessitate some type of micro-mechanics design/analysis cycle. Instead unidirectional materials became even more standardized than fabrics. Test data replaced micro-mechanics.

The search for improved impact resistance has brought about a renewal of interest in more complex reinforcing geometries. Meanwhile, computing capability has kept pace with materials development. This increased computing capability now allows design and analysis of fabrics at a level comparable to design and analysis of unidirectional materials. The number of geometric variables present and the requirements of impact resistance suggest fabric reinforcements will play a role in developing impact resistant composites.

First attempts to extend composite mechanics beyond the realm of planar analysis arose in conjunction with carbon-carbon development for reentry vehicles (Ref 2). These attempts ranged from 3-D versions of the rules of mixture and netting

analysis to finite element solutions. Fiber curvature was seldom considered.

Two-dimensional analysis of wavy fiber reinforced composites was considered by some to be an initial step toward the analysis of true fabric reinforced composites (Ref. 3). In this approach a single wavy fiber is treated as a curved beam on an elastic foundation.

Another step toward geometric reality (Ref. 4) involved modeling of orthogonal fiber arrays. However, the problem was reduced to two dimensions and solved by finite elements.

Among the first to treat fabric mechanics as a true 3-D problem were Ishikawa, Chou, et al., (Refs. 5 through 11). Based on assumed fiber paths and cross-sectional shapes these authors developed a variety of models based largely on "strength of materials" type idealizations and extended some of this work into the nonlinear property realm.

Materials Sciences Corporation developed a simple fabric model based on earlier work on random fiber reinforcements (Ref. 12).

Another more refined approach was the attempt to fit fabric mechanics directly into the context of laminated plate theory (Ref. 13). This analysis also occasionally relies on "strength of materials" assumptions (Ref. 14).

The primary legacy of the previous work lies not in analytical details, but in the modeling of complex fabric microgeometry with unit cells and subcells. Not only does this reduce the geometry problem to smaller, "more digestible" pieces; it also meshes with the finite element scheme of reducing a complex structure to an assemblage of simpler ones which can be characterized, reassembled, and manipulated to predict the response of the unit cell and the composite.

4. FABRIC ANALYSIS

For convenience in establishing thickness direction properties, each fabric reinforced composite ply hereafter will be considered to be imbedded in a thick laminate of identical plies layered such that each unit cell in each ply represents one level in a vertical stacking of unit cells extending through the full thickness of the laminate (like stories in a multi-story building). For example, treat each unit cell as a single brick in a stack bond wall (Figure 6).

A wide variety of other stacking arrangements are equally valid and can be observed in laminates. Cursory investigations show these stacking variations to be of secondary importance to the principal ply stiffness. A more thorough investigation would be appropriate to strength analysis but of lower priority to this study.

4.1 Determination of Overall Elastic Constants

Now consider a large cube of fabric reinforced composite material in which dimensions of the cube are orders of magnitude greater than dimensions of the unit cell. For most engineering purposes such a composite material can be considered homogeneous and anisotropic with a linear stress-strain law of the form:

$$
\begin{Bmatrix} \bar{\varepsilon}_{xx} \\ \bar{\varepsilon}_{yy} \\ \bar{\varepsilon}_{zz} \\ \bar{\gamma}_{yz} \\ \bar{\gamma}_{xz} \\ \bar{\gamma}_{xy} \end{Bmatrix} = \begin{bmatrix} S_{11} & S_{12} & S_{13} & S_{14} & S_{15} & S_{16} \\ S_{21} & S_{22} & S_{23} & S_{24} & S_{25} & S_{26} \\ S_{31} & S_{32} & S_{33} & S_{34} & S_{35} & S_{36} \\ S_{41} & S_{42} & S_{43} & S_{44} & S_{45} & S_{46} \\ S_{51} & S_{52} & S_{53} & S_{54} & S_{55} & S_{56} \\ S_{61} & S_{62} & S_{63} & S_{64} & S_{65} & S_{66} \end{bmatrix} \begin{Bmatrix} \bar{\sigma}_{xx} \\ \bar{\sigma}_{yy} \\ \bar{\sigma}_{zz} \\ \bar{\tau}_{yz} \\ \bar{\tau}_{xz} \\ \bar{\tau}_{xy} \end{Bmatrix}
\tag{4.1}
$$

where: $\bar{\varepsilon}_{ii}$ = average normal strain,

$\bar{\gamma}_{ij}$ = average shear strain,

$\bar{\sigma}_{ii}$ = average normal stress (psi)

$\bar{\tau}_{ij}$ = average shear stress (psi)

S_{ij} = flexibility coefficient (in^2/lb).

If the cube of material is subjected to a unit average strain in the x-direction, with all other average strains held to zero, then $\bar{\sigma}_{xx}$, $\bar{\sigma}_{yy}$, $\bar{\sigma}_{zz}$, $\bar{\tau}_{yz}$, $\bar{\tau}_{xz}$, $\bar{\tau}_{xy}$ represent average stresses corresponding to this strain state. In a hypothetical test these stresses could be considered to be measured quantities. The stress-strain law given above would then consist of six independent equations in the 36 unknown S_{ij} coefficients. Repeating this test with $\bar{\varepsilon}_{yy}$ = 1 and all other average strains held at zero would yield six more equations in the S_{ij} unknowns. All six independent unit strain states would yield 36 equations in the 36 unknown S_{ij}. These terms are the flexibility coefficients of the composite.

Inverting the matrix of flexibility coefficients yields the stiffness matrix [D]:

$$
\begin{Bmatrix} \bar{\sigma}_{xx} \\ \bar{\sigma}_{yy} \\ \bar{\sigma}_{zz} \\ \bar{\tau}_{yz} \\ \bar{\tau}_{xz} \\ \bar{\tau}_{xy} \end{Bmatrix} = \begin{bmatrix} D_{11} & D_{12} & D_{13} & D_{14} & D_{15} & D_{16} \\ D_{21} & D_{22} & D_{23} & D_{24} & D_{25} & D_{26} \\ D_{31} & D_{32} & D_{33} & D_{34} & D_{35} & D_{36} \\ D_{41} & D_{42} & D_{43} & D_{44} & D_{45} & D_{46} \\ D_{51} & D_{52} & D_{53} & D_{54} & D_{55} & D_{56} \\ D_{61} & D_{62} & D_{63} & D_{64} & D_{65} & D_{66} \end{bmatrix} \begin{Bmatrix} \bar{\varepsilon}_{xx} \\ \bar{\varepsilon}_{yy} \\ \bar{\varepsilon}_{zz} \\ \bar{\gamma}_{yz} \\ \bar{\gamma}_{xz} \\ \bar{\gamma}_{xy} \end{Bmatrix}
$$

(4.2)

where: D_{ij} = stiffness coefficient of composite (psi).

E_{ii}, V_{ij}, G_{ij} etc. for the composite can be obtained by considering the material response to single nonzero components of each of the six average stresses

where: E_{ii} = modulus of elasticity of material (psi),

V_{ij} = Poisson's Ratio,

G_{ij} = modulus of rigidity of material (psi).

4.2 Unit Cell Boundary Conditions

Now return to the initial problem of obtaining the average composite stress components $\overline{\sigma}_{xx}$, $\overline{\sigma}_{yy}$, $\overline{\sigma}_{zz}$, $\overline{\tau}_{yz}$, $\overline{\tau}_{xz}$, $\overline{\tau}_{xy}$ resulting from the average strain state

$$\overline{\varepsilon}_{xx} = 1, \quad \overline{\varepsilon}_{yy} = \overline{\varepsilon}_{zz} = \overline{\gamma}_{yz} = \overline{\gamma}_{xz} = \overline{\gamma}_{xy} = 0. \tag{4.3}$$

This problem can be resolved by considering a single unit cell of the material, sufficiently far removed from the surfaces to be free from edge, corner, or surface effects. Since all such unit cells in the material are indistinguishable from one another the response of any two unit cells to any uniform average stress or strain state must be similar, except for rigid body motion.

Relative displacement of the eight corners of the unit cell are shown in Figure 7. Any other set of relative displacements would be incompatible, inhomogeneous (in the average strain sense), or in violation of the unit strain case that it represents.

Now consider boundary conditions on surfaces of the unit cell. First consider interlamina upper and lower surfaces of the cell. For every point on the upper surface there is a corresponding point directly below it on the bottom surface (Figure 8). Call these two points "image points" because the top image point on

one unit cell is coincident with the bottom image point on the unit cell directly

above it. Similarly the bottom image point on any cell coincides with the top

image point on the unit cell below it. Since there is no reason to expect any two

cells to deform differently under uniform average strain, the displacements of

image points can differ only by the amount of displacement associated with the

homogeneous unit strain case (plus some arbitrary rigid motion). Ignoring rigid

motion, the displacement boundary conditions (corresponding to unit strain case

4.3) for image points i,j (Figure 8) have the form:

$$U_i = U_j, \quad V_i = V_j, \quad W_i = W_j \qquad (4.4)$$

where U,V,W designate displacements in the positive x,y,z coordinate directions,

respectively. This condition provides three equations in the six displacement

components of the two image points. Three additional equations are required for a

complete statement of a 3-D elastic problem.

Stress continuity considerations provide these equations. The stress vector at any

point on the lower surface of one unit cell is the reaction to the stress vector

at the same point on the upper surface of the unit cell lying directly below it.

Also, surface stresses on one unit cell are assumed to be identical to stresses on

any other cell. Therefore, stress vectors at image points of the same cell must

be equal in magnitude but oppositely directed. These conditions

$$\sigma_{zz}(i) = \sigma_{zz}(j), \quad \tau_{xz}(i) = \tau_{xz}(j), \quad \tau_{yz}(i) = \tau_{yz}(j) \qquad (4.5)$$

where σ, τ represent surface stress components, provide three more equations at

each pair of image points. These conditions (4.4 and 4.5) place the problem in

the category of a mixed boundary value problem in elasticity; i.e. both stress and

displacement conditions apply. A similar argument may be applied to image points

on any other pair of opposite sides of the unit cell. On sides perpendicular to

the x-axis the U displacement condition has the more general form $U_i = U_j + A$, where A is a constant that accounts for the stretching in the x-direction. Similar conditions can be specified for the other two normal strain cases.

Boundary conditions for the three unit shear strain cases differ from normal strain cases only in that the constant terms that appear in some of the displacement boundary conditions are associated with displacement components that are parallel rather than normal to sides of the unit cell where they apply.

4.3 Symmetry Boundary Conditions

Structural symmetry often can be used to reduce the portion of the unit cell that needs to be analyzed. However, boundary conditions on the plane of symmetry, and the cell face parallel to the plane of symmetry, will differ from those conditions previously stated. Consider only the special case where two parallel faces of the reduced unit cell are both planes of symmetry.

First consider the three unit normal strain problems. All eight corners of the reduced (by symmetry) unit cell now lie on planes of structural (and loading) symmetry, but their pure displacement boundary conditions are not changed from the previous discussion; i.e. their displacements are what establish the particular unit strain case under consideration. Points lying on one plane of symmetry have the traditional symmetry conditions of zero (or constant) normal displacement and zero shear stress. Thus, stresses and displacements at image points that lie on parallel planes of symmetry are no longer related through their boundary condition equations.

Unit shear strain load cases divide into two categories: symmetric loading categories and antisymmetric ones. Symmetric loading cases do not differ from unit normal strain cases. Antisymmetric loading categories have boundary conditions that are the converse of the symmetric ones; i.e., displacements parallel to a plane of structural symmetry are zero (or constant), and stresses normal to that plane are zero.

5. SUBELEMENT MECHANICS

The previous section (4.) of this report describes the elastic structure (the unit cell), the various load (or displacement) cases applied to that structure, and the boundary conditions prevailing on surfaces of the structure. This section considers a numerical method for estimating internal (and surface) displacements of the unit cell for each set of loads and boundary conditions. This analysis is a direct application of the finite element method in which the unit cell structure is idealized into a number of smaller polyhedra (subcells) joined together at common vertices. The presumption is that stress, strain, and displacement fields are simpler to approximate within the subcell, than in the larger structure. Each subcell is then analyzed for the most general set of loads (or displacements) at each of the vertices and reassembled into the unit cell structure.

If the unit cell is in the shape of a rectangular prism it is convenient to consider only subdivisions of the unit cell into smaller rectangular prisms (subcells). The advantage of this restriction is that it simplifies the geometry and the analysis, and eases coding for digital computation. This restriction is one of convenience and is not particularly restrictive because fabric microgeometries are often rectangular to some degree. For example, consider the plain weave unit cell of Figure 9.[*] This unit cell of Figure 9 can be subdivided into 16 subcells as shown. These subcells are all rectangular prisms, like the unit cell.

---

[*] A subsequent section contains photomicrographs of actual fabric reinforced composites, including a plain weave. The similarities between cross sections of the more realistic unit cells which model the composite microstructure and the photomicrographs are apparent.

If the warp and fill tows are similar and their paths are the same, then the 16 subcells are all simple transformations of each other; i.e., any one of their reinforcing microgeometries can be reproduced by a combination of rigid motions and reflections about the face planes of any one of the subcells. The transformation makes the chore of describing microgeometry much simpler since a detailed description of one subcell (mastercell) and a set of instructions for the series of coordinate transformations will suffice to reconstruct the unit cell. As another example consider the unit cell of the 2/2 rib weave construction with similar warp and fill yarn geometries (Figure 2). This unit cell can be constructed from a sequence of transformations of two master subcells designated I and II in Figure 2.

5.1 Subcell Analysis

Now consider the elastic analysis of a single rectangular subcell. For incorporation into a finite element analysis at the simplest level, it is necessary first to obtain a stiffness matrix relating the three components of force, acting at each corner of the subcell, to the three components of displacement at each corner. The method of obtaining this matrix is the central problem in fabric reinforced composite stiffness analysis. Many possible approaches exist. Simpler approaches often overlook fiber reinforcing detail. Refined analyses lead to greater computational efforts than the problem warrants. Hence, a compromise is needed. One compromise is suggested by the general energy formulation for the stiffness matrix of rectangular finite element hexahedra (Ref. 15); i.e.,

$$[k] = \iiint\limits_{vol} [B]^T [D] \; [B] \; d(vol) \tag{5.1}$$

where: [D] = 3-D material stiffness matrix,

           [B] = strain/displacement matrix,

           vol = volume

[D] contains only local material property distribution functions and [B] contains only derivatives of displacement mode shapes. Superscript T designates matrix transposition. [D] is usually obtained by inverting the flexibility matrix [S]. [S] is usually obtained by transforming the stresses and strains from material coordinates of orthotropy into the coordinate of integration.[*] In the natural coordinates of the material (x_1, x_2, x_3):

$$[S] = \begin{bmatrix}
1/E_1 & -V_{21}/E_2 & -V_{31}/E_3 & 0 & 0 & 0 \\
-V_{12}/E_1 & 1/E_2 & -V_{32}/E_3 & 0 & 0 & 0 \\
-V_{13}/E_1 & -V_{23}/E_2 & 1/E_3 & 0 & 0 & 0 \\
0 & 0 & 0 & 1/G_{23} & 0 & 0 \\
0 & 0 & 0 & 0 & 1/G_{13} & 0 \\
0 & 0 & 0 & 0 & 0 & 1/G_{12}
\end{bmatrix} \tag{5.2}$$

Formulae for [B] depend on the form of the assumed displacements U(x,y,z), V(x,y,z), and W(x,y,z). A variety of displacements have been associated with hexahedra. The first hexahedra were formed from various combinations of tetrahedra whose displacements were assumed to be linear. Higher order tetrahedra

---

[*]Assuming the constitent materials to be orthotropic rather than generally anisotropic does not restrict the response of the unit cell to be less than generally anisotropic.

were also used. Later, isoparametric families of hexahedra were used with 8, 20, 32 nodes. All nodes were located on element edges. Elements with internal nodes were also investigated. Also used were super-elements formed from smaller hexahedra. Displacement derivatives were used as nodal degrees of freedom also. The intent of this study was to begin with simple elements, increasing their complexity only as required to obtain acceptable accuracy for moduli predictions. The first displacements chosen were those associated with eight-node isoparametric hexahedra (Ref. 15); i.e.:

$$8abc\{U,V,W\} = (a+2x)(b-2y)(c-2z)\{U_1,V_1,W_1\}$$

$$+(a+2x)(b+2y)(c-2z)\{U_2,V_2,W_2\}$$

$$+(a-2x)(b+2y)(c-2z)\{U_3,V_3,W_3\}$$

$$+(a-2x)(b-2y)(c-2z)\{U_4,V_4,W_4\}$$

$$+(a+2x)(b-2y)(c+2z)\{U_5,V_5,W_5\}$$

$$+(a+2x)(b+2y)(c+2z)\{U_6,V_6,W_6\}$$

$$+(a-2x)(b+2y)(c+2z)\{U_7,V_7,W_7\}$$

$$+(a-2x)(b-2y)(c+2z)\{U_8,V_8,W_8\}$$

where:

a = subelement side length in x-direction,

b = subelement side length in y-direction,

c = subelement side length in z-direction.

Later, additional internal degrees of freedom associated with incompatible mode corrections (Refs. 16, 17) were incorporated into the current analysis.

All elements of the [B] and [D] matrices are functions of spatial coordinates within the subcell. If more than one material is present in the subcell, [D] is discontinuous in the region of interest and derivatives of true displacements will

also be discontinuous. Nevertheless, the integration for obtaining the stiffness matrix can still be performed. Mathematically, functions of class C_o (without continuous first derivatives), can be approximated by a series of functions of class C_1 (with continuous first derivatives).

Formation of the stiffness matrix from [B] and [D] requires numerical integration of the matrix product $[B]^T [D] [B]$. Integration of a matrix product is the integration of each element of the product matrix. Various mensuration formulae exist which are applicable to the formation of this integral; e.g., Gaussian or Newton-Cotes quadrature. In this report only the simplest step-function approximation to the integrand is used for computing stiffness matrices. The integral is formed independently for each different material appearing in the subcell, and then is summed over all materials in the subcell.

For integration purposes, a 3-D grid is superimposed on the subcell volume as follows. First, each set of parallel subcell edges is divided into N unequal segments. N can be different for each coordinate direction. Planes are constructed through these points of subdivision, normal to the edges of the subcell. Intersections of these three sets of planes, within (or on) boundaries of the subcell, are the integration points (Figure 10). Each element of the $[B]^T [D] [B]$ matrix is evaluated at each integration point.

For each material a local average value of a fiber reinforcing direction is input at each integration point. Each average value is estimated by considering all of the material closest to that integration point. The fiber direction is established by specifying the two spherical angles (ϕ_1, ϕ_2) that the fiber principal axis makes within a local coordinate system parallel to the axes of integration (See Figure 11). Elastic properties of the material are then transformed into the subcell reference system of integration. The value of each

18

element of the matrix product $[B]^T[D][B]$, for that material, is then computed at the integration point and multiplied by the product of the volume fraction of the material at that point times the total rectangular volume of neighboring space associated with that integration point (Figure 12A). The resulting matrix quantity is then totaled over each integration point and material.

Since the integration grid spacing is variable, the volume of any material associated with any integration point can be obtained by summing the material volumes of the eight octants of volume adjacent to the integration point (See Figure 12B).

For simplicity it is often convenient to consider one volume of impregnated tow (for example a warp tow) as one material, while another volume of impregnated tow (for example a fill tow) is considered to be a different material, even though they may have the same elastic properties. This avoids the assigning of more than one fiber direction to a material at an integration point. Many details of reinforcing microgeometry are lost in the integration process. Examples include the fiber location with respect to an integration point and local fiber curvature.

5.2 Subcell Transformations

As mentioned previously, the ability to transform the stiffness matrix of a subcell into the global coordinate system of the unit cell is essential. For rectangular hexahedral subcells, only a limited number of transformations are needed, namely, rigid rotations about the coordinate axes and reflections about those axes. First consider a reflection about the x-coordinate axis of Figure 13. This is the coordinate transformation $x = -\bar{x}$, $y = \bar{y}$, $z = \bar{z}$. Let the node points of the subcell be ordered in the sequence shown in Figure 13 and forces (X_i, Y_i, Z_i) and displacements (U_i, V_i, W_i) associated with those nodes ordered as follows:

$$\{X_1, Y_1, Z_1, X_2, Y_2, Z_2, \cdots , X_8, Y_8, Z_8\}$$

$$\{U_1, V_1, W_1, U_2, V_2, W_2, \cdots , U_8, V_8, W_8\}.$$

The rearrangement of the microgeometry caused by reversal of the x-axis is reflected in the rearrangement of rows and columns of the [k] matrix as follows:

$$\{-X_5, Y_5, Z_5, -X_6, Y_6, Z_6, -X_7, Y_7, Z_7, -X_8, Y_8, Z_8,$$

$$-X_1, Y_1, Z_1, -X_2, Y_2, Z_2, -X_3, Y_3, Z_3, -X_4, Y_4, Z_4\}$$

$$\{-U_5, V_5, W_5, -U_6, V_6, W_6, -U_7, V_7, W_7, -U_8, V_8, W_8,$$

$$-U_1, V_1, W_1, -U_2, V_2, W_2, -U_3, V_3, W_3, -U_4, V_4, W_4\}$$

Similar exchanges of rows, columns, and signs can characterize a reversal of fiber geometry about the y or z-axes.

Now consider changes in fiber reinforcing geometry brought about by rotation of the subelement about a coordinate axis. Look at rotation about the x-axis of 90° as shown in Figure 14. The following rearrangement of rows and columns of the [k] matrix achieves this reinforcing geometry modification:

$$\{X_4, Z_4, -Y_4, X_1, Z_1, -Y_1, X_2, Z_2, -Y_2, X_3, Z_3, -Y_3,$$

$$X_8, Z_8, -Y_8, X_5, Z_5, -Y_5, X_6, Z_6, -Y_6, X_7, Z_7, -Y_7\}$$

$$\{U_4, W_4, -V_4, U_1, W_1, -V_1, U_2, W_2, -V_2, U_3, W_3, -V_3,$$

$$U_8, W_8, -V_8, U_5, W_5, -V_5, U_6, W_6, -V_6, U_7, W_7, -V_7\}$$

A similar rotation of 180° about the x-axis leads to the following rearrangement of forces and displacements:

$$\{X_3, -Y_3, -Z_3, X_4, -Y_4, -Z_4, X_1, -Y_1, -Z_1, X_2, -Y_2, -Z_2,$$

$$X_7, -Y_7, -Z_7, X_8, -Y_8, -Z_8, X_5, -Y_5, -Z_5, X_6, -Y_6, -Z_6\}$$

$$\{U_3, -V_3, -W_3, U_4, -V_4, -W_4, U_1, -V_1, -W_1, U_2, -V_2, -W_2,$$

$$U_7, -V_7, -W_7, U_8, -V_8, -W_8, U_5, -V_5, -W_5, U_6, -V_6, -W_6\}$$

A rotation of 270° about the x-axis is produced by the following row/column substitution:

$$\{X_2, -Z_2, Y_2, X_3, -Z_3, Y_3, X_4, -Z_4, Y_4, X_1, -Z_1, Y_1,$$

$$X_6, -Z_6, Y_6, X_7, -Z_7, Y_7, X_8, -Z_8, Y_8, X_5, -Z_5, Y_5\}$$

$$\{U_2, -W_2, V_2, U_3, -W_3, V_3, U_4, -W_4, V_4, U_1, -W_1, V_1,$$

$$U_6, -W_6, V_6, U_7, -W_7, V_7, U_8, -W_8, V_8, U_5, -W_5, V_5\}$$

In an analogous manner, stiffness matrices corresponding to subelement rotations or reflections about the y and z-axes may be obtained. Any sequence of rotations and/or reflections may follow one another in order.

6. ASSEMBLY AND SOLUTION

The process of assembling various subcell stiffness matrices into a unit cell stiffness matrix is similar to any other finite element assembly. First, nodal forces and displacements are arranged in some convenient order. Each element of each subcell stiffness matrix is then placed in its appropriate location within the unit cell stiffness matrix. All terms in any location of the unit cell matrix are summed to obtain the unconstrained stiffness matrix of the assembled unit cell. Now consider the manner in which the nodal displacements are obtained from the unit cell stiffness matrix, the applied displacements (at corners of the cell), and the surface boundary conditions.

6.1 Discrete Unit Cell Boundary Conditions

Unit cell corner displacements are established by the particular applied unit strain and by the location of the zero displacement reference axis. In this report the unit cell is always located wholly within the positive octant of a right hand x,y,z coordinate system with one corner of the unit cell at the origin (Figure 7), the zero displacement reference point. If the unit cell has dimensions A,B,C in the x,y,z directions respectively, then the eight corner nodes have the coordinate locations shown in Figure 7. Corner node displacements for the six average unit strain cases of interest are given in Table 1.

Next consider boundary conditions that apply at a finite element node point situated on either the upper or lower surface of the unit cell, a common point on two adjacent plies (Figure 8). The nodal boundary conditions are equivalent to the continuum elastic boundary conditions discussed previously (Section 4.). Nodal forces at two image points (i,j) must be equal but oppositely directed (Figure 8), i.e.,

$$X_i = -X_j, \quad Y_i = -Y_j, \quad Z_i = -Z_j \qquad (6.1)$$

while the corresponding displacement boundary conditions at the same two nodes are:

Unit Strain Case (1) $\quad \overline{\varepsilon}_{xx} = 1^*; \quad U_i = U_j; \ V_i = V_j; \ W_i = W_j$

Unit Strain Case (2) $\quad \overline{\varepsilon}_{yy} = 1^*; \quad U_i = U_j; \ V_i = V_j; \ W_i = W_j$

Unit Strain Case (3) $\quad \overline{\varepsilon}_{zz} = 1^*; \quad U_i = U_j; \ V_i = V_j; \ W_i - C = W_j$

Unit Strain Case (4) $\quad \overline{\gamma}_{yz} = 1^*; \quad U_i = U_j; \ V_i - C = V_j; \ W_i = W_j$

Unit Strain Case (5) $\quad \overline{\gamma}_{xz} = 1^*; \quad U_i - C = U_j; \ V_i = V_j; \ W_i = W_j$

Unit Strain Case (6) $\quad \overline{\gamma}_{xy} = 1^*; \quad U_i = U_j; \ V_i = V_j; \ W_i = W_j$

$$\left. \right\} \qquad (6.2)$$

If there is more than one subcell per ply thickness then there may be node points on all four vertical faces of the unit cell that are not edge or corner nodes. If these vertical faces are not planes of structural symmetry then the mixed boundary conditions at these node points will be similar to those just stated for upper and lower surface image points. Only the magnitude and location of the constants in the displacement constraints will differ.

6.2 Discrete Symmetry Boundary Conditions

Where structural symmetry conditions exist on a vertical face of the unit cell, nodal force conditions become, for all nodes (except corner nodes) on planes of symmetry perpendicular to the

*All other average strain components equal zero.

$$\text{x-axis} \begin{cases} Y = Z = 0 & \text{for Unit Strain Cases (1),(2),(3),(4)} \\ X = 0 & \text{for Unit Strain Cases (5),(6)} \end{cases} \quad (6.3)$$

$$\text{y-axis} \begin{cases} X = Z = 0 & \text{for Unit Strain Cases (1),(2),(3),(5)} \\ Y = 0 & \text{for Unit Strain Cases (4),(6)} \end{cases} \quad (6.4)$$

Displacement constraints, on planes of symmetry perpendicular to the x-axis, are:

$$\left. \begin{array}{ll} U = 0 \text{ (or A)} & \text{for Unit Strain Case (1)} \\ U = 0 & \text{for Unit Strain Case (2), (3), (4)} \\ V = W = 0 & \text{for Unit Strain Case (5), (6)} \end{array} \right\} \quad (6.5)$$

For planes of symmetry perpendicular to the y-axis:

$$\left. \begin{array}{ll} V = 0 \text{ (or B)} & \text{for Unit Strain Case (2)} \\ V = 0 & \text{for Unit Strain Case (1), (3), (5)} \\ U = W = 0 & \text{for Unit Strain Case (4), (6)} \end{array} \right\} \quad (6.6)$$

Similar sets of boundary conditions can be specified for all other unit average strain cases with the chief difference being size and location of the constant terms in the displacement constraints. The general form of the system of equations for nodal forces and displacements can now be written.

6.3 General Statement of the Discrete Problem.

The assembled unit cell stiffness matrix, $[K]$, relates all nodal forces, $\{F\}$, and displacements $\{\delta\}$, as follows:

$$\{F\} = [K] \{\delta\}. \quad (6.7)$$

The homogeneous force boundary conditions at surface and edge nodes can be written symbolically in matrix form as:

$$\{O\} = [H] \{F\} \quad (6.8)$$

where $\{O\}$ is the null vector and $[H]$ the coefficient matrix.

The homogeneous and inhomogeneous displacement boundary conditions at surface, edge and corner nodes can similarly be written in matrix form as:

$$\{O,A,B,C\} = [J] \{\delta\} \qquad\qquad (6.9)$$

where $\{O,A,B,C\}$ is a vector containing only the values O,A,B or C and $[J]$ is the coefficient matrix. Implicit is the absence of force resultants at all internal nodes.

The foregoing system of equations $(6.7, 6.8, 6.9)$ has dimension $6n$ by $6n$ where n is the number of node points in (or on) a unit cell . The size of the system can be substantially reduced before attempting a solution.

All nodal forces must be eliminated by first setting to zero those forces that are zero in the stiffness matrix. Remaining nonzero force equations involving the stiffness matrix are then used to eliminate all nonzero force terms from the homogeneous force boundary conditions. The combination of zero-force stiffness equations and the force boundary conditions (in terms of displacements) comprise a set of homogeneous equations in nodal displacement variables only. Each displacement boundary condition is so simple that it can be used to eliminate one surface displacement variable in the foregoing set of homogeneous equations. Over half of the displacement variables on the faces of the unit cell are eliminated in this manner. The remaining equations can now be solved for all unconstrained displacements. The foregoing procedure is not standard finite element procedure. Most general purpose finite element programs do not treat boundary conditions of this complexity.

Displacement boundary conditions and corner conditions are then used to obtain constrained displacement values. All surface and corner forces can be obtained by substituting the complete set of nodal displacements into the original stiffness equations. Nodal force components on any side of the unit cell can then be summed and divided by the area of the side. This dividend is the average stress on that side. These stress values are the coefficients of the 3-D composite stress/strain

law, [D].   Elastic solutions for the six unit strain cases provide all 36 coefficients of the stress/strain law which can be inverted to provide the composite flexibility matrix.   Recourse to definitions of engineering constants provides formulae for these quantities.

One remaining simplification eliminates the need for reformulating and resolving each elastic displacement problem for each of the six unit strain cases.   Each unit strain case is considered to be a combination of a homogeneous (uniform) strain field plus an inhomogeneous (nonuniform) one.   Nodal displacements for the six uniform strain fields are obvious from knowledge of the response of homogeneous material to uniform surface stress states.   The six sets of equations for the nonuniform displacements turn out to differ only in the inhomogeneous portions of their algebraic equations.   Thus only one large matrix inversion is required (as opposed to six).   If NX is the number of subcells along the x-parallel side of a unit cell and NY is the number along a y-parallel side then the size of the inversion is $3[(NX)(NY)-1]$ square.

The use of planes of structural symmetry to reduce the amount of unit cell structure that must be analyzed complicates matters somewhat.   Strain cases representing symmetric loads (with respect to planes of symmetry) do not reduce to the same set (or number) of unconstrained displacement equations as the shear strain cases which represent asymmetric loadings.   Thus, the computational effort is approximately doubled.   Despite this increased effort, it is still advantageous to use structural symmetry when it exists.

7.   COMPUTER PROGRAM DESCRIPTION

A computer code, based on the foregoing analysis, has been written in Fortran 77 language for use on the CDC 6600 computer at NASA Langley Research Center's central computing facility.   A listing for the program is given in Appendix I. The core of the program consists of a set of three nested do loops.   The outer do loop computes the stiffness matrix for each elastically different subcell in the finite element model of the unit cell, transforms it into the global unit cell coordinates, and inserts each element of the subcell stiffness matrix into its proper location in the larger unit cell stiffness matrix.

The intermediate do loop ranges over each material within the subcell.   In other words, the subcell stiffness matrix is assembled, one material at a time, and the contribution that each material makes to the stiffness matrix is computed and added into the subcell stiffness matrix, which maintains a running total of each material contribution, in the same manner that the unit cell stiffness matrix consists, at any point in time, of a running total of the different subcell contributions.

The third and inner most do loop ranges over each integration point in the integration grid.   The contribution of one material to one subcell stiffness matrix represents the sum of its contributions at each integration point.   As the fiber directions and constituent material volumes are read in, for any integration point, the contribution to the appropriate subcell stiffness matrix is calculated and added into the proper matrix locations.   As the last constituent material associated with the last integration point for the last subcell is read into the program the last contribution to the unit cell stiffness matrix is put into place and the unconstrained stiffness matrix of the unit cell is completed.   There is no further input data required.   The six unit strain problems are solved in sequence

and the mean stresses corresponding to each unit strain tabulated. The elastic constants for the composite are then computed and displayed.

Prior to entering the nested do loops the necessary information to characterize the constituent materials, set the number of master subcells, size the unit cell, divide the unit cell into subcell compartments, and fill each compartment with a properly transformed subcell, must be specified. The subcells are sized in the outermost portion of the nested do loops. The input data details are discussed in Appendix II. Appendix III contains an interactive sample problem input and output for a simple woven composite architecture. Figure 15 contains a flow chart of the program.

The math subroutines that invert matrices and solve simultaneous equations (MATOPS and GELIM) are not included in the listing. Similar subroutines are included in any math library package.

8. SIMPLE APPLICATIONS

In this section fabric analysis is applied to a set of problems that are not representative of any actual fabric reinforced composite, but are simple enough to illustrate some basic features of the analysis. The simplest possible application is the prediction of the stiffness of a bulk orthotropic material, for example, a graphite/epoxy with the following elastic properties:

$$E_{11} = 20.0 \text{ msi} \qquad \nu_{12} = \nu_{13} = 0.25$$

$$E_{22} = E_{33} = 1.5 \text{ msi} \qquad \nu_{23} = 0.35 \qquad\qquad (8.1)$$

$$G_{12} = G_{13} = G_{23} = 0.7 \text{ msi}$$

where planes perpendicular to the fiber axis are planes of transverse isotropy. The fiber direction is denoted by 1, the direction perpendicular to the fiber (in the plane of the laminate) by 2, and the ply thickness direction by 3.

The unit cell of this reinforcing geometry can be any size of rectangular prism with a minimum side length several orders of magnitude larger than the average fiber diameter. This unit cell can be assembled from a single subcell which contains only one material, the graphite/epoxy composite with fibers paralleling the x-axis. The subcell is the unit cell. The simplest 3-D integration grid and integration scheme is adequate in this case. Let the eight corners of the subcell be the integration points. The subcell stiffness matrix generated by integration represents a homogeneous material uniformly distributed throughout the subcell. The unit cell stiffness matrix is identical to the subcell stiffness matrix. Subsequent calculation of the composite stiffness coefficients and E,V,G values yields the same numbers as the material property input. Analyzing the same material with the fibers at an angle to (rather than parallel to) the global x-

axis gives the composite moduli in a different reference system from the input data.

8.1 Fiber Path Variation

The effect of $\pm 45^{\circ}$ zigzag ($\bigwedge\!\!\bigwedge$) or rickrack fiber paths on the moduli can also be evaluated with this analysis. For example, consider the 2-D rickrack reinforcing pattern of Figure 16A. The unit cell shown contains one repeat of this geometry. The unit cell can be subdivided into two subcells (I and II) with constant fiber direction in each (Figure 16B). One subcell can be generated from the other via a 180° rotation about the z-axis. Thus only one master subcell and a pair of rigid transformations are required to orient fibers properly in the unit cell. Using the previous unidirectional composite properties (Equation 8.1), the analysis of the unit cell gives the following results:

$$E_x = 1.89 \text{ msi}, \ V_{yz} = 0.18, \ G_{yz} = 0.70 \text{ msi}, \ \eta_{xz,x} = 0$$

$$E_y = 1.50 \text{ msi}, \ V_{xz} = 0.35, \ G_{xz} = 2.04 \text{ msi}, \ \eta_{xz,y} = 0$$

$$E_z = 1.89 \text{ msi}, \ V_{xy} = 0.23, \ G_{xy} = 0.70 \text{ msi}, \ \eta_{xz,z} = 0$$

where the coefficient of mutual influence $(\eta_{ij,k})$ designates shear strain in the ij plane as a result of a unit normal strain in the k direction. The comparable results for unidirectional material oriented at an angle of $\pm 45^{\circ}$ to the x-axis (in the xy-plane) without the rickrack pattern are:

$$E_x = 1.89 \text{ msi}, \ V_{yz} = 0.18, \ G_{yz} = 0.70 \text{ msi}, \ \eta_{xz,x} = 0.81$$

$$E_y = 1.50 \text{ msi}, \ V_{xz} = 0.35, \ G_{xz} = 1.40 \text{ msi}, \ \eta_{xz,y} = 0.36$$

$$E_z = 1.89 \text{ msi}, \ V_{xy} = 0.23, \ G_{xy} = 0.70 \text{ msi}, \ \eta_{xz,z} = 0.81$$

The Young's moduli and Poisson's ratios of the rickrack pattern are the same as the skewed unidirectional material. However, the G_{xz} shear modulus and all of the non-zero coefficients of mutual influence differ.

Neither of these examples shows how multiple materials can be mixed in the same subelement. The previous example problem could have been approached in this way; i.e., the unit cell could have been modeled by a single subcell containing both fiber angles in the rickrack pattern (see Figure 16C). If half of the subcell contained only $+ 45^{\circ}$ material and the other half -45° material then (using the same eight corner integration points) the volume of material associated with the four integration points on the $x = 0$ plane would consist only of $+45^{\circ}$ material while integration points on the $x = A$ plane would have only -45° material associated with them. The complete subcell stiffness matrix includes all eight integration points and both $+ 45^{\circ}$ and -45° material. Resulting moduli predictions are identical to the previous model based on two homogeneous subcells per unit cell.

Three-dimensional rickrack reinforcements, shown in Figure 17A, can be analyzed almost as easily as 2-D ones. A unit cell of this fiber reinforcing pattern is shown in Figure 17B. Solid lines indicate fiber direction in an entire subcell. All four subcells (Figure 17C) are rigid transformations of each other. Variation in Young's modulus of this material with the z-axis fiber orientation angle (for the same graphite/epoxy) is shown in Figure 18. This figure also contains a plot of Young's moduli for the 2-D rickrack pattern of Figure 16. Internal constraints from adjacent subcells increase the 3-D moduli very slightly over the 2-D case.

8.2 Void Analysis

Consider another example problem in which the material is homogeneous and isotropic except for a periodic array of continuous, parallel, square holes. The

major axis of these holes is parallel to the z-axis, as shown in Figure 19A. One unit cell of this microgeometry consists of a cube of material with one hole in its center (Figure 19B). Since there is no variation of geometry along the axis of the hole, there is no need for more than one subelement in that direction. The simplest conceivable representation of hole geometry is a single subelement with the volume integration for it's stiffness matrix extending only over the volume of the actual material present. With the eight corners as integration points, Figure 20 shows the Young's modulus and shear modulus predictions as a function of hole volume fraction for an epoxy unit cell. Similar estimates may be obtained using 3x3x2 and 4x4x2 integration grids depicted in Figure 21. However, the single eight-node subcell is not capable of yielding better stiffness estimates than the rule of mixtures (for elements in parallel) for this example, irrespective of integration grid refinements.

Now consider a model of the same microstructure with more subcells of smaller size. The unit cell model in Figure 22 contains 12 subcells. However, only two are elastically different, the square subcells at the four corners and the eight rectangular ones between the corners. Stiffness estimates for this model are shown in Figure 23. Both 2x2x2 and 3x3x2 grids are used for subcell stiffness integrations. There is a small difference in results for the 2x2x2 and 3x3x2 grids but there is no major improvement in accuracy with this or further grid refinement. However, a large improvement has resulted from the use of smaller, more numerous subelements (Compare Figures 20 and 23). The standard of comparison in Figure 23 is the strength of materials calculation for stretching and bending of two orthogonal sets of parallel plates, welded together at their lines of intersection. This model is not an exact solution but is very accurate for hole volume fractions of more than 50%.

For high void fractions, moduli prediction of the fabric analysis and predictions of the strengths of materials model are generally in agreement; except for the G_{xy} shear modulus case. These predictions differ by almost a constant factor of 2. The reason for this difference is that the G_{xy} shear modulus is dependent on bending stiffness of the thin cellular walls between the square holes. The eight node hexahedral element used to represent these cell walls is deficient in its ability to model linear bending strain distributions.

9. WOVEN FABRIC APPLICATIONS

This section considers application of the preceeding analysis to woven fabric microgeometry. First consider the most common weave construction, plain weave. Idealizing the geometry is traditionally the first step in analyzing any structure. For fabrics this usually implies replacing tow bundles with elastic tubes of constant cross section. In textile mechanics these interwoven tubes are referred to as channel models (Ref. 18). In composite mechanics these tubes are assumed to consist of unidirectional orthotropic material with a plane of isotropy normal to the principal axis of each tube. Figure 24A contains one such idealization in which tow cross-sections are assumed to have a diamond shape. Dissimilar materials in the unit cell are separated by a series of flat planar areas. As mentioned previously, if warp and fill materials and their geometries are identical, and if a rule of four subcells per yarn crossover is adopted, then only one master subcell plus 16 transformations of that subcell are required to model the unit cell, (Figure 24B,C). If a 2x2x2 integration grid is superimposed on the idealized subcell microgeometry, then the small volumes of dissimilar materials associated with each integration point can be visualized, characterized, and tabulated from geometric considerations (Figures 25 and Table 2). Table 2 presents the two spherical fiber angles (ϕ_1, ϕ_2) and eight material volume fractions $(v_1, v_2, \cdots v_{,8})$ associated with each octant of volume surrounding each integration point for each of the three constituent materials, namely, the unidirectional warp composite (1), the unidirectional fill composite (2), and the bulk matrix (3). The subscripts 1 through 8 on the material volume fractions refer to the following x,y,z octants respectively: +++, ++-, +-+, +--, -++, -+-, --+, and --- as shown in Figure 12.

The volume fraction of impregnated tow in this composite is 50%. The other 50% is

interstitial bulk matrix. If elastic properties of the transversely isotopic tow material have the same values as the unidirectional material of the previous section (Equation 8.1) and the bulk matrix properties are

$$E = 0.5 \text{ msi}, \ G = 0.185 \text{ msi}, \ V = 0.35, \qquad\qquad (9.1)$$

then the analytical predictions of the fabric reinforced composite properties are:

$$E_x = E_y = 4.40 \text{ msi} \quad , \quad E_z = 1.14 \text{ msi}$$

$$G_{yz} = G_{xz} = 0.48 \text{ msi} \quad , \quad G_{xy} = 0.42 \text{ msi}$$

$$V_{yz} = V_{xz} = 0.425 \quad , \quad V_{xy} = 0.132$$

If this same graphite/epoxy composite was unwoven unidirectional material in the form of a thick blended 0/90 laminate with 50% bulk matrix material between the plies, the laminate properties would be:

$$E_x = E_y = 5.67 \text{ msi} \quad , \quad E_z = 1.02 \text{ msi}$$

$$G_{yx} = G_{xz} = 0.29 \text{ msi} \quad , \quad G_{xy} = 0.44 \text{ msi}$$

$$V_{yz} = V_{xz} = 0.422 \quad , \quad V_{xy} = 0.051$$

The weave microgeometry is thus responsible for an approximate 22% reduction in Young's moduli E_x and E_y, but a much smaller reduction in the in-plane shear moduli.

This sample problem serves only as an example of the application of fabric analysis to a reinforcing geometry resembling a plain weave microstructure. A true fabric microstructure has more complex tow paths and tow cross-sectional variations than this example. However, the analysis is not limited by any of these geometric complications, as the next example illustrates.

9.1 Realistic Plain Weave Model

Now consider the microgeometry of Figure 26 for a graphite/epoxy, plain weave, reinforced composite which is magnified approximately 70X. This laminate is an 8-

ply composite consisting of T-300 untwisted tow yarns at 18 ends and 18 picks per inch. The matrix designation is 5208; average thickness per ply is 0.011 inches; fiber volume fraction is 66.7%. Closer examination of Figure 26 reveals that warp and fill fibers have a maximum angle of approximately $\pm 6^{O}$ with the middle plane of the fabric as they undulate over and under one another. Using the concept of a somewhat irregular unit cell and subcell of Figure 9 with a 2x2x2 integration network (the corners of the subcell are the integration points), Table 3 contains all necessary remaining geometric input data for computation of the subcell stiffness matrix. As before, υ_i designates the fraction of volume associated with the i th octant of volume (surrounding an integration point) that is occupied by one of the three constituent materials. Octants containing both warp and fill tows are considered to contain two different orthotropic materials. Bulk matrix is the third material.

Subcell cross-section sketches and 3-D yarn bundle models, based on photomicrographs, assist in establishing the υ_i quantities. For simplicity, fiber angles are obtained from observed values at integration points rather than from averages over neighborhoods of the integration points. There is no attempt in this example to force reinforcing geometry to coincide with any idealized model.

The fiber volume fraction within a tow bundle is taken to be 75% based on electronic scanning of similar composite photomicrographs using only those areas within the tow cross sections. The void content of the composite is assumed to be zero. The volume fraction of fiber in the tow (75%), times the volume fraction of impregnated tow within the composite must equal the total fiber volume fraction of 64%.

The volume fraction of impregnated tow is thus 85% of the total volume.* The volume fraction of the composite occupied by unreinforced matrix material must therefore be 15%. This is necessary to arrive at an overall composite fiber volume fraction of 64% which is the approximate average measured value for all of the test materials considered in this section (as determined by acid digestion).

There is some difficulty associated with the assignment of principal moduli to the impregnated tow material. Neither existing test data or micromechanics provides reliable estimates. Test data from unidirectional material seldom extends into the 75% fiber volume fraction range. Also, unidirectional test data does not include the inevitable degradation to tow properties that result from the weaving and related fabric forming processes. The latter objection also applies to micromechanics estimates of moduli. A semi-empirical application of the rule of mixtures (for elements in parallel) described subsequently seems to provide the best basis for establishing E_1 of the impregnated tows.

In Ref. 19 twelve different unidirectional graphite composite materials were characterized experimentally. Their measured longitudinal moduli were lower in eleven out of twelve cases from the rule of mixtures prediction. The mixtures rule overestimated measured moduli (E_1) by almost 10% based on an average of the twelve materials. This shortfall in the measured E_1 can be attributed in part to fiber loss, misalignment, and breakage in the unidirectional prepregging and curing processes. The weaving process is considerably more damaging than the unidirectional prepregging process.

*For analysis purposes 64% fiber volume fraction was used rather than 66.7% because it was desired to have a common basis of comparison for each of the different weaves in this correlation.

37

Thus it seems reasonable to anticipate a greater reduction in E_1 due to weaving than unidirectional tow placement. Another 10% reduction in E_1 might be appropriate to account for weaving factors. Therefore, if the fiber volume fraction of a graphite/epoxy unidirectional material, with a 20 msi longitudinal modulus, were increased from 65% to 75% the rule of mixtures would predict about a 15% longitudinal modulus increase. However, the weaving reduction factor would decrease this gain to only 5% and the resulting longitudinal modulus of the impregnated tow material within the weave would be about 21 msi. A truly reliable alternative to such an estimate would be an experimental study that measured impregnated tow modulus before and after weaving. This was beyond the scope of this program.

The weaving process often includes beaming, sizing, weaving, scouring, drying and packaging. Each of these steps abrades, damages and misaligns the reinforcing fibers to some degree. The floor of any weaving room is a testament to the degradation and loss of reinforcing material. Also, T300 fibers showed more evidence of property reduction as a result of the unidirectional prepregging process than most of the graphite fibers studied in Ref. 19.

Only the longitudinal modulus of the tow composite is assumed to be significantly degraded by weaving. Micromechanics considerations indicate a 15% increase in the transverse Young's modulus and shear moduli are appropriate to a fiber volume fraction increase from 65% to 75%. The principal Poisson's ratios should decrease a few percent as the fiber content increases.

The principal moduli values for the impregnated tow composite are thus estimated to be (using the Rule of Mixtures for elements in series and parallel):

$$E_1 = 21.0 \text{ msi} \qquad\quad V_{12} = 0.23$$

$$E_2 = E_3 = 1.7 \text{ msi} \qquad\quad V_{23} = 0.30 \qquad\qquad (9.2)$$

$$G_{12} = 0.8 \text{ msi} \qquad\quad G_{23} = 0.8 \text{ msi}$$

Matrix properties are equivalent to those in the prior example (Equation 9.1). The fabric analysis predictions are given in Table 4 along with the experimental data. Experimental values and photomicrographs were provided by NASA Langley Research Center and were previously published in Reference 12.

The comparison between analysis and experiment is generally good. The small differences in Young's moduli would indicate that the assumptions regarding tow property reduction resulting from the weaving processes were reasonable. The experimental difference between the moduli in the warp and fill direction could be accounted for in two ways. There are possibly some small variations in undulation angles between warp and fill tows that are not in evidence in the small area samples that were subject to microscopic examination. Also, there is ample reason to believe that property damage due to weaving is not evenly distributed between the warp and fill tows.

There is a major discrepancy between the analytical and measured in-plane Poisson's ratio. The experimental value is suspect in this case because it is much greater than other analytical predictions, similar graphite/epoxy data, and 0/90 cross ply analysis and data.

The reduction in the principal in-plane moduli due to the weave microstructure is about 5% based on a cross-ply unidirectional laminate with the same fiber volume.

Consider the possible loss of accuracy resulting from doubling the subcell x,y

side lengths while reducing the number of subcells in the unit cell from 16 to 4. One subcell then represents one warp/fill yarn crossover. This increases the maximum subcell side length ratio from 5/4 to 5/2, which is not excessive for finite element analysis. If a 3x3x2 integration grid is applied to the subcell then all the fiber angle and material volume fraction data associated with each integration point carries over unchanged from the 16 subcell model to the 4 subcell model.

Use of this larger subcell leads to the following plain weave fabric reinforced composite moduli predictions:

	Small Subcell (msi)	Large Subcell (msi)
E_x, E_y	9.25	9.22
E_z	1.65	1.65
G_{yz}, G_{xz}	0.721	0.720
G_{xy}	0.699	0.744

	Small Subcell	Large Subcell
v_{yz}, v_{xz}	0.329	0.333
v_{xy}	0.031	0.028

Results from the two models are almost identical.

9.2 Other Weaves

Using the same fiber and matrix, NASA has made composite laminates in four weave patterns: plain, 2/2 Oxford, five harness satin and eight harness satin. All weaves have 18 ends and 18 picks per inch. Figure 27 shows photomicrographs of the latter three weave geometries after lamination. Different weave patterns

yield slight variations in fiber undulation angles. The maximum angle that satin weave fibers make with the plane of the fabric is approximately one degree smaller than the maximum plain weave fiber angle. Oxford weave angles are smaller than plain weave angles but larger than satin weave angles. Fiber volume fractions of the four weaves also vary slightly. In the analysis a fiber volume fraction of 64% was maintained for all weaves.

Figure 28 shows an Oxford weave unit cell and three possible subdivisions. The first possibility (Figure 28C), with four subcells per yarn crossing, requires 32 transformations of two master subcells to model the unit cell. This model leads to a matrix inversion of dimension 93 square; probably larger than warranted. The second possibility (Figure 28D), with two subcells per yarn crossover, leads to a matrix inversion of order 45. Only 16 transformations of a single master subcell are required with this model. A third possible model is shown in Figure 28E. It is a coarser subdivision than either previous model. Each subcell represents one warp/fill tow crossover. All three models are shown to illustrate the point that many variations are possible with this type of analysis. The fabric reinforced composite moduli prediction, based on the medium subcell division model, using a 2x3x2 integration grid, are given in Table 4.

Comparison of the Oxford weave and plain weave moduli predictions shows a slightly greater Young's moduli for the Oxford weave. This reflects the differences in yarn crossover angles and crossover frequency. Fiber volume fraction for the Oxford weave was 64% for the analysis and 62% for the experiment.

Consider the five harness satin weave geometry shown in the photomicrograph of Figure 27 and the sketch of Figure 29. If a subcell division of the unit cell is based on a rule of four subcells per yarn crossing then the largest matrix inversion is of order 297. Use of one subcell per crossover reduces this

dimension to 72. Thus, the subcell division shown in Figure 29C was adopted. Two different master subcell stiffness matrices are required for this model. A 3x3x2 integration grid is used on each subcell. Matrix and unidirectional properties used are equivalent to those used in the Oxford and plain weave models. Analytical and experimental moduli are given in Table 4.

Analysis again predicts the trend toward higher in-plane moduli with decreasing density of yarn undulations. The frequency of undulations has little effect on shear moduli or Poisson's ratios. Both analytical and experimental fabric volume fractions of the five-harness satin weave are 64%.

The in-plane Young's moduli correlation is not as good as was obtained on the plain weave or Oxford weave. This raises a question concerning the use of a constant unidirectional tow composite property reduction factor to account for tow damage in weaving. It would appear from the correlation that the amount of tow damage is a function of the weave style. The lower than expected analytical Young's moduli for the satin weave, with relatively few warp/fill crossovers per unit of fabric area, indicates a possible lower level of tow damage than was evidenced in the plain or Oxford weave forming process with many more warp/fill crossovers. The beat up process following pick yarn insertion could be more of a localized damage phenomenon in the vicinity of warp/fill crossovers than an overall damage mechanism.

The eight harness satin weave is shown in the photomicrograph of Figure 27 and sketched in Figure 30. One unit cell is shown in Figure 30B. Using four subcells per yarn crossing leads to a reduced stiffness matrix of 765 square. One subcell per yarn crossing gives a stiffness matrix of order 189. In addition, three different master subcells are required. Thus, it is of interest to consider a

cruder single subcell that includes four yarn crossovers. Only two different master subcells require consideration with such a model. This subdivision of the unit cell is shown in Figure 30C. The unit cell reduced stiffness matrix is of order 45. Use of the previous constituent material properties with the 5x5x2 integration grid of Figure 30D yields the results given in Table 4.

The lower than expected analytical Young's moduli in the plane of the fabric for the eight harness satin reflects the same trend as was observed for the five harness satin and again suggests less weave damage with fewer warp/fill crossovers.

In general the correlation between analysis and experiment was satisfactory for most engineering applications. A linearly varying tow property reduction factor based upon the number of warp/fill crossovers per inch of tow would have very much improved the correlation. However, this correction should be verified more thoroghly before adoption.

In summary, a general rule of "four subcells per yarn crossover with crude integration schemes and networks" is adequate for modeling conventional woven fabric reinforcing geometries. Larger subcells can be used with little compromise in accuracy if corresponding refinements are made in the integration network. One subcell per ply in the thickness direction seems adequate under the same circumstances.

10. BRAIDED FABRIC APPLICATIONS

A variety of industrial braided fabrics have application as composite reinforcing materials. Their microgeometries are often similar to woven fabrics. The simplest 2-D braids (Figure 31A) are analogous to skewed plain weaves.

One important braid characteristic is braid angle, i.e., the average angle (in the plane of the fabric) that yarns (tows) make with the fabric output (machine take-up) direction. A braid angle of $\pm$ 45° corresponds to an orthogonal plain weave (although some microgeometry differences may result from differences in tow handling). For analytical purposes $\pm$ 45° plain braid and plain weave microgeometry can be considered equivalent. Furthermore, when the braiding tows are identical and have identical spacing, it is possible to isolate a unit cell that is a rectangular prism (Figure 31B). This particular unit cell can be subdivided into four subcells (Figure 31D), each of which can be obtained from the other by various coordinate transformations. Thus, it is necessary to obtain a stiffness matrix for only one master subcell in order to model the unit cell. The stiffness matrix for the subcell is obtained by the same method used for weaves. First, a 3x3x2 integration grid is superimposed on the subcell volume. Fractional values of octant volumes (surrounding each integration point) containing the three constituent materials (two sets of impregnated braid tows and bulk matrix insterstices) are given in Table 5. Two spherical angles describing local fiber directions at each of the 18 integration points are also tabulated. This data corresponds to a braid angle of $\pm$ 45°. The unidirectional composite properties are given in equation (9.2). Bulk matrix properties are given in equation (9.1).

Moduli predictions for the 64% fiber volume fraction braid and for the 64% fiber volume fraction plain weave from Section 9. should be close to equivalent after the plain weave moduli are transformed into the coordinate system of the braid.

44

The predicted moduli are:

	$\pm\,45^{\circ}$ Braid	Transformed Plain Weave
E_x, E_y (msi)	2.48	2.44
E_z (msi)	1.66	1.65
G_{xy} (msi)	4.57	4.49
V_{xy}	0.73	0.51

Small differences in the descriptions of the microgeometry of the master subcells would account for the small moduli differences. The reason for the large difference in the Poisson's ratio of the two models is not clear.

Figure 32 contains a plot of variation in braid moduli as a function of braid angle. Reinforced and unreinforced material volumes associated with integration points are assumed to remain constant as the braid angle varies. Actually, some of the braid angles are not possible to achieve without "jamming" of the two braid tow systems. Distortions of local geometry begin as the braid angle approaches these limits. Braid moduli plots are qualitatively similar to the corresponding plots for symmetric angle-ply laminates made from unidirectional materials.

Braids with different sets of braid tows may be analyzed by the same procedure, but more than one master subcell is needed to build the unit cell. Different tow spacings in the two sets of braided tows would present a greater modelling problem.

10.1 Triaxial Braids

A triaxial braid reinforced composite, as shown in Figure 33, consists of three sets of tows, intertwined together. Besides the pair of conventional braider tows

the 0° or longitudinal "stuffer" tows are introduced into the 2-D braid through a set of stationary tow carriers around which the braider carriers pass during the fabric formation. The 0° tows remain essentially straight in the final fabric and lie in the machine take up direction. The braid pattern must be modified to make room for the 0° tows. Instead of each braid tow intertwining over and under each braid tow that it crosses, each braid tow is allowed to float alternately over and under each pair of braid tows it crosses. This relates the braid to a 2/2 twill weave in the same way that the previous braid relates to a plain weave. The triaxial braid introduces an additional 0° tow size parameter of choice. For the particular triaxial braid to be modeled the tows were all made from AS-4 graphite fibers. The braid angle was $\pm$ 70°. The braider tows contained 6000 strands per tow. The 0° longitudinal tows contained 18,000 strands. Both tows were untwisted. The composite fiber volume fraction was 52% as measured by acid digestion. The matrix matrial was Shell 1895 epoxy.

Figure 34 shows the smallest rectangular unit cell for the triaxial braid. It contains two 0° stuffer tows and portions of four tows from each of the two sets of $\pm$70° braider tows. The spacing of the stuffer tows establish the width of the unit cell. The stuffer tow spacing was 4.4 tows per inch making the unit cell (2/4.4) = 0.455 inches wide. The braid angle of $\pm$70° established the unit cell height of (1/2)(0.455)/(tan 70°) = 0.166 inches. The thickness per ply was 0.0275 inches. The laminate was five plies thick. Figure 35 shows two photomicrographs of the actual material which was made by the Boeing Co. and tested at NASA Langley Research Center (Ref. 20). The braider tows had an average crossover angle of $\pm$9°. The unit cell was divided into eight subcells, as shown in Figure 34. The eight subcells reduce to two master subcells whose stiffness matrices were assembled using a 2x2x2 integration network. The fiber volume fraction within a tow bundle

was taken to be 75%. Thus, the volume of unidirectional tow composite within the unit cell was (100)(52/75)= 70%. The remaining 30% is bulk interstitial or unreinforced matrix material. The same elastic properties that were attributed to the bulk matrix and the unidirectional tow composite in the prior braid analysis were applied to the triaxial braid analysis. The percentages of fiber in the three different tow directions were almost equal. Since the braid angle was close to 60° it is expected that the resulting composite will have close to quasi-isotropic laminate properties for the same volume fraction of the same fiber. The principal triaxial composite moduli from both the fabric analysis and test are, with reference to the coordinate system of Figure 34:

	Analysis	Test
E_x (msi)	7.41	7.03
E_y (msi)	6.32	6.31
E_z (msi)	1.75	N.A.
G_{xy} (msi)	1.80	N.A.
ν_{xy}	0.214	0.190
ν_{yx}	0.169	0.183

The analysis and test are in good agreement, particularly as relates to measured strains in a tow diection.

11. KNITTED FABRIC APPLICATIONS

The foregoing braided and woven fabric composite analysis proceedures also apply to composites with knitted reinforcement. Low fiber content and the absence of long fiber floats in the microgeometry render this form of reinforcement inefficient for highly-loaded structural applications. However, knitting is used in nonstructural applications because of its ability to conform to complex surfaces prior to curing and because of its availability in tubular form.

One of the most common knit patterns is the Jersey (plain) knit. Jersey microgeometry and a rectangular unit cell (Ref. 21) are shown in Figure 5. This pattern resembles some forms of chain link fencing which have almost the same unit cell. One possible subdivision of the unit cell into subcells is shown in Figure 36. This subdivision is convenient because all four subcells can be formed from transformations of one master subcell. A 2x2x2 integration network serves to form the stiffness matrix for the master subcell. Spherical fiber direction angles and composite and bulk matrix volume fractions associated with each integration point are given in Table 6. The fiber volume fraction within the impregnated tow is assumed to be 75% and the volume fraction of unidirectional material within the composite is assumed to be 33.3%. Thus, the overall fiber volume fraction of the composite is (0.75 x 0.33 x 100) = 25% and interstitial or unreinforced matrix volume fraction is 66.7%. Unidirectional composite and matrix constituent properties are the same as the previous braided fabric constituent properties. The predicted knit fabric reinforced composite moduli are as follows:

$$E_x = 1.70 \text{ msi} \quad , \quad V_{yz} = 0.33 \quad , \quad G_{yz} = 0.52 \text{ msi}$$

$$E_y = 2.16 \text{ msi} \quad , \quad V_{xz} = 0.27 \quad , \quad G_{xz} = 0.41 \text{ msi}$$

$$E_z = 1.02 \text{ msi} \quad , \quad V_{xy} = 0.32 \quad , \quad G_{xy} = 0.74 \text{ msi} \quad .$$

The in-plane composite Young's moduli are lower than (0/90) laminates of unidirectional material with the same fiber content. The in-plane shear modulus and Poisson's ratio are higher for the knit.

In braids, weaves, and knits prestress can distort microgeometry within the unit cell and cause large changes in moduli of the composite material. Prestretching of knits in the layup process is almost unavoidable. This phenomena is one reason for the absence of reliable test data on knits. Figure 37 shows the effects of prestretching or elongating the unit cell. As in the case of braids, tow compaction may prevent some of these microgeometries from being achievable.

12. CONCLUDING REMARKS

This report describes a method for applying general 3-D finite element analysis to predict all of the linear elastic constants of fabric reinforced composite laminates. The analysis presumes the reinforcing microstructure can be condensed into a small repeating rectangular unit cell. The generic composite structure is presumed to consist of an infinite array of these unit cells joined together at matching surfaces. The analysis of a single unit cell is sufficient to predict all the global elastic properties of the composite. The approach avoids some of the difficulties associated with matching of finite element node point locations and element boundaries to internal material boundaries. Partially reinforced elements are used, along with the general energy formula for their stiffness matrix. This formula accounts for material property variations within the element. This approach should work if element dimensions are small with respect to the tow cross-sectional dimensions and interstitial matrix volume dimensions. This report shows that for many reinforcing geometries it is not essential (within the requirements of engineering accuracy) that the element size be that small. With most common reinforcing weaves and with the eight-node hexahedral element, a general rule for sizing of elements is one element per ply in the thickness direction and one to four elements per tow crossover. This rule applies to braids as well. Its application to knits is suggested but unverified.

Since most general purpose finite element codes are awkward to use with the boundary conditions associated with moduli prediction, a special purpose computer code was written to facilitate application to these problems. This code is much quicker and easier to use than general finite element codes. Appendices I, II and III contain a listing, discussion of input data and sample problem for this Fortran code.

One advantage to this analysis is that it easily adapts to most forms of reinforcing microgeometry. The method does not require difficult logic or multiple option choices and enables the calculation of the all 3-D elastic contants. Hence, this method is useful for estimating material property inputs required of impact damage analysis codes. Another advantage of this analysis is that it remains within the scope of finite elements, which is familair to many engineers. No depth of knowledge in textile structures is required.

Examples of application of this analysis to weaves, braids and knits are included to familiarize readers with fabric microgeometry and modeling of yarn constructions, and to impart some appreciation for the effects of varying these construction parameters. It is possible, with this code, to generate a catalogue of moduli predictions based on microgeometry and constituent property variations. However, the goal of this report is simply to show that reinforced composite microgeometry is amenable to routine structural analysis and that this analysis is useful in the search for impact damage resistant composite designs.

The analytical predictions of fabric reinforced composite moduli have been compared to test data for several weave and braid reinforced composite laminates. The predictions are largely within the desired range of accuracy required of most materials engineering applications.

If a laminate consists of several different plies of different fabrics then it is necessary to apply the fabric reinforced composite analysis to each different fabric. This ply level analysis is followed by a conventional laminate analysis in order to obtain the elastic properties of the complete laminate. Laminates that are made from many plies of the same fabric reinforcement, oriented at different angles with respect to each other require a single fabric reinforced composite analysis followed by a conventional laminate analysis. Thin laminate

51

response may only be approximated using this analysis. Corrections may be necessary to account for free surface effects and possible single ply bending and stretching/bending coupling effects.

Historically very few special elements have been developed which contain more than one material within the elements (except for laminated plate and shell elements). The potential for new 3-D elements exists within the context of this analysis. However, this work is beyond the scope of the present effort.

LIST OF REFERENCES

1. Wu, Hsi-Yung T. and Springer, G.S., "Impact Induced Stresses, Strains, and Delaminations", _Journal of Composite Materials_, Vol. 22, No. 6 (June 1988), pp. 533-560.

2. Jortner, J., "Effects of Weave Geometry and Yarn Waviness on Thermomechanical Properties of Multi-Directional Composites", 3-D Composite Materials, _NASA Conference Publication 2420_, (1986), pp 53-73.

3. Harris, Charles E. and Lee, Jong-Won, "A Micromechanics Model of the Stiffness and Strength of Laminates With Fiber Waviness", _NASA Contractor Report 181670_ (July 1988).

4. Kriz, R.D., "Influence of Damage on Mechanical Properties of Woven Composites at Low Temperatures", _Journal of Composites Technology & Research_, Vol. 7, No. 2 (Summer 1985), pp 55-58.

5. Ishikawa, T. and Chou, Tsu-Wei, "Elastic Behavior of Woven Hybrid Composites", _Journal of Composite Materials_, Vol 16 (January 1982), pp. 2-19.

6. Ishikawa, T. and Chou, Tsu-Wei, "Thermoelastic Analysis of Hybrid Fabric Composites" _Journal of Composite Materials Sciences_, Vol. 18 (1983), pp. 2260-2268.

7. Ishikawa, T. and Chou, Tsu-Wei, "Nonlinear Behavior of Woven Fabric Composites", _Journal of Composite Materials_, Vol 17 (September 1983), pp. 399-413.

8. Ishikawa, Takashi, "Anti-Symmetric Elastic Properties of Composite Plates of Satin Weave Cloth", _Fiber Sciences and Technology_, Vol 15 (1981), pp. 127-145.

9. Ishikawa, T. and Chou, T.W., "Stiffness and Strength Behavior of Woven Fabric Composites", _Journal of Materials Science_, Vol. 17 (1982), pp. 3211-3220.

10. Ko, Frank K.,; Pastore, C.M.; Yang, J.M. and Chou, T.W., "Structure and Properties of Multilayer Multidirectional Warp Knit Fabric Reinforced Composites", _Composites 86: Recent Advances in Japan and the United States_, Proc. Japan-U.S. CCM-III, Tokyo, 1986.

11. Chou, Tsu-Wei, "Modeling and Characterization of Three-Dimensional Braided Metal-Matrix Composites", 3-D Composite Materials, _NASA Conference Publication 2420_, (1986), pp. 31-52.

12. Dow, Norris F. and Ramnath, V., "Analysis of Woven Fabrics for Reinforced Composite Materials", _NASA Contractor Report 178275_ (1987).

13. Mai, H. Ulv, "A Soft Mosaic Theory for Elastic and Strength Properties of Hybrid Woven Composites", _DFVLR Report B435-85/20_ (1985).

14. Whitney, Thomas J.; Chou, Tsu-Wei; Taske, Leo and Majidi, Azar P., "Performance Maps of 3-D Textile Structural Composites", Fiber-Tex 1987, _NASA Conference Publication 3001_ (1988), pp. 153-168.

15. Bathe, Klaus-Jurgen, _"Finite Element Procedures in Engineering Analysis"_, Prentice-Hall, Inc., Englewood Cliffs, New Jersey 07632 (1982).

16. Wilson, E.L.; Taylor, R.L.; Doherty, W. and Ghaboussi, "Incompatible Displacement Models", _Numerical and Computer Methods in Structural Mechanics_, Academic Press, Inc., New York, N.Y. (1973).

17.   Taylor, Robert L.,; Beresford, Peter J. and Wilson, Edward L., "A Non-Conforming Element for Stress Analysis", _International Journal for Numerical Methods in Engineering_, Vol. 10 (1976), pp. 1211-1219.

18.   Davidson, D.A., "The Mechanical Behavior of Fabrics Subjected to Biaxial Stress: Channel Model Theory of Plain Weave" _Air Force Materials Lab. Technical Documentary Report No. MD-TDR-64-23_, (July 1964).

19.   Coquill, Scott L. and Adams, Donald F., "Mechanical Properties of Several Neat Polymer Matrix Materials and Unidirectional Carbon Fiber-Reinforced Composites", _NASA Contractor Report 181805_ (April 1989).

20.   Masters, John E.; Foye, Raymond L., Pastore,Christopher M.; and Gowayed, Yasser A. "Mechanical Properties of Triaxially Braided Composites: Experimental and Analytical Results", _Ninth DOD,NASA,FAA Conference on Fibrous Composites in Structural Design_, Lake Tahoe, NV (November 1991).

21.   Epting, James and Whitney, James, "An Investigation of the Reliability of a Mathematical Model Which Describes Knitted Fabrics Subjected to Biaxial Stresses", _Air Force Materials Lab. Technical Documentary Repot. No. ASD-TDR-63-450_, (June 1963).

| | CORNER NODE LOCATION (x,y,z) | | | | | | | | | | | | | | | | | | | | | | |
| (x,y,z) = | (0,0,0) | | | (0,0,C) | | | (0,B,0) | | | (0,B,C) | | | (A,0,0) | | | (A,0,C) | | | (A,B,0) | | | (A,B,C) | | |
UNIT STRAIN CASE	U	V	W	U	V	W	U	V	W	U	V	W	U	V	W	U	V	W	U	V	W	U	V	W
(1) $\bar{\varepsilon}_{xx} = 1$	O	O	O	O	O	O	O	O	O	O	O	O	A	O	O	A	O	O	A	O	O	A	O	O
(2) $\bar{\varepsilon}_{yy} = 1$	O	O	O	O	O	O	O	B	O	O	B	O	O	O	O	O	O	O	O	B	O	O	B	O
(3) $\bar{\varepsilon}_{zz} = 1$	O	O	O	O	O	C	O	O	O	O	O	C	O	O	O	O	O	C	O	O	O	O	O	C
(4) $\bar{\tau}_{yz} = 1$	O	O	O	O	C	O	O	O	O	O	C	O	O	O	O	O	C	O	O	O	O	O	C	O
(5) $\bar{\tau}_{xz} = 1$	O	O	O	C	O	O	O	O	O	C	O	O	O	O	O	C	O	O	O	O	O	C	O	O
(6) $\bar{\tau}_{xy} = 1$	O	O	O	O	O	O	B	O	O	B	O	O	O	O	O	O	O	O	B	O	O	B	O	O

TABLE 1: UNIT CELL CORNER DISPLACEMENTS FOR UNIT STRAIN CASES

INTEGRATION POINT (Fig.25)	ϕ_1 (Fig.11)	ϕ_2 (Fig. 11)	V_i (i = 1-8)								MATL. NO.
			i=1 (+++)	i=2 (++-)	i=3 (++)	i=4 (+--)	i=5 (-++)	i=6 (-+-)	i=7 (--+)	i=8 (---)	
1	90	10	0.04	–	–	–	–	–	–	–	1
2	90	10	–	0.21	0	–	–	–	–	–	1
3	90	10	–	–	–	–	–	–	–	–	1
4	90	10	–	–	–	0.25	–	–	–	–	1
5	90	10	–	–	–	–	0.25	–	–	–	1
6	90	10	–	–	–	–	–	0.50	–	–	1
7	90	10	–	–	–	–	–	–	0.04	–	1
8	90	10	–	–	–	–	–	–	–	0.71	1
1	0	-10	0.21	–	–	–	–	–	–	–	2
2	0	-10	–	0.04	0.50	–	–	–	–	–	2
3	0	-10	–	–	–	–	–	–	–	–	2
4	0	-10	–	–	–	0.25	–	–	–	–	2
5	0	-10	–	–	–	–	0.25	–	–	–	2
6	0	-10	–	–	–	–	–	0	–	–	2
7	0	-10	–	–	–	–	–	–	0.71	–	2
8	0	-10	–	–	–	–	–	–	–	0.04	2
1	0	0	0.75	–	–	–	–	–	–	–	3
2	0	0	–	0.75	0.50	–	–	–	–	–	3
3	0	0	–	–	–	–	–	–	–	–	3
4	0	0	–	–	–	0.50	–	–	–	–	3
5	0	0	–	–	–	–	0.50	–	–	–	3
6	0	0	–	–	–	–	–	0.50	–	–	3
7	0	0	–	–	–	–	–	–	0.25	–	3
8	0	0	–	–	–	–	–	–	–	0.25	3

TABLE 2: DIAMOND CROSS-SECTION PLAIN WEAVE INPUT DATA

56

INTEGRATION POINT (Fig. 9)	ϕ_1 (Fig.11)	ϕ_2 (Fig. 11)	υ_i (i = 1 - 8)								MATL. NO.
			i=1 (+++)	i=2 (++-)	i=3 (+-+)	i=4 (+--)	i=5 (-++)	i=6 (-+-)	i=7 (--+)	i=8 (---)	
1	90	0	0.70	-	-	-	-	-	-	-	1
2	90	0	-	0	-	-	-	-	-	-	1
3	90	6	-	-	0.45	-	-	-	-	-	1
4	90	6	-	-	-	0.24	-	-	-	-	1
5	90	0	-	-	-	-	1.00	-	-	-	1
6	90	0	-	-	-	-	-	0	-	-	1
7	90	6	-	-	-	-	-	-	0.86	-	1
8	90	6	-	-	-	-	-	-	-	0.16	1
1	0	6	0.16	-	-	-	-	-	-	-	2
2	0	6	-	0.86	-	-	-	-	-	-	2
3	0	6	-	-	0.24	-	-	-	-	-	2
4	0	6	-	-	-	0.45	-	-	-	-	2
5	0	0	-	-	-	-	0	-	-	-	2
6	0	0	-	-	-	-	-	1.00	-	-	2
7	0	0	-	-	-	-	-	-	0	-	2
8	0	0	-	-	-	-	-	-	-	0.70	2
1	0	0	0.14	-	-	-	-	-	-	-	3
2	0	0	-	0.14	-	-	-	-	-	-	3
3	0	0	-	-	0.31	-	-	-	-	-	3
4	0	0	-	-	-	0.31	-	-	-	-	3
5	0	0	-	-	-	-	0	-	-	-	3
6	0	0	-	-	-	-	-	0	-	-	3
7	0	0	-	-	-	-	-	-	0.14	-	3
8	0	0	-	-	-	-	-	-	-	0.14	3

TABLE 3: PLAIN WEAVE INPUT DATA FROM PHOTOMICROGRAPHS

WEAVE	E_x* (msi)	E_y** (msi)	E_z*** (msi)	G_{yz} (msi)	G_{xz} (msi)	G_{xy} (msi)	ν_{yz}	ν_{xz}	ν_{xy}
Plain	9.25 (9.13)	9.25 (8.83)	1.65 (N.A.)	0.72 (N.A.)	0.72 (N.A.)	0.70 (N.A.)	0.33 (N.A.)	0.33 (N.A.)	0.03 (0.11)
Oxford	9.33 (9.63)	9.55 (9.68)	1.65 (N.A.)	0.72 (N.A.)	0.73 (N.A.)	0.70 (0.77)	0.34 (N.A.)	0.35 (N.A.)	0.04 (0.06)
5 Harness Satin	9.57 (10.05)	9.57 (10.09)	1.65 (N.A.)	0.73 (N.A.)	0.73 (N.A.)	0.72 (0.76)	0.32 (N.A.)	0.32 (N.A.)	0.03 (0.06)
8 Harness Satin	9.68 (10.59)	9.68 (10.35)	1.66 (N.A.)	0.73 (N.A.)	0.73 (N.A.)	0.72 (0.98)	0.32 (N.A.)	0.32 (N.A.)	0.03 (0.06)

58

x,y plane is the plane of the fabric

*   Warp Direction
**   Fill Direction
***   Thickness Direction

( )   Experimental Data
(N.A.) Not Available

Table 4:   WOVEN FABRIC RESULTS

INTEGRATION POINT	ϕ_1 (Fig.11)	ϕ_2 (Fig. 11)	υ_i (i = 1-8)							
			i=1 (+++)	i=2 (++-)	i=3 (+-+)	i=4 (+--)	i=5 (-++)	i=6 (-+-)	i=7 (--+)	i=8 (---)
1	-45	0	-	-	-	-	-	-	-	-
2	-45	0	-	1.0	-	-	-	-	-	-
3	-45	3	-	-	-	-	-	-	-	-
4	-45	3	-	0.8	-	0.9	-	-	-	-
5	-45	-6	-	-	0.4	-	-	-	-	-
6	-45	6	-	-	-	0.4	-	-	-	-
7	-45	-3	-	-	-	-	-	-	-	-
8	-45	-3	-	0.8	-	-	-	0.9	-	-
9	-45	0	0.3	-	0.2	-	0.2	-	-	-
10	-45	0	-	-	-	0.2	-	0.2	-	0.3
11	-45	-3	-	-	0.9	-	-	-	0.8	-
12	-45	-3	-	-	-	-	-	-	-	-
13	-45	6	-	-	-	-	0.4	-	-	-
14	-45	-6	-	-	-	-	-	0.4	-	-
15	-45	3	-	-	-	-	0.9	-	0.8	-
16	-45	3	-	-	-	-	-	-	-	-
17	-45	0	-	-	-	-	-	-	1.0	-
18	-45	0	-	-	-	-	-	-	-	-
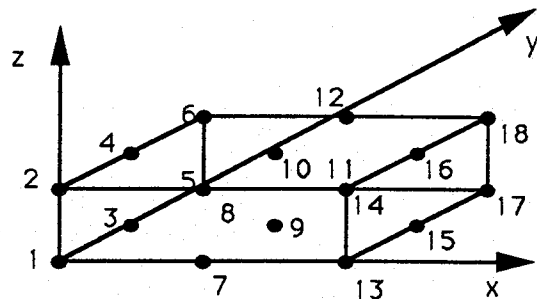
Integration Points
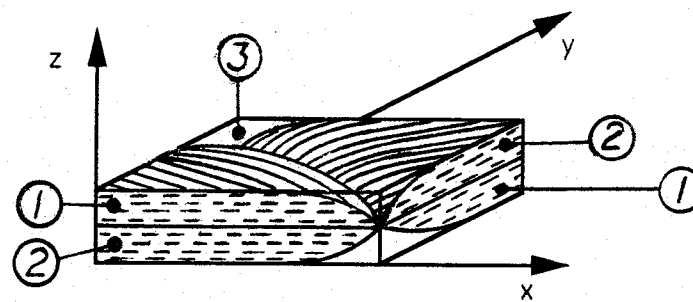
Subcell

TABLE 5A: BRAID INPUT DATA (MATERIAL 1)

INTEGRATION POINT	φ1 (Fig.11)	φ2 (Fig. 11)	V_i (i = 1–8) i=1 (+++)	i=2 (++-)	i=3 (+-+)	i=4 (+--)	i=5 (-++)	i=6 (-+-)	i=7 (--+)	i=8 (---)
1	45	0	1.0	–	–	–	–	–	–	–
2	45	0	–	–	–	–	–	–	–	–
3	45	3	0.9	0.1	1.0	–	–	–	–	–
4	45	3	–	–	0.2	0.1	–	–	–	–
5	45	6	–	–	–	0.2	–	–	–	–
6	45	6	0.9	0.1	–	–	–	–	–	–
7	45	3	–	–	–	0.4	1.0	0.1	–	–
8	45	3	0.5	0.7	0.4	0.4	–	–	–	–
9	45	6	–	–	–	–	0.4	0.4	0.7	0.5
10	45	6	–	–	–	1.0	–	–	0.1	0.9
11	45	3	–	–	0.1	–	–	–	–	–
12	45	3	–	–	–	–	0.2	–	0.1	–
13	45	6	–	–	–	–	0.2	0.2	–	0.9
14	45	6	–	–	–	–	–	0.2	–	–
15	45	3	–	–	–	–	0.1	–	0.1	–
16	45	3	–	–	–	–	–	1.0	–	0.9
17	45	0	–	–	–	–	–	–	–	–
18	45	0	–	–	–	–	–	–	–	1.0

TABLE 5B: BRAID INPUT DATA (MATERIAL 2)

60

INTEGRATION POINT	ϕ_1 (Fig.11)	ϕ_2 (Fig. 11)	V_i (i = 1-8)							
			i=1 (+++)	i=2 (++-)	i=3 (++-+)	i=4 (+--)	i=5 (-++)	i=6 (-+-)	i=7 (--+)	i=8 (---)
1	0	0	—	—	—	—	—	—	—	—
2	0	0	0.1	—	—	—	—	—	—	—
3	0	0	—	0.1	—	—	—	—	—	—
4	0	0	—	—	0.4	0.4	—	—	—	—
5	0	0	0.1	—	—	—	0.4	—	—	—
6	0	0	—	0.1	—	—	—	—	—	—
7	0	0	0.2	0.3	0.4	0.4	—	—	—	—
8	0	0	—	—	—	—	0.4	0.4	0.3	0.2
9	0	0	—	—	—	—	—	—	—	—
10	0	0	—	—	—	—	0.4	—	0.1	0.1
11	0	0	—	—	—	—	—	—	—	—
12	0	0	—	—	—	—	—	0.4	—	—
13	0	0	—	—	—	—	—	—	0.1	—
14	0	0	—	—	—	—	—	—	—	0.1
15	0	0	—	—	—	—	—	—	—	—
16	0	0	—	—	—	—	—	—	—	—
17	0	0	—	—	—	—	—	—	—	—
18	0	0	—	—	—	—	—	—	—	—

TABLE 5C: BRAID INPUT DATA (MATERIAL 3)

61

INTEGRATION POINT (Fig.36B)	ϕ_1 (Fig.11)	ϕ_2 (Fig. 11)	V_i (i = 1 - 8)								MATL. NO.
			i=1 (+++)	i=2 (++-)	i=3 (+-+)	i=4 (+--)	i=5 (-++)	i=6 (-+-)	i=7 (--+)	i=8 (---)	
1	120	0	0.0	-	-	-	-	-	-	-	1
2	120	0	-	0.3	-	-	-	-	-	-	1
3	120	-20	-	-	0.2	-	-	-	-	-	1
4	120	-20	-	-	-	0.4	-	-	-	-	1
5	120	0	-	-	-	-	0.0	-	-	-	1
6	120	0	-	-	-	-	-	0.2	-	-	1
7	120	-20	-	-	-	-	-	-	0.0	-	1
8	120	-20	-	-	-	-	-	-	-	0.1	1
1	0	0	0.4	-	-	-	-	-	-	-	2
2	0	0	-	0.0	-	-	-	-	-	-	2
3	0	0	-	-	0.1	-	-	-	-	-	2
4	0	0	-	-	-	0.0	-	-	-	-	2
5	45	5	-	-	-	-	0.3	-	-	-	2
6	45	5	-	-	-	-	-	0.1	-	-	2
7	100	20	-	-	-	-	-	-	0.3	-	2
8	100	20	-	-	-	-	-	-	-	0.3	2
1	O	O	0.6	-	-	-	-	-	-	-	3
2	O	O	-	0.7	-	-	-	-	-	-	3
3	O	O	-	-	0.7	-	-	-	-	-	3
4	O	O	-	-	-	0.6	-	-	-	-	3
5	O	O	-	-	-	-	0.7	-	-	-	3
6	O	O	-	-	-	-	-	0.7	-	-	3
7	O	O	-	-	-	-	-	-	0.7	-	3
8	O	O	-	-	-	-	-	-	-	0.6	3

Integration Grid

TABLE 6:   JERSEY KNIT INPUT DATA

Subcell

62

Structural element — **Laminate element** — **Fabric element** — **Micromechanics element**
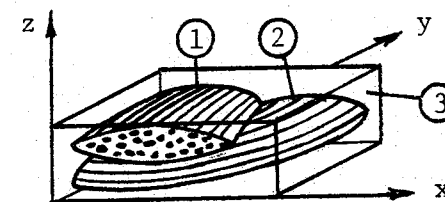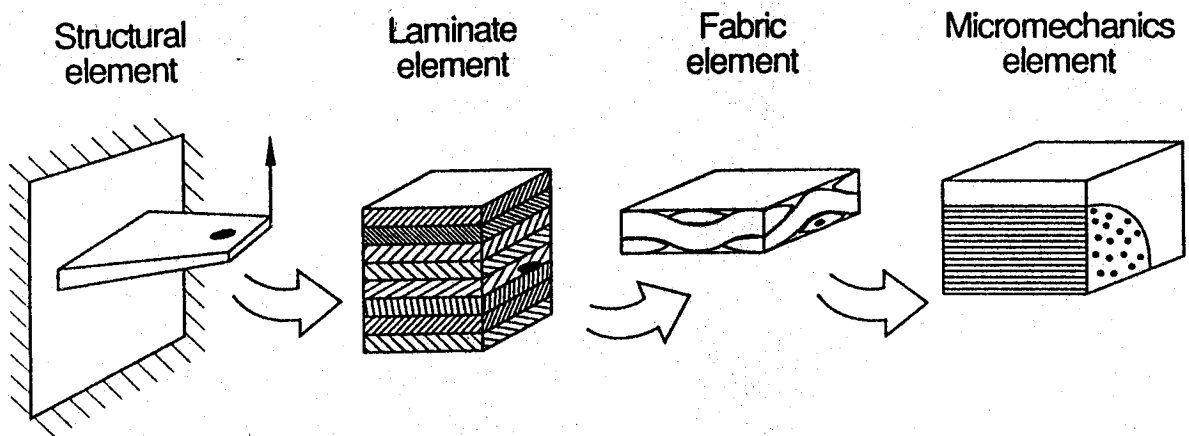
FIGURE 1: ROLE OF FABRIC MECHANICS IN COMPOSITE MECHANICS

Unit Cell

Subcells

I   II

Subcell Distribution
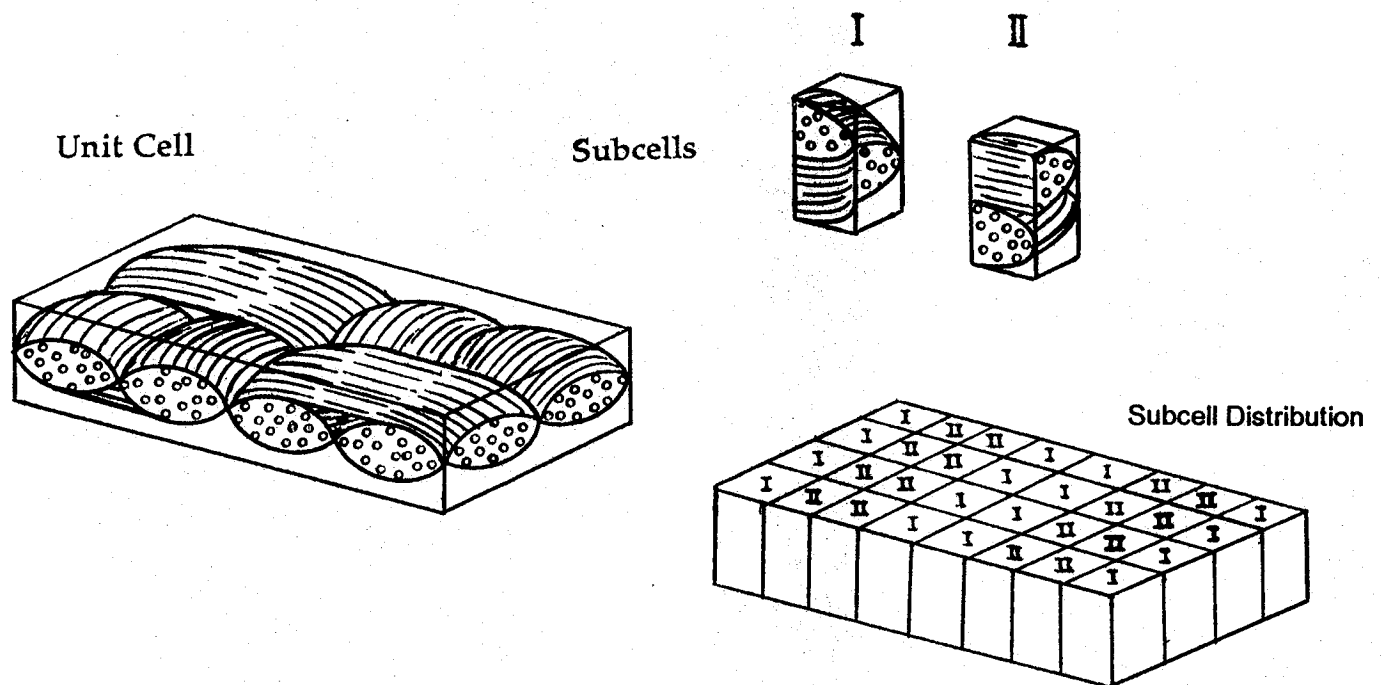
FIGURE 2: 2 x 2 RIB WEAVE MICROSTRUCTURE

63

Unit Cell
(A)

Design Plan
(B)
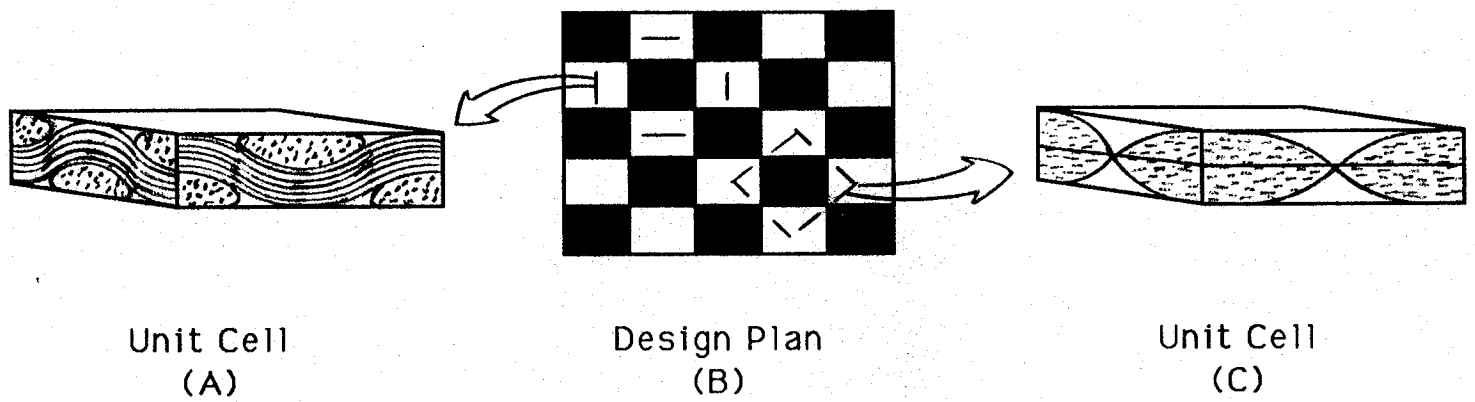
Unit Cell
(C)

FIGURE 3: PLAIN WEAVE DESIGN PLAN AND UNIT CELLS

Design Plan
(A)

Unit Cell
(B)
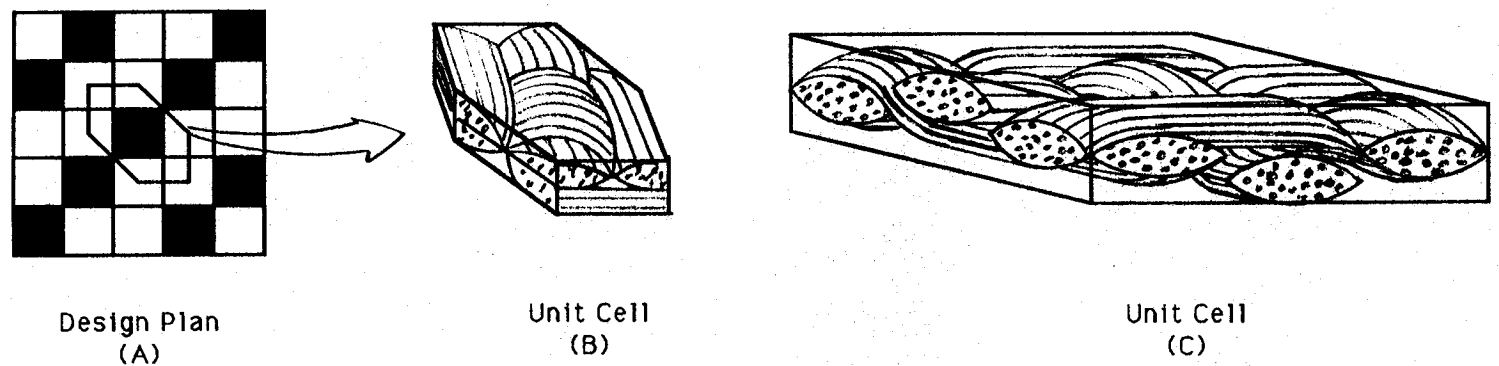
Unit Cell
(C)

FIGURE 4: TWILL WEAVE DESIGN PLAN AND UNIT CELL
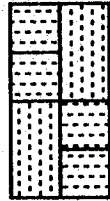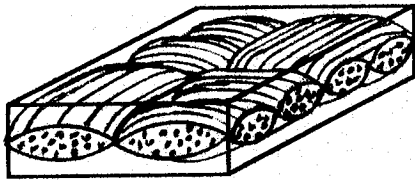
2 x 2 Warp Rib Weave
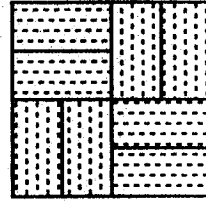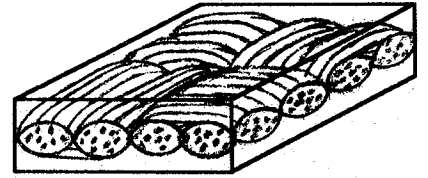
2 x2 Basket Weave
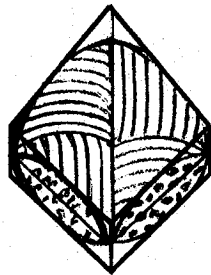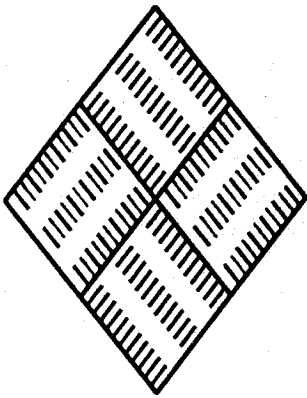
2-D Braid
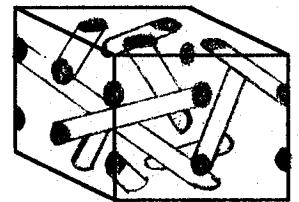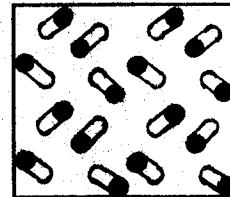
3-D Braid
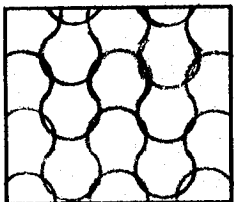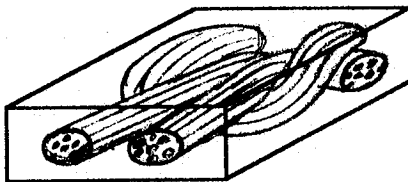
Jersey Knit
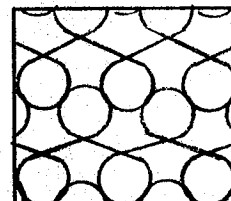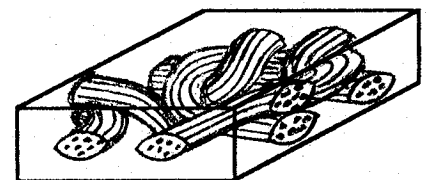
Tricot Knit

FIGURE 5: UNIT CELLS FOR WEAVES, BRAIDS, AND KNITS
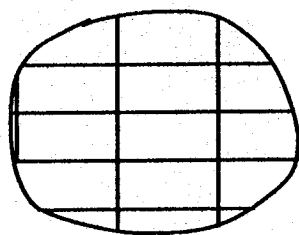
Stack Bond Brick
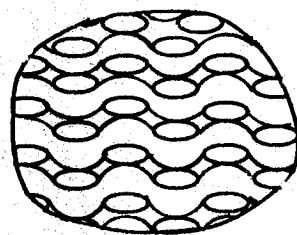
Plain Weave Stacking

FIGURE 6: UNIT CELL ARRAY
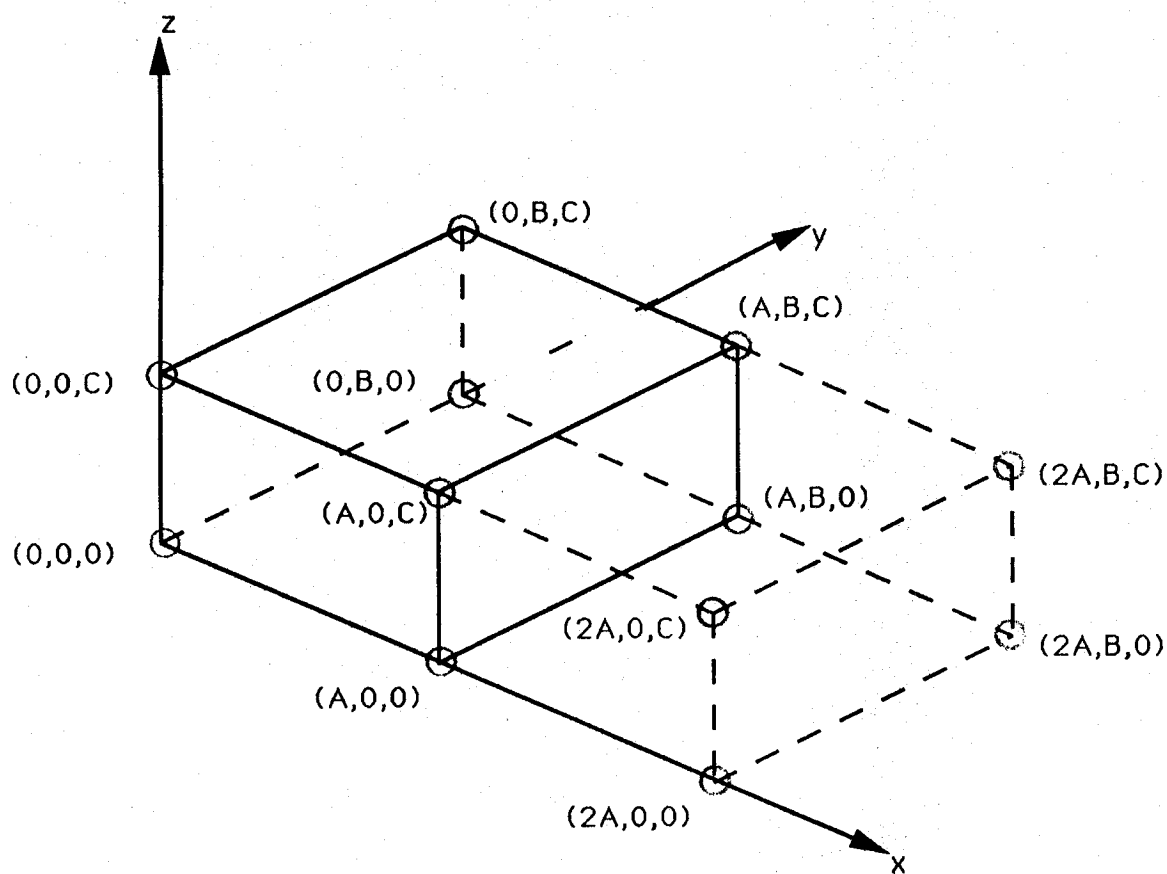
FIGURE 7: UNIT CELL CORNER DISPLACEMENT FOR STRAIN CASE (1) : $\bar{\bar{\varepsilon}}_{xx} = 1$

66
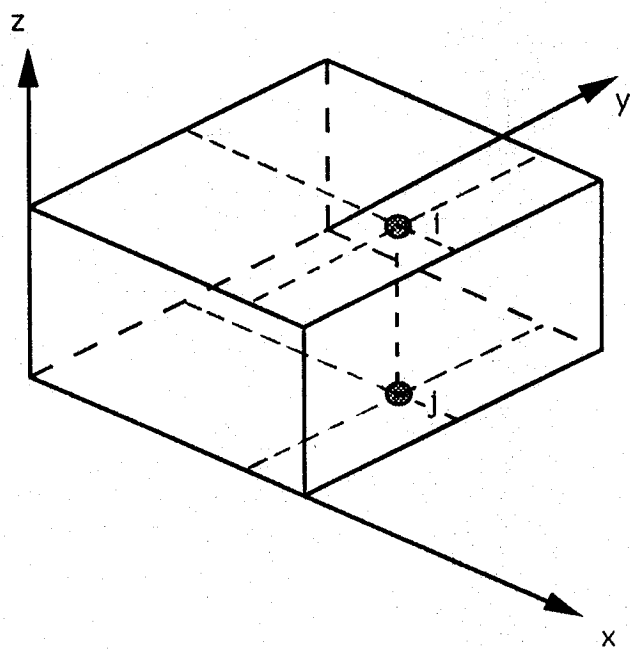
FIGURE 8: IMAGE POINTS ON UPPER AND LOWER SURFACE OF UNIT CELL

Material (3)

Material (2)

Material (1)

Subcell

z

y

x

Subcell Assembly

Unit Cell
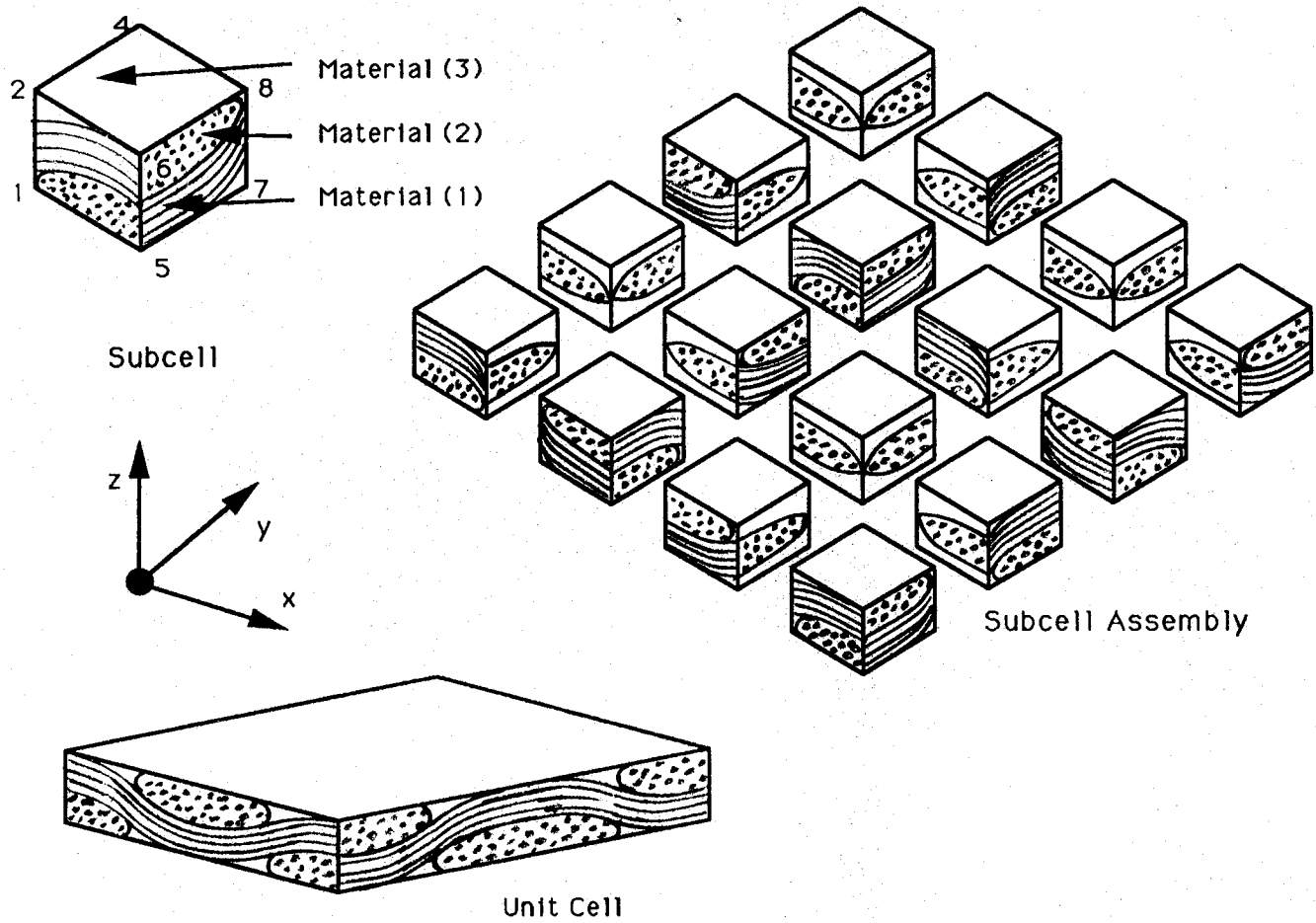
FIGURE 9: PLAIN WEAVE GEOMETRY

68
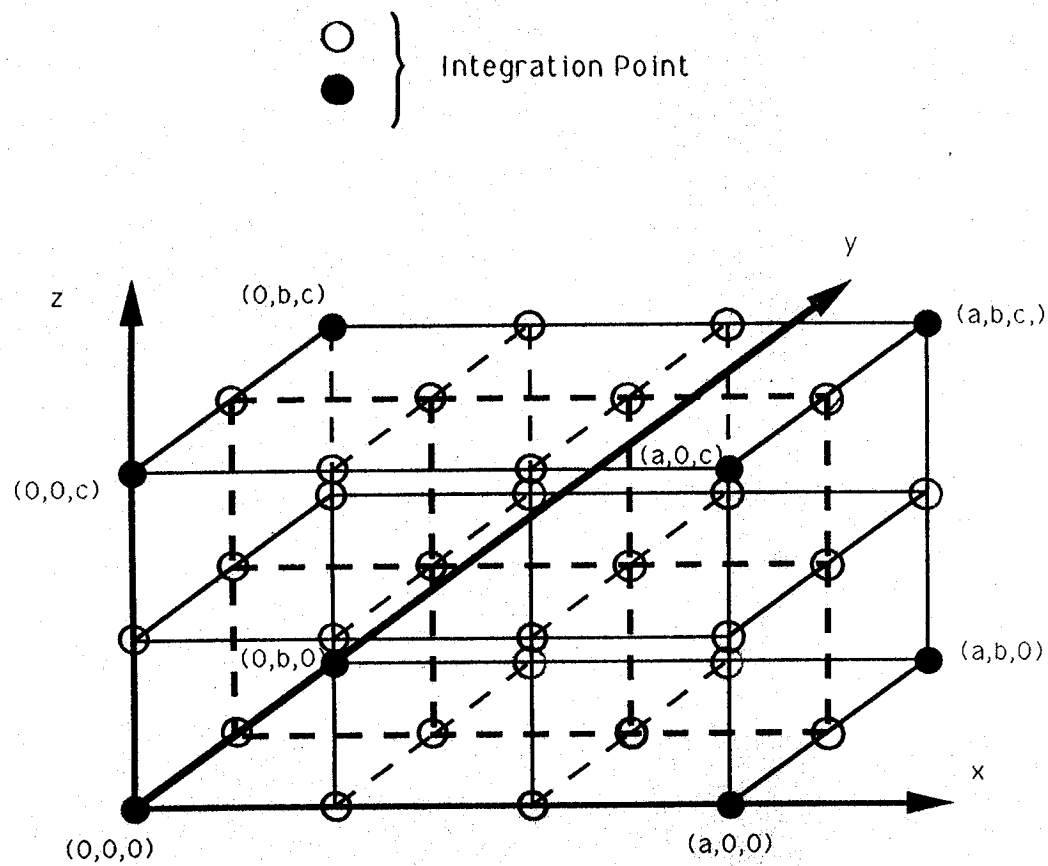
FIGURE 10: INTEGRATION NETWORK FOR THE SUBCELL
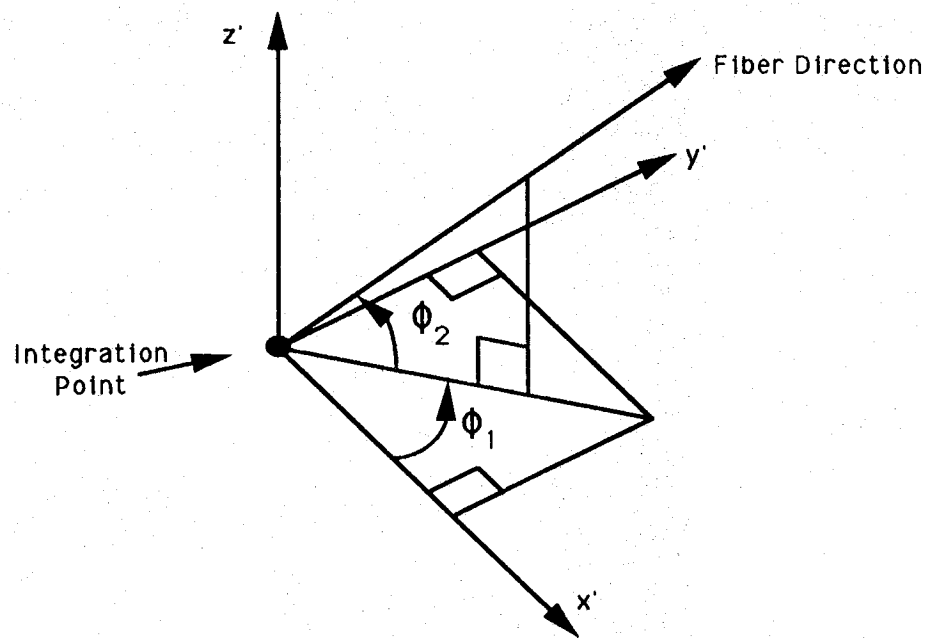
Parallel Local Coordinate System
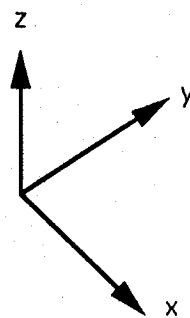
Global Coordinates of Integration

FIGURE 11: FIBER DIRECTION IN SPHERICAL COORDINATES   (Φ_1, Φ_2)
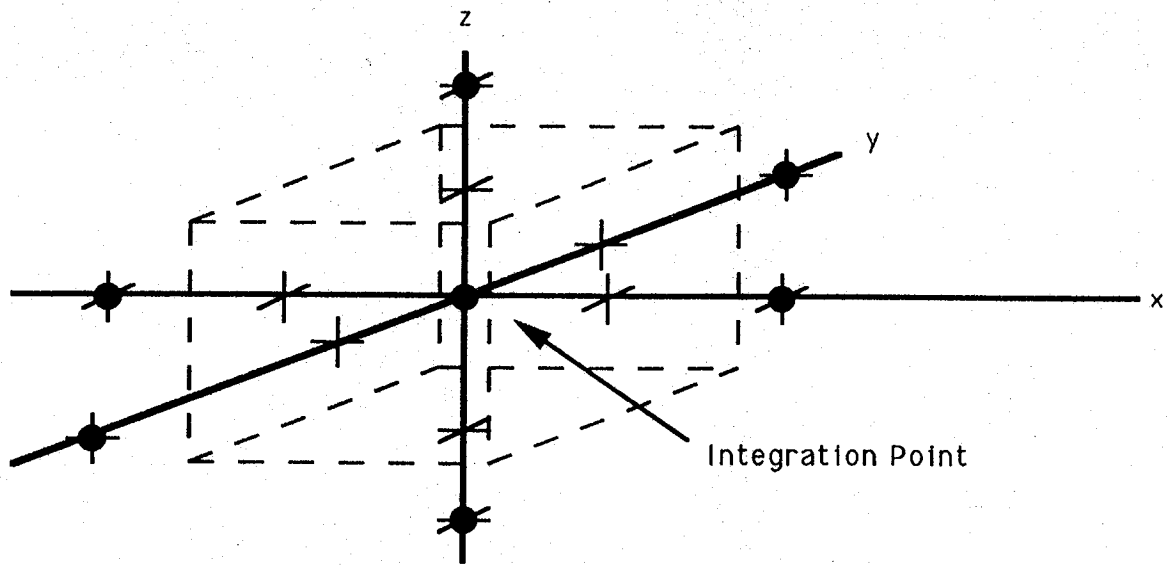
(A) Volume Associated with an Integration Point
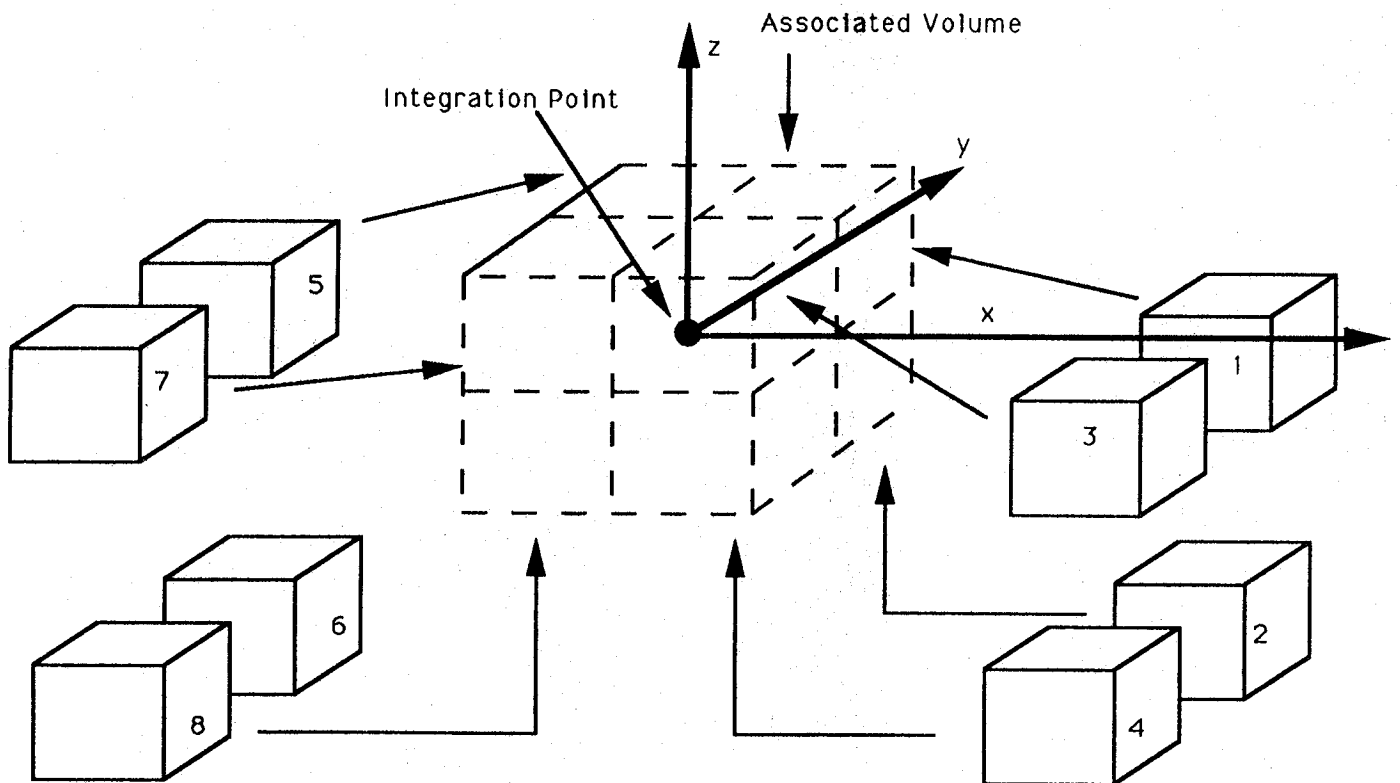
(B) Octants of Volume at an Integration Point

FIGURE 12: INTEGRATION GRID GEOMETRY DETAILS
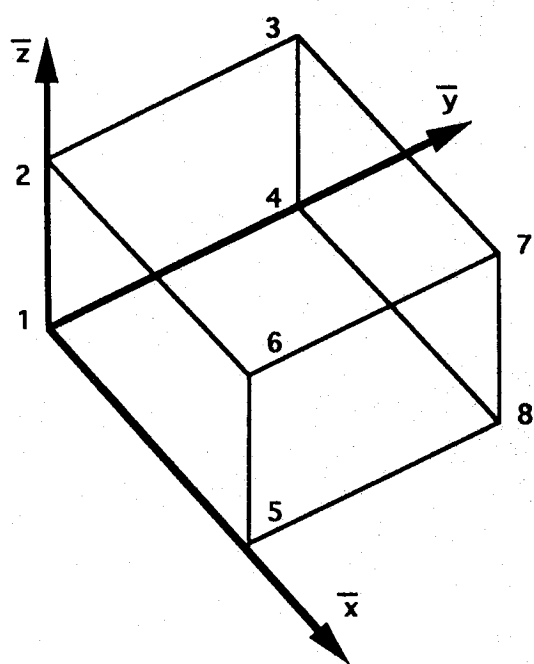
Transformation $\begin{cases} x = -\bar{x} \\ y = \bar{y} \\ z = \bar{z} \end{cases}$
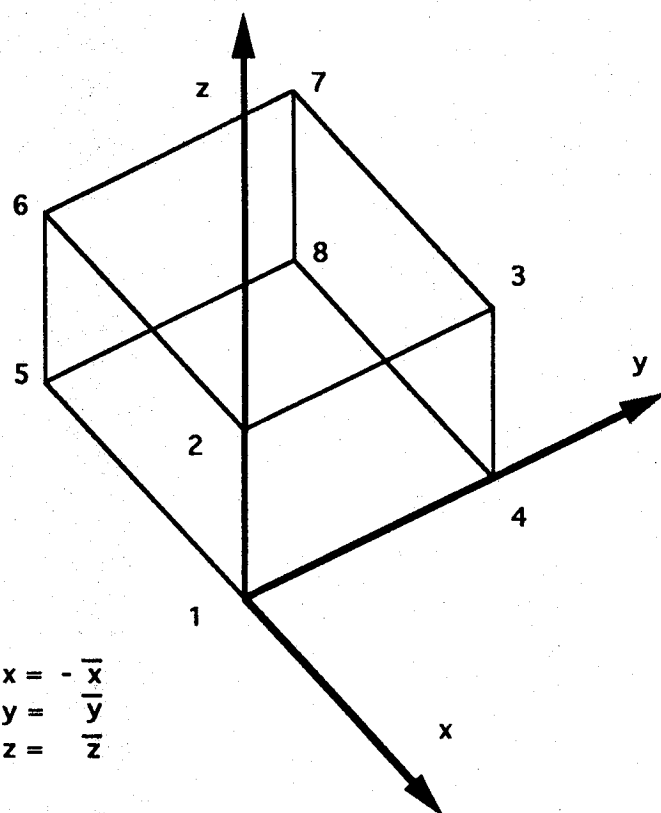
FIGURE 13: REFLECTION ABOUT THE $\bar{X}$ AXIS
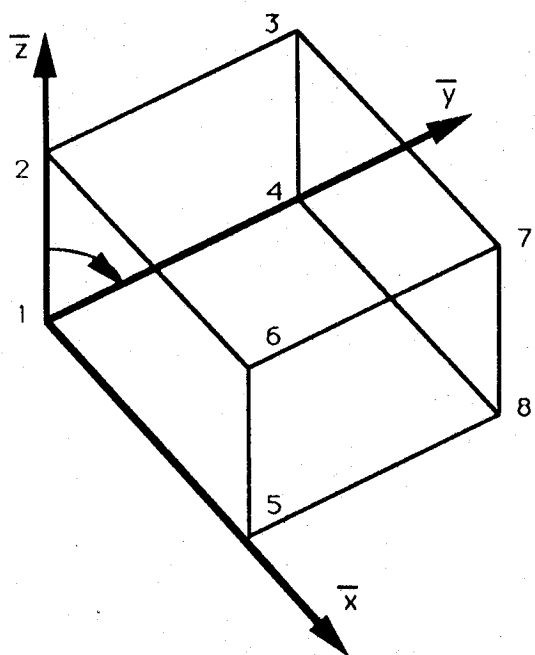
$$\text{Transformation} \begin{cases} x = \bar{x} \\ y = \bar{z} \\ z = -\bar{y} \end{cases}$$
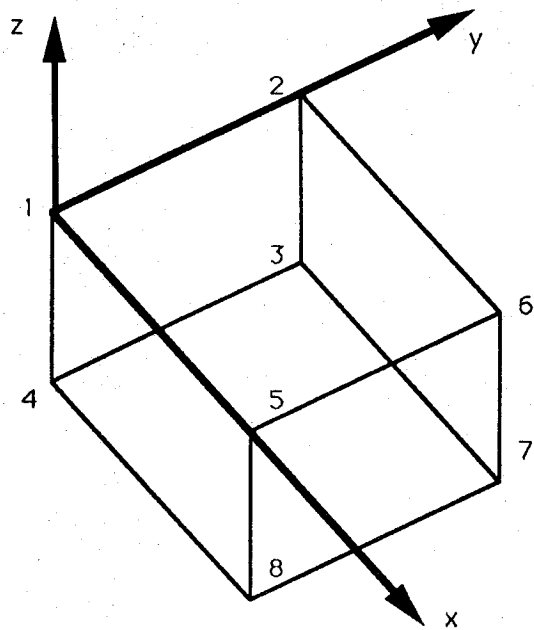
FIGURE 14: ROTATION OF 90° ABOUT THE $\bar{X}$ AXIS
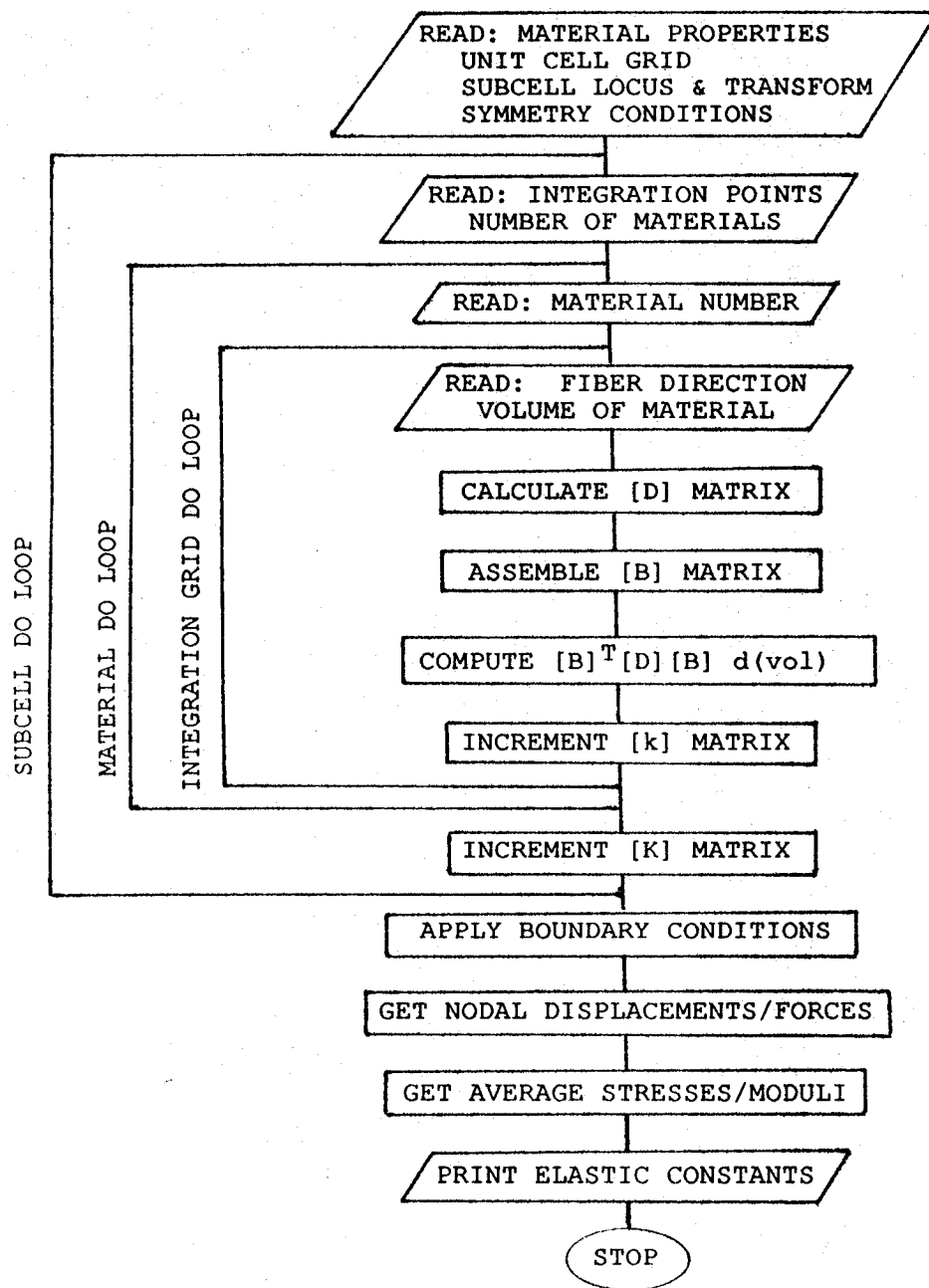
FIGURE 15: FLOW CHART FOR THE COMPUTER CODE

74
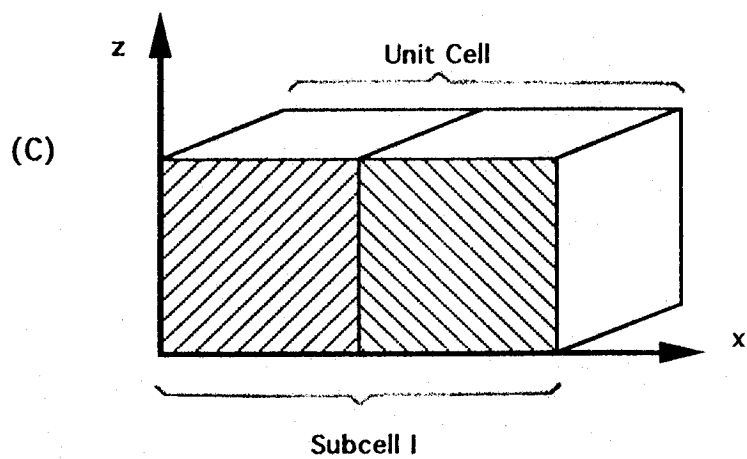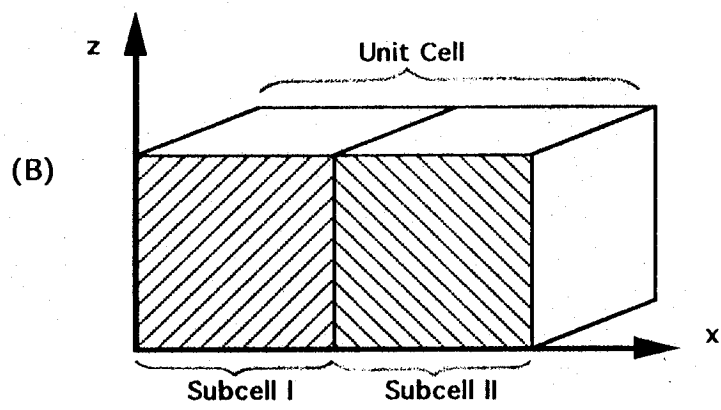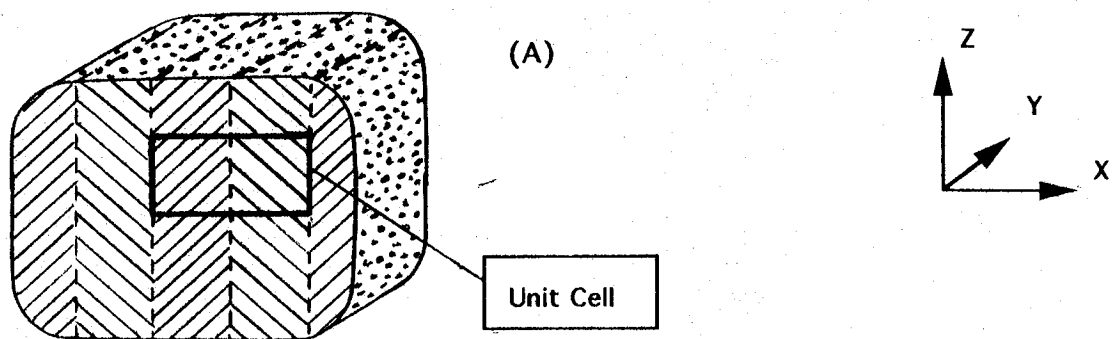
FIGURE 16: 2-D RICKRACK COMPOSITE GEOMETRY
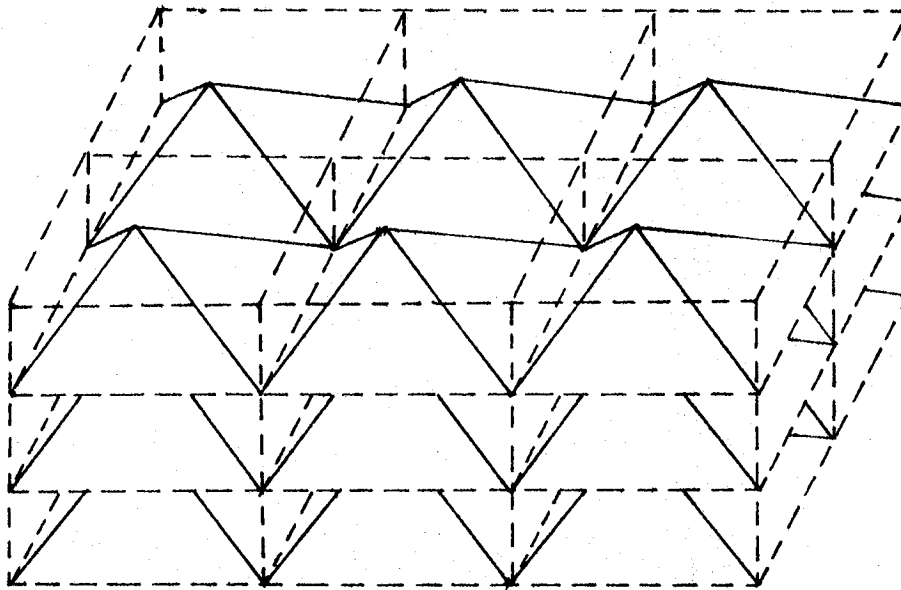
(A) Geometry
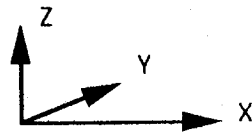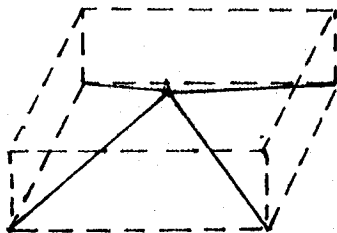
(B) Unit Cell   (C) Subcells
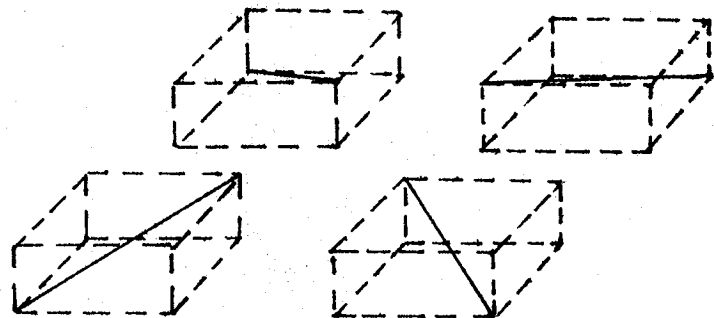
FIGURE 17: 3-D RICKRACK COMPOSITE GEOMETRY

2-D Subcell
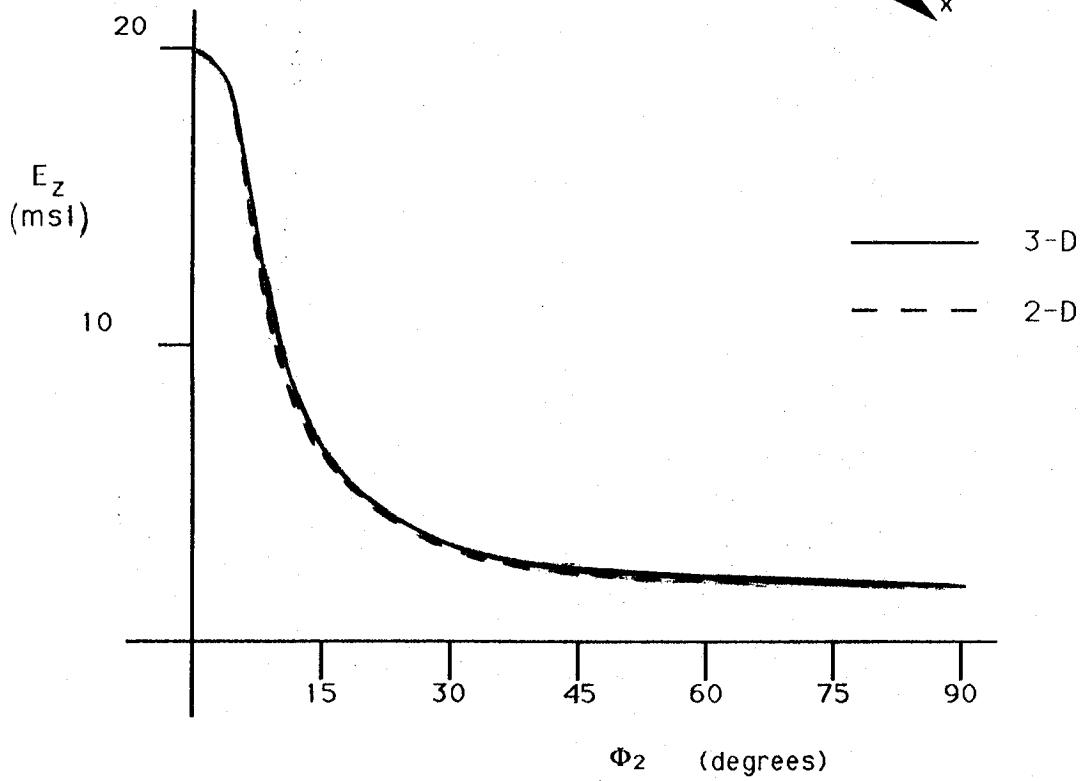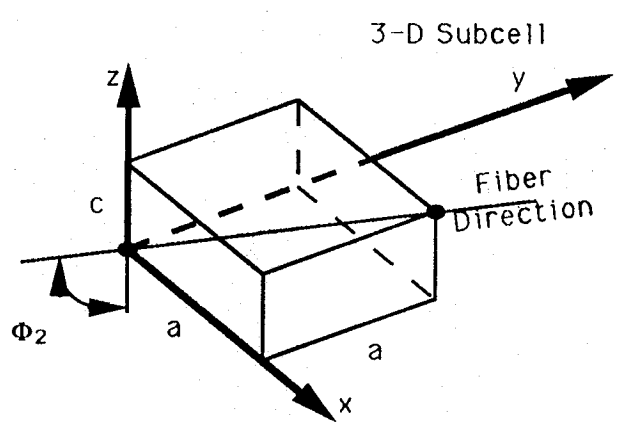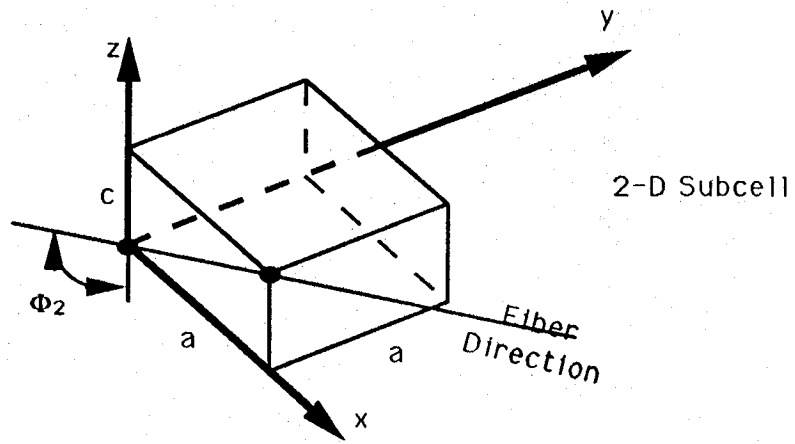
3-D Subcell

FIGURE 18: MODULUS OF RICKRACK COMPOSITE

(A) Void Geometry
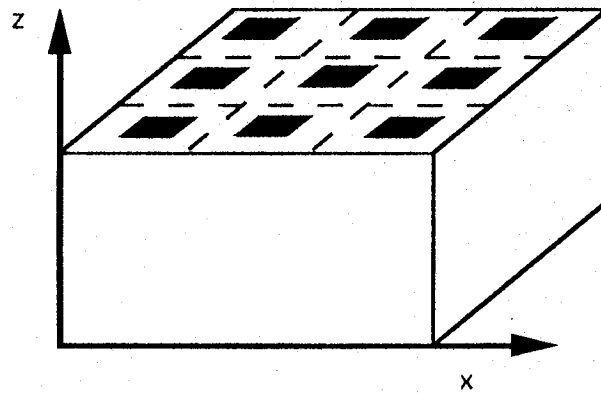
(B) Unit Cell
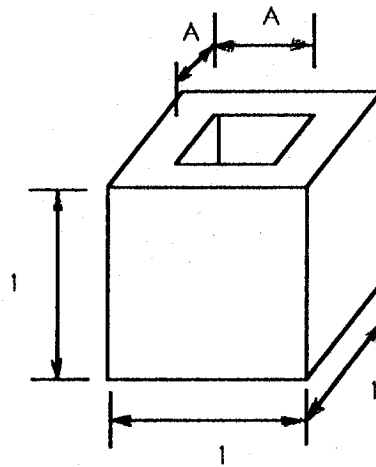
FIGURE 19: VOIDED MATERIAL
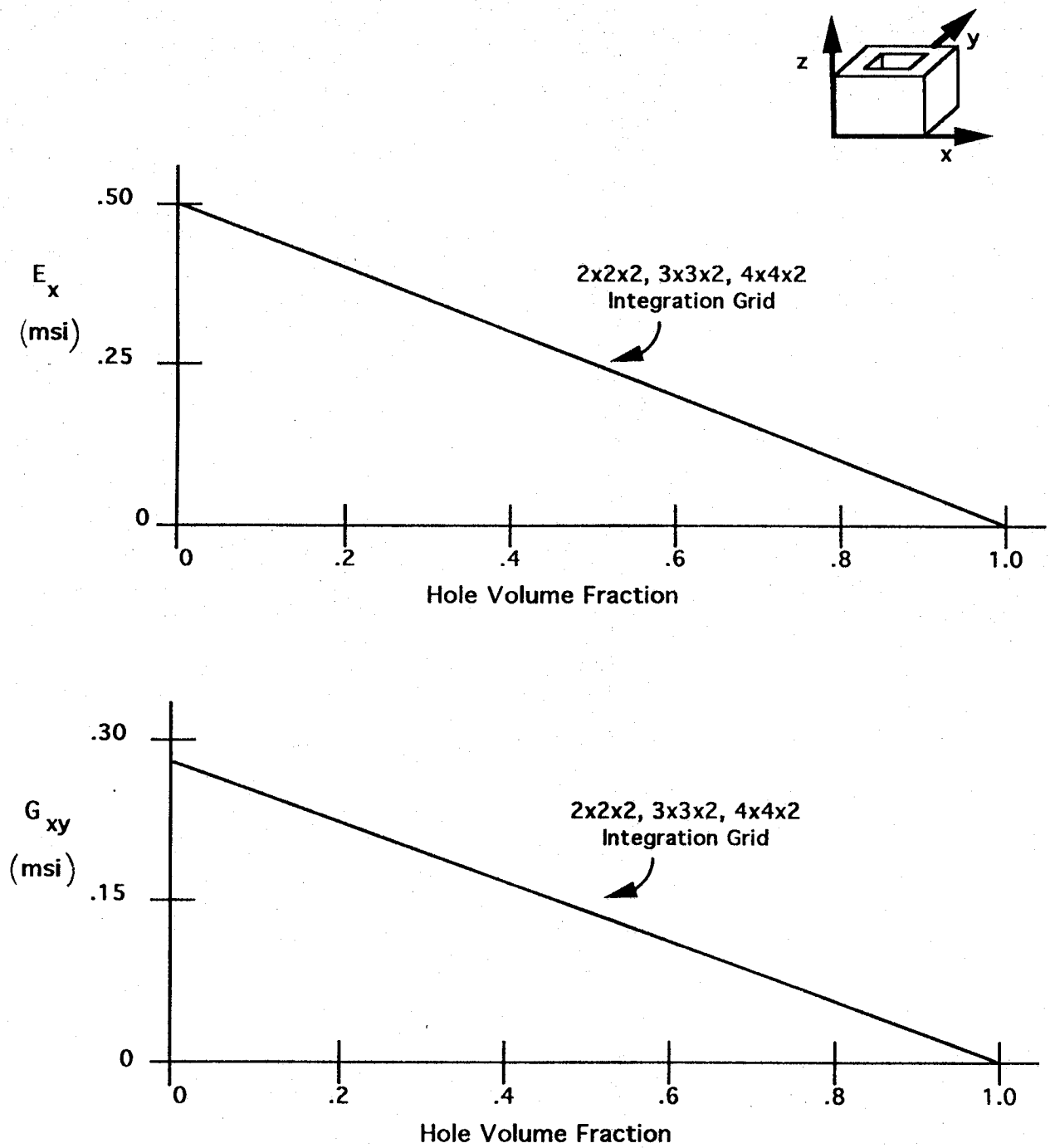
FIGURE 20: MODULI OF VOIDED MATERIAL BASED ON A SINGLE SUBCELL
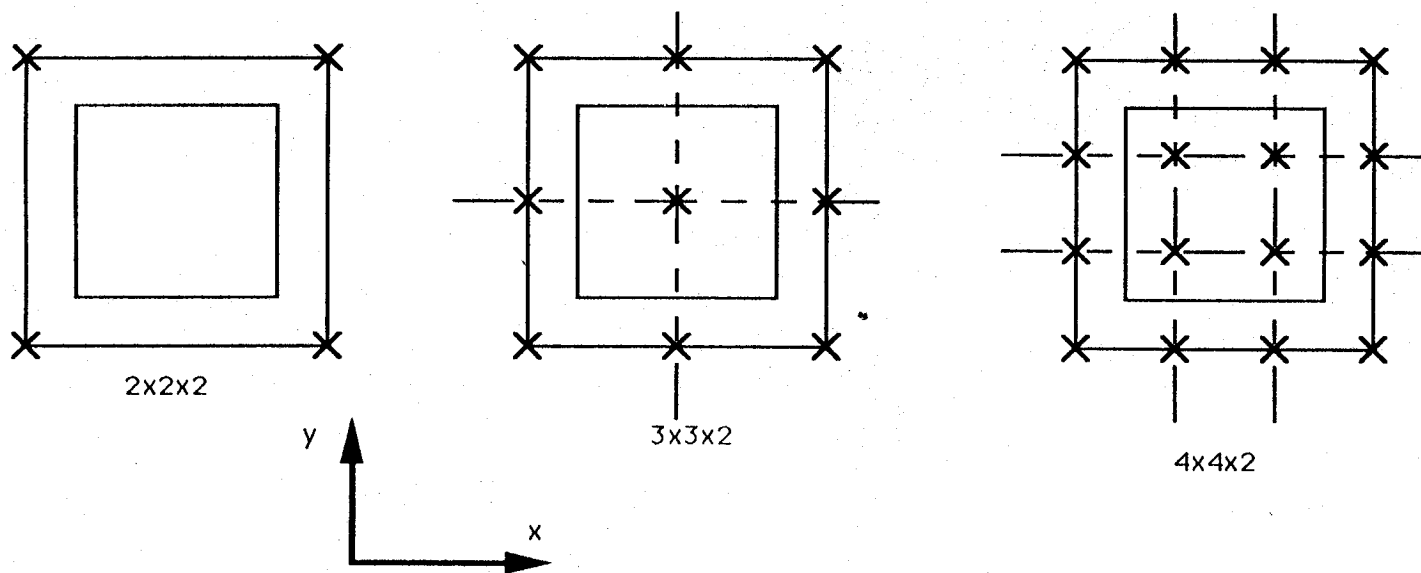
FIGURE 21: REFINING THE INTEGRATION GRID

2x2x2

3x3x2

4x4x2

(A) Unit Cell

(B) Subcells

I   II
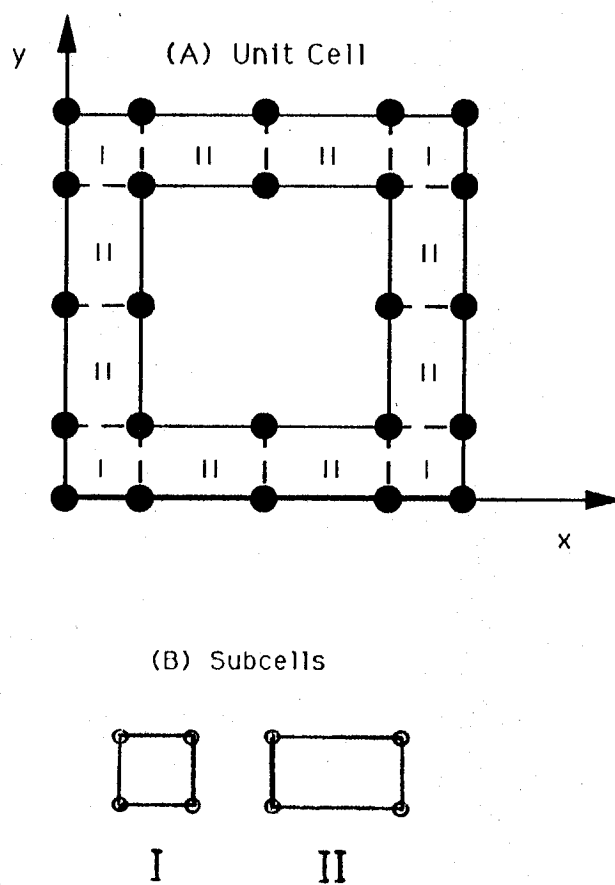
FIGURE 22: TWELVE SUBCELL MODEL
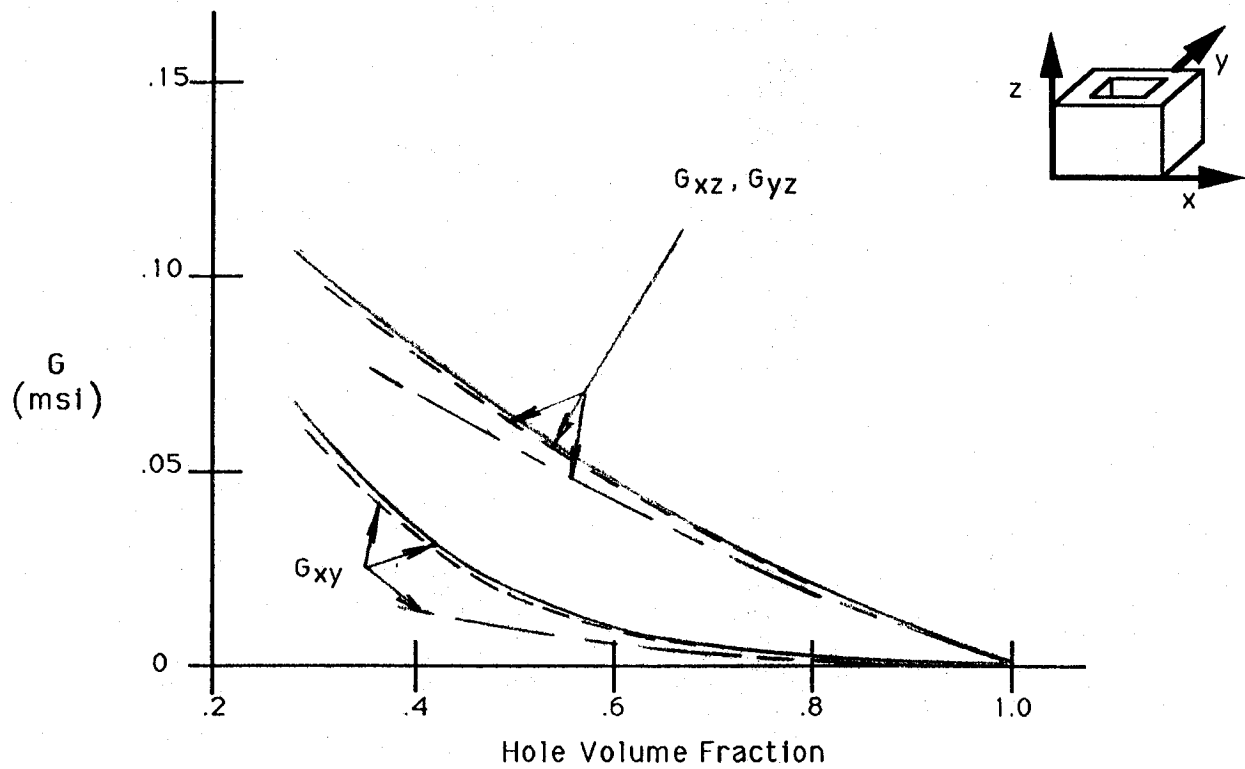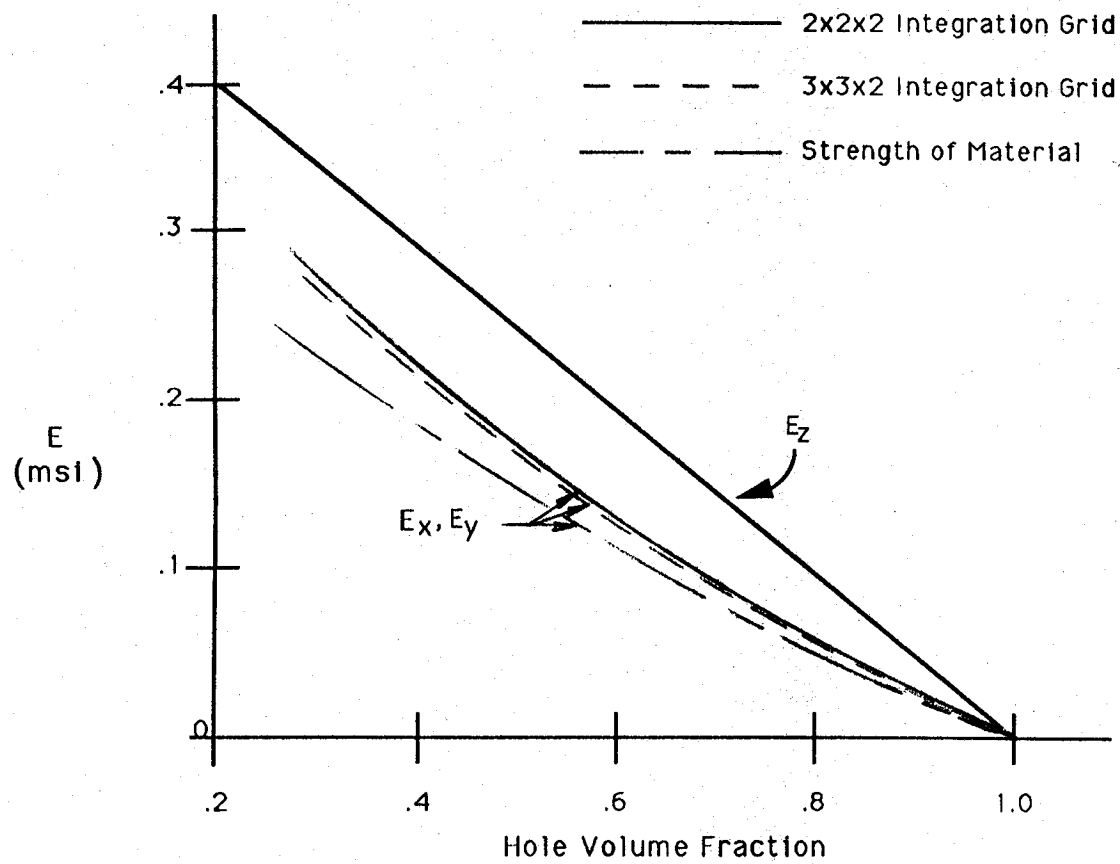
FIGURE 23: CELLULAR EPOXY MODULI
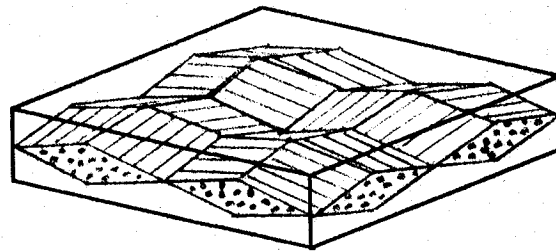
(A) Idealized Unit Cell
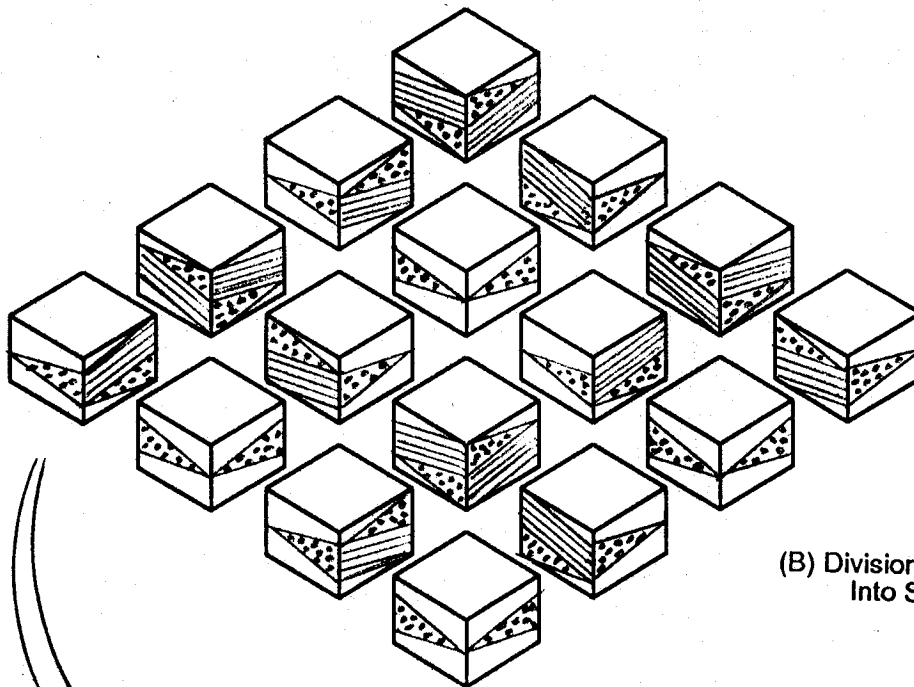
(B) Division of Unit Cell Into Subcells
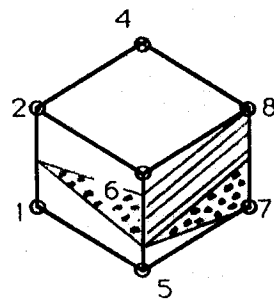
(C) Master Subcell

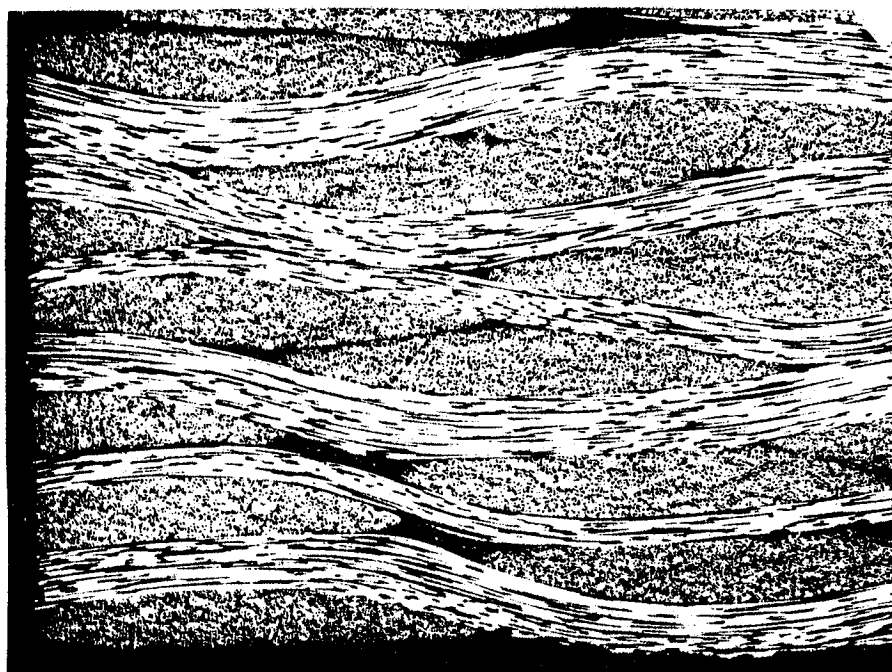FIGURE 24: IDEALIZED PLAIN WEAVE MODEL

82
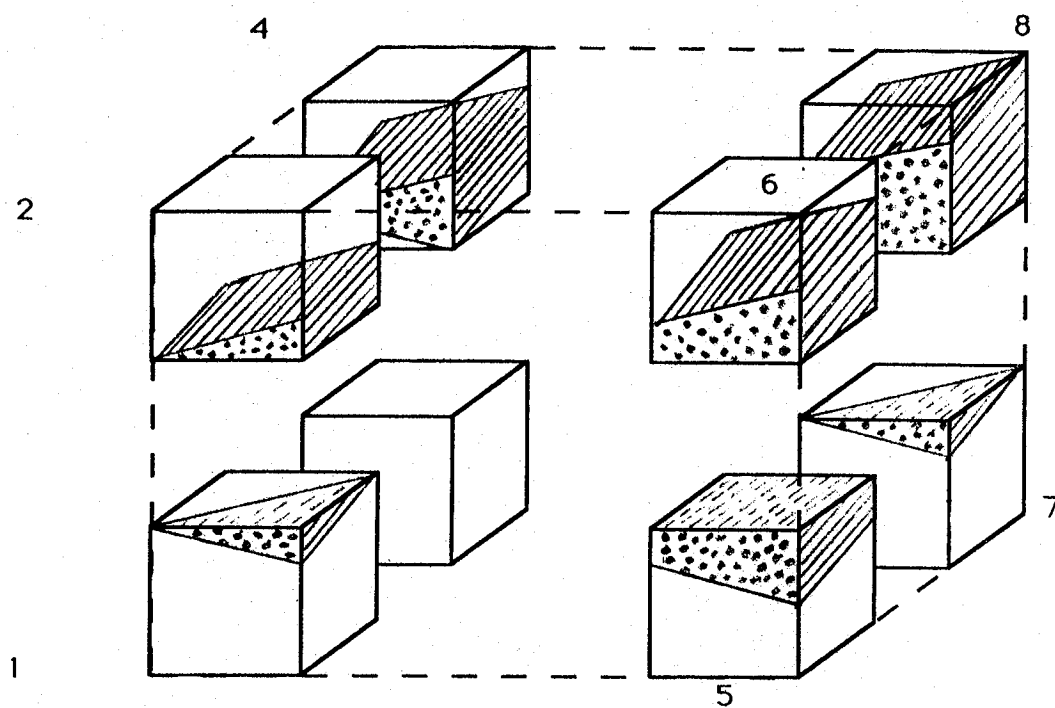
(A) Distribution of Warp Material Only
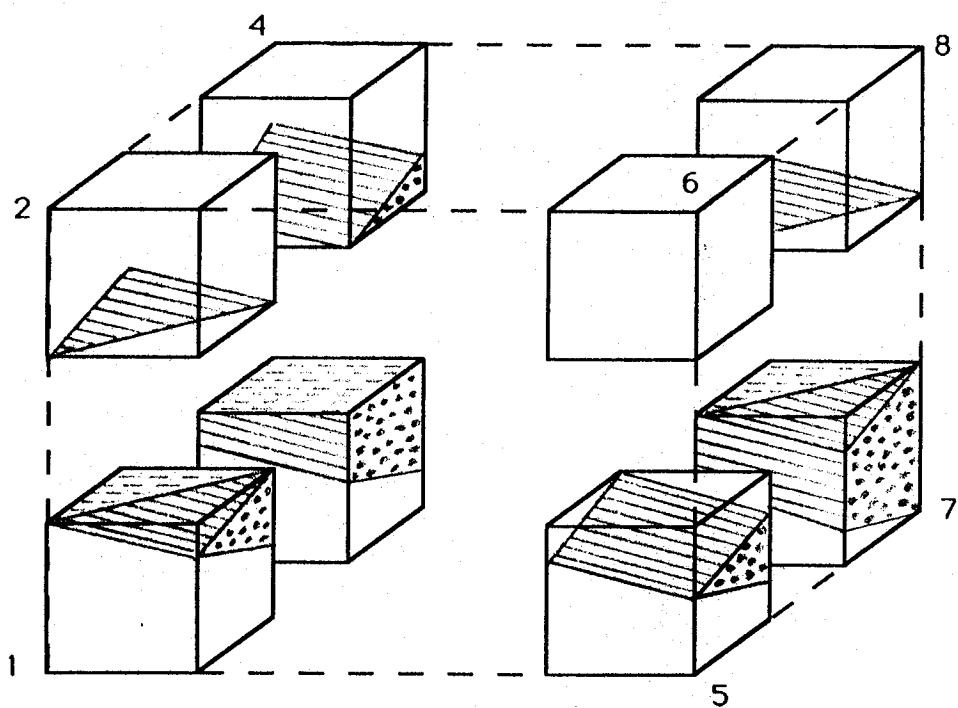
(B) Distribution of Fill Material Only

FIGURE 25: EXPLODED VIEW OF MASTER SUBCELL FROM FIG. 24(C)
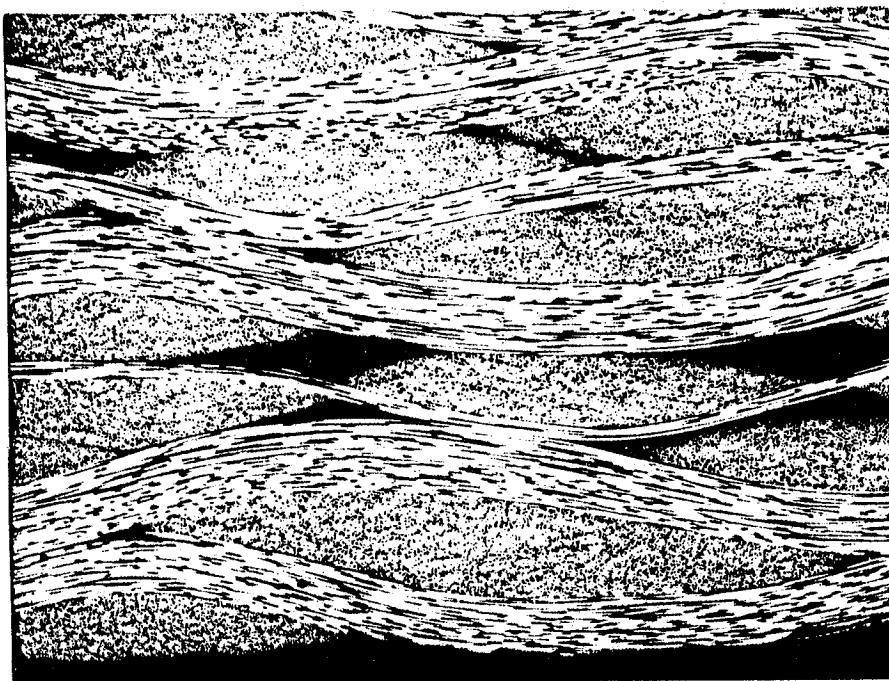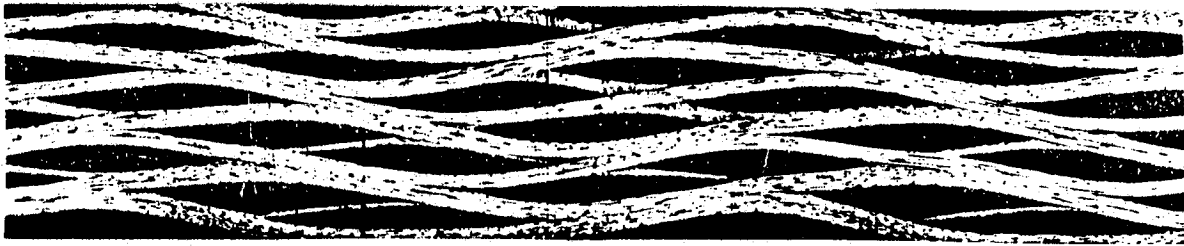
(A)   Warp Direction

(B)   Filling Direction

FIGURE 26: LAMINATED PLAIN WEAVE PHOTOMICROGRAPHS (70X)

Oxford Weave - 8 plies

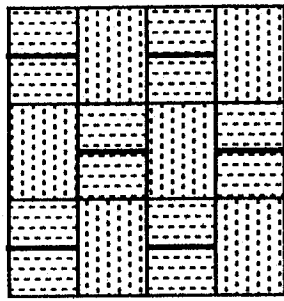← Warp direction →

5 Harness Satin Weave - 8 plies
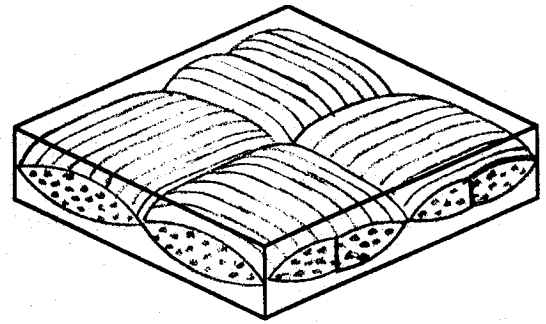
← Warp direction →
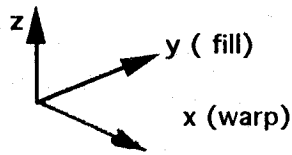
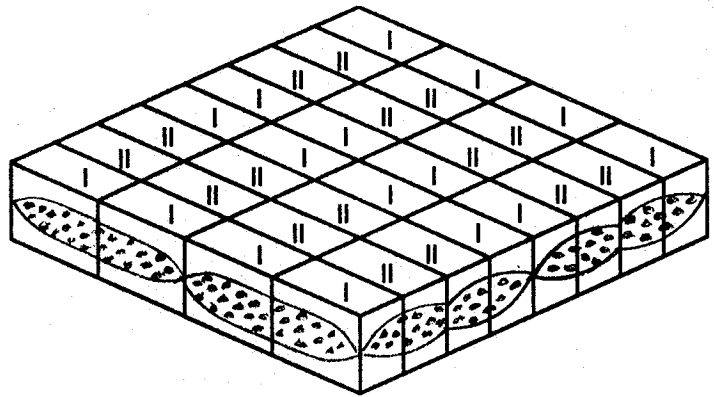

8 Harness Satin Weave - 8 plies
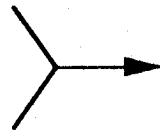
← Filling direction →

FIGURE 27: LAMINATED OXFORD AND SATIN WEAVE PHOTOMICROGRAPHS

(A) Fabric Pattern

(B) Unit Cell

z

y (fill)

x (warp)
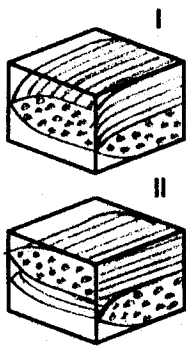
(C) Refined Subcell Division
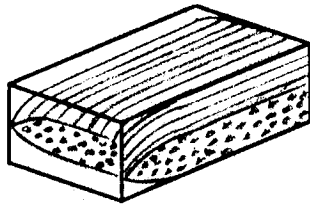
(D) Medium Subcell Division
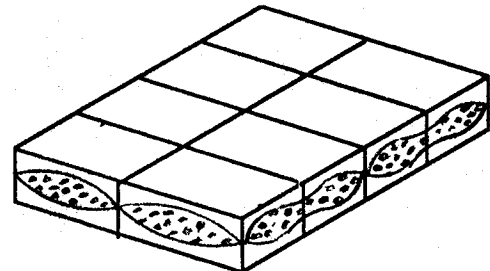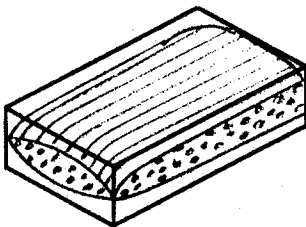
(E) Coarse Subcell Division

FIGURE 28: 2/2 OXFORD WEAVE MODELS

(A) Fabric Pattern

(B) Unit Cell

z

y

x

I

II
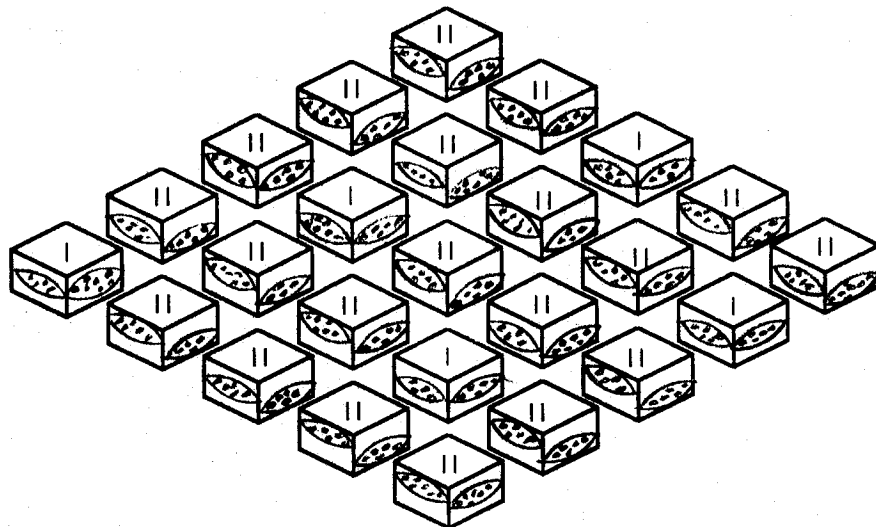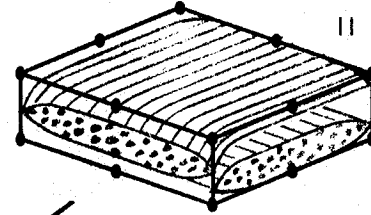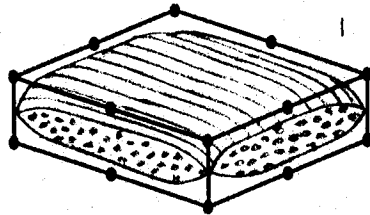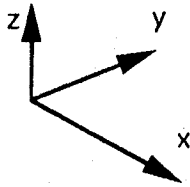
(C) Subcell Division

FIGURE 29: FIVE HARNESS SATIN WEAVE MODEL

87
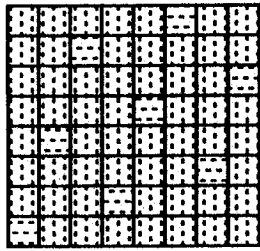
(A) Fabric Pattern

(B) Unit Cell

(C) Subcell Division
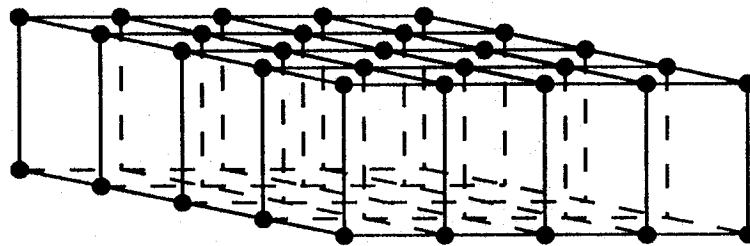
(D) Subcell Intergration Network

FIGURE 30: EIGHT HARNESS SATIN WEAVE MODEL

(A) Fabric Pattern

(B) Unit Cell

z

y

x

4

2

8

6

1

7

(C) Subcell

5
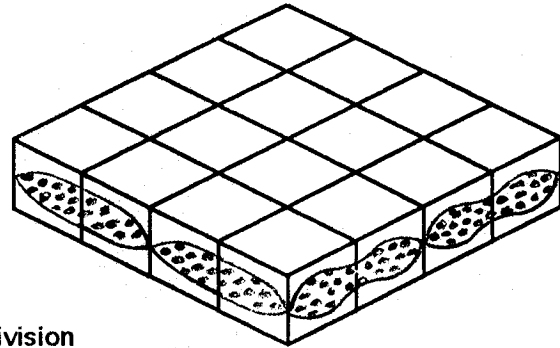
(D) Subcell Assembly
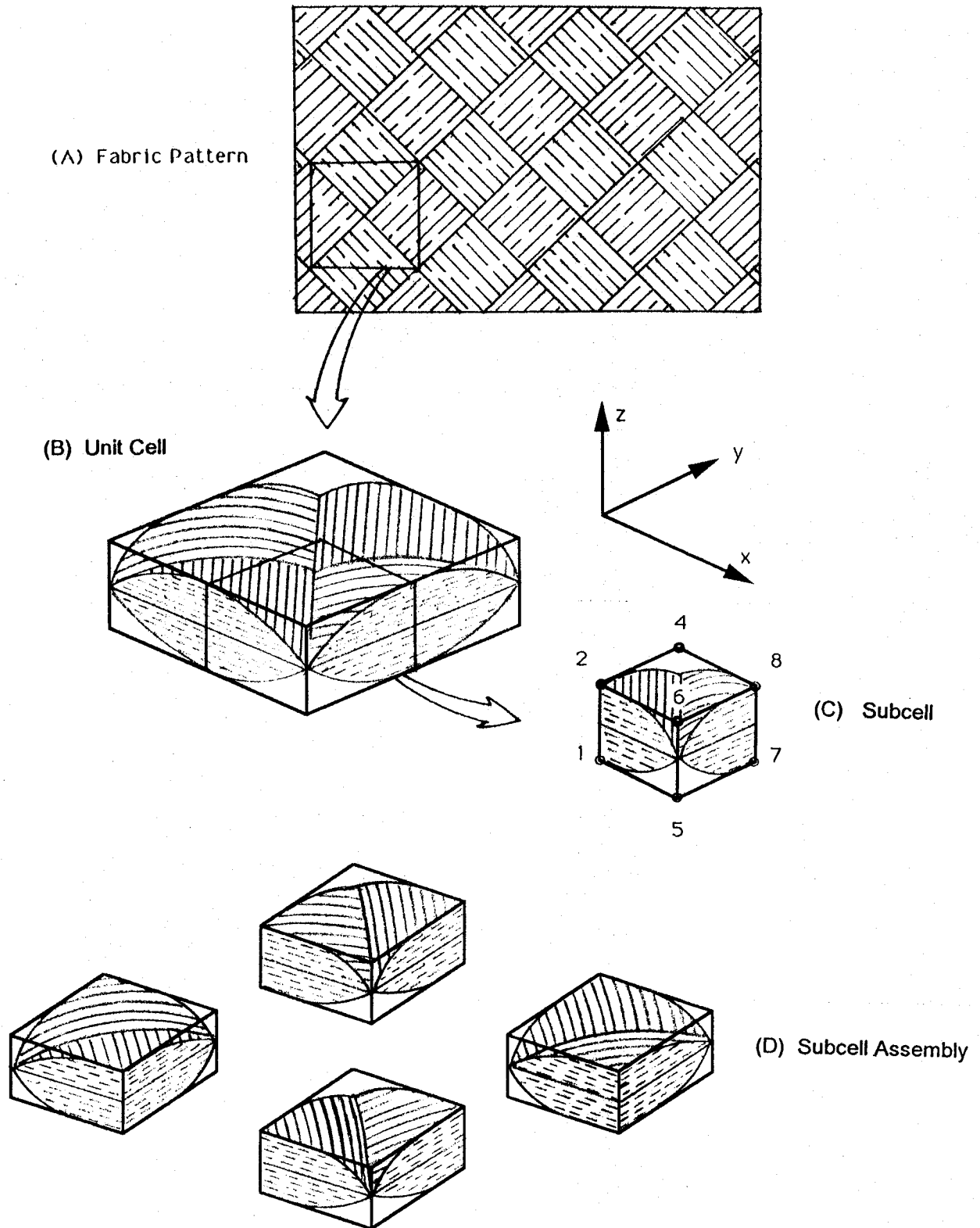
FIGURE 31: 2-D BRAID MICROGEOMETRY MODEL
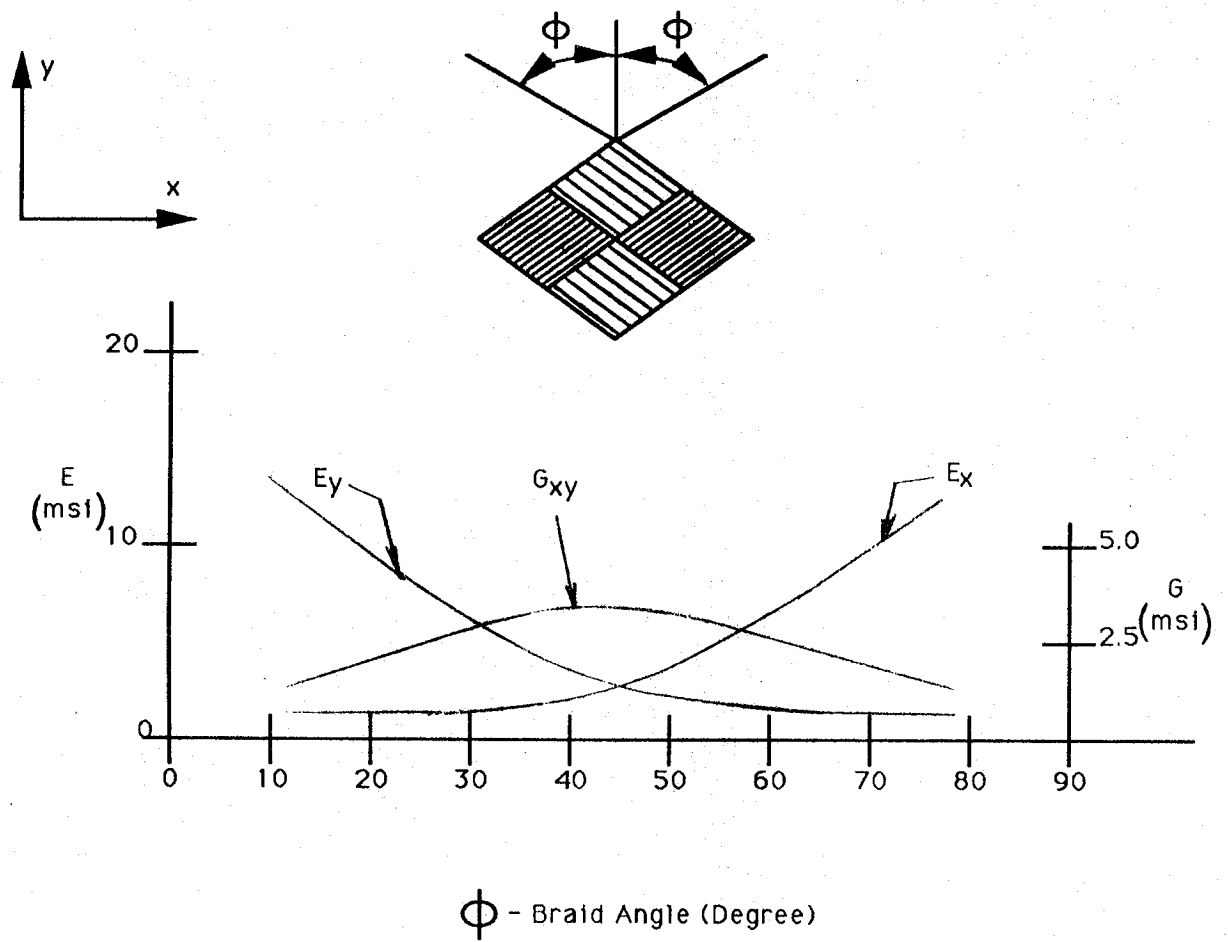
FIGURE 32: VARIATION IN STIFFNESS WITH BRAID ANGLE

O° Stuffer

Braiders
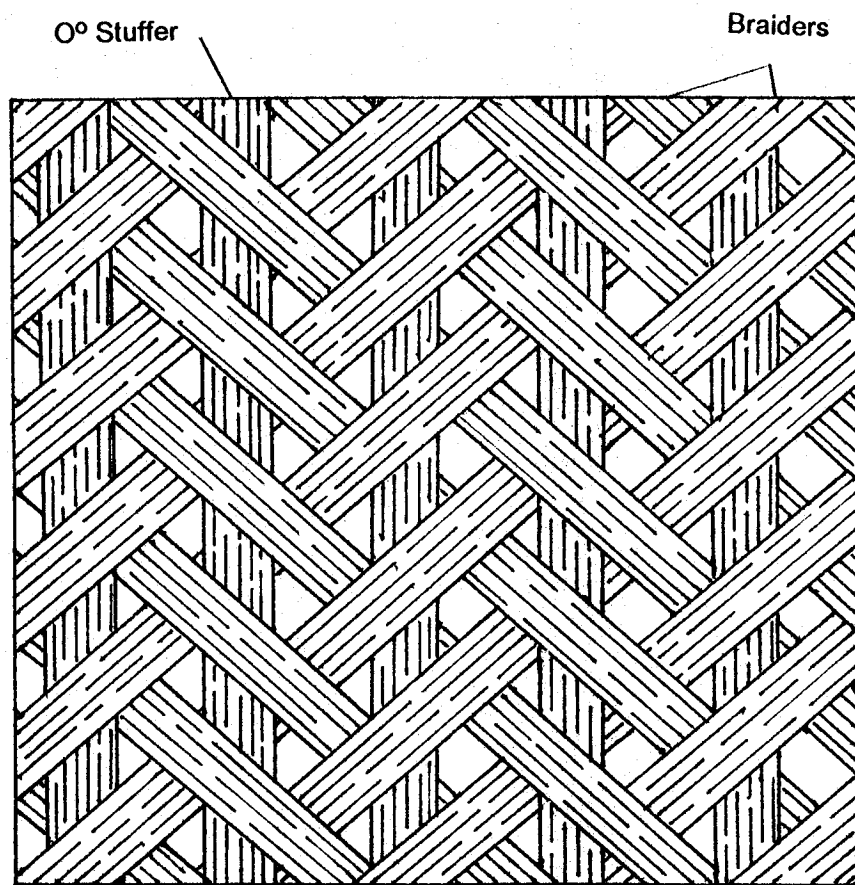
FIGURE 33: 2-D TRIAXIAL BRAID

(A) Unit Cell

(B) Master Subcells
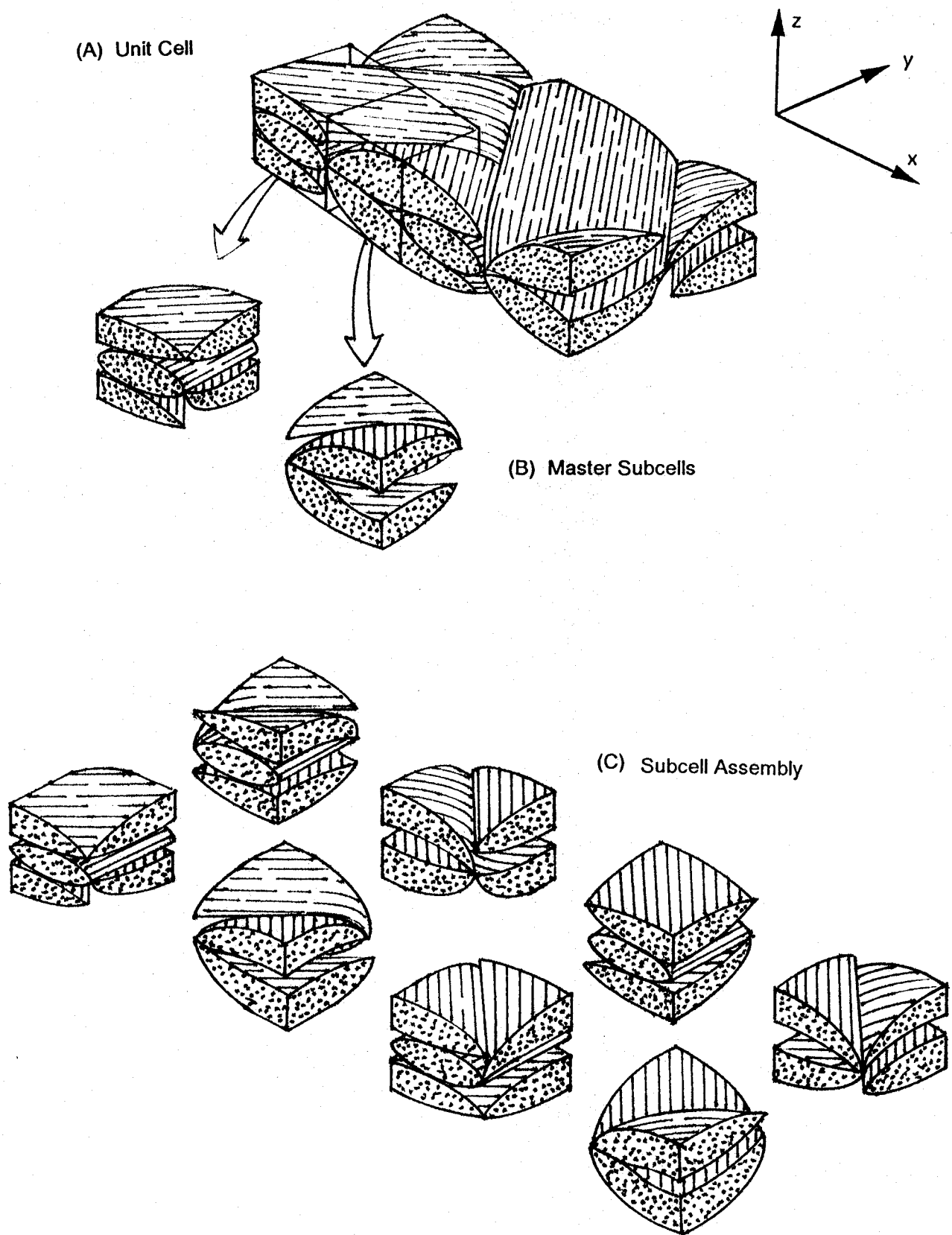
(C) Subcell Assembly

FIGURE 34: 2-D TRIAXIAL BRAID MODEL

92

Braider Tow   Stuffer Tow
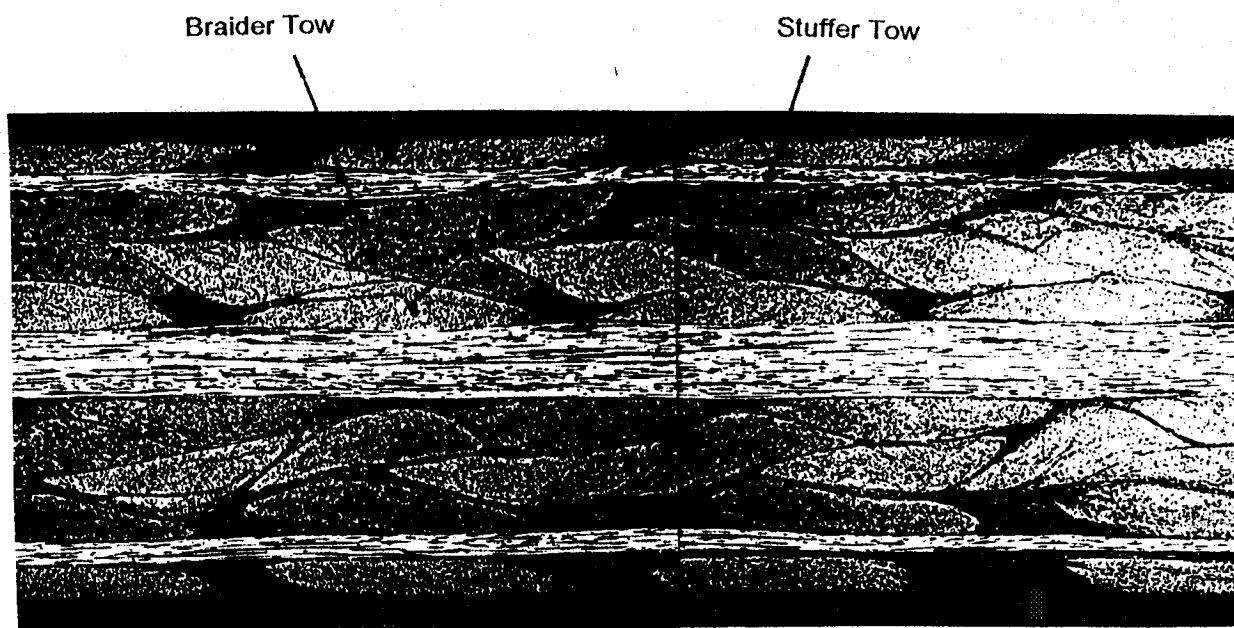
Longitudinal Cross-Section (20x)

Braider Tow   Stuffer Tow
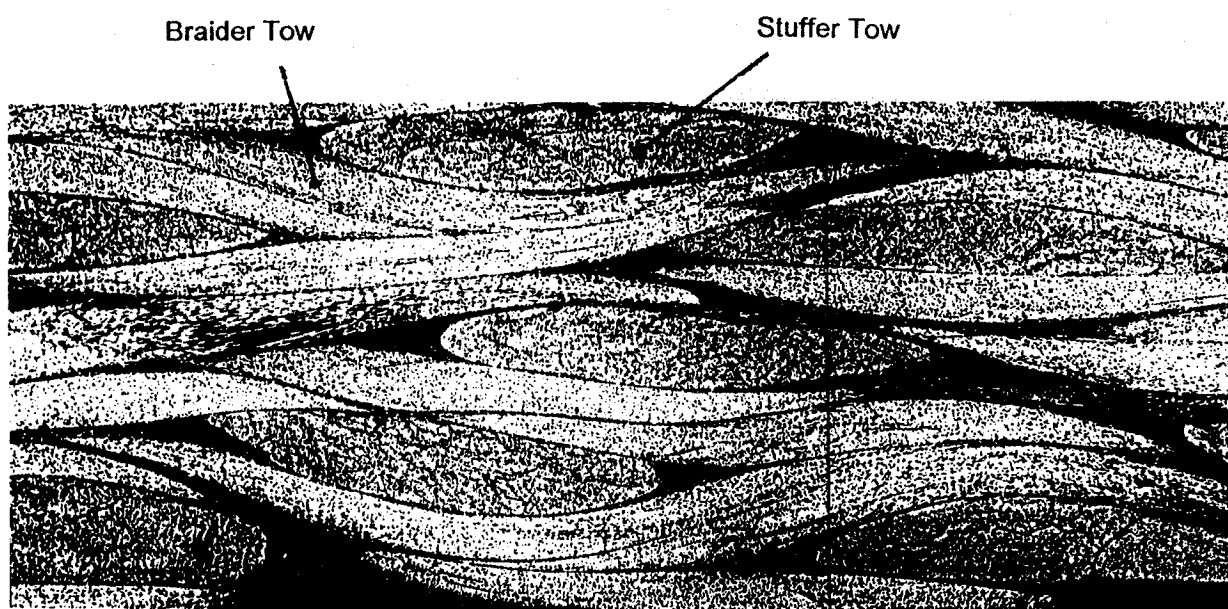
Transverse Cross-Section (20x)

FIGURE 35: PHOTOMICROGRAPHS OF TRIAXIAL BRAID
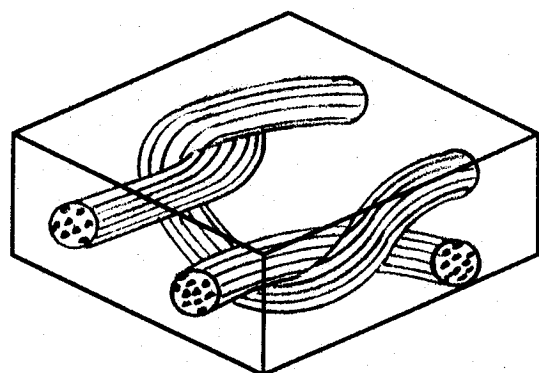
(A) Unit Cell
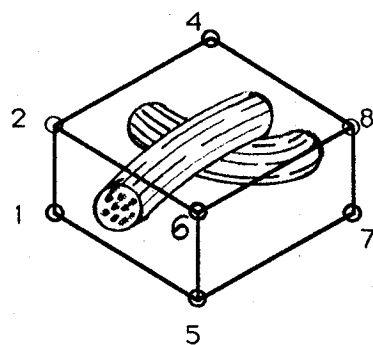
(B) Subcell
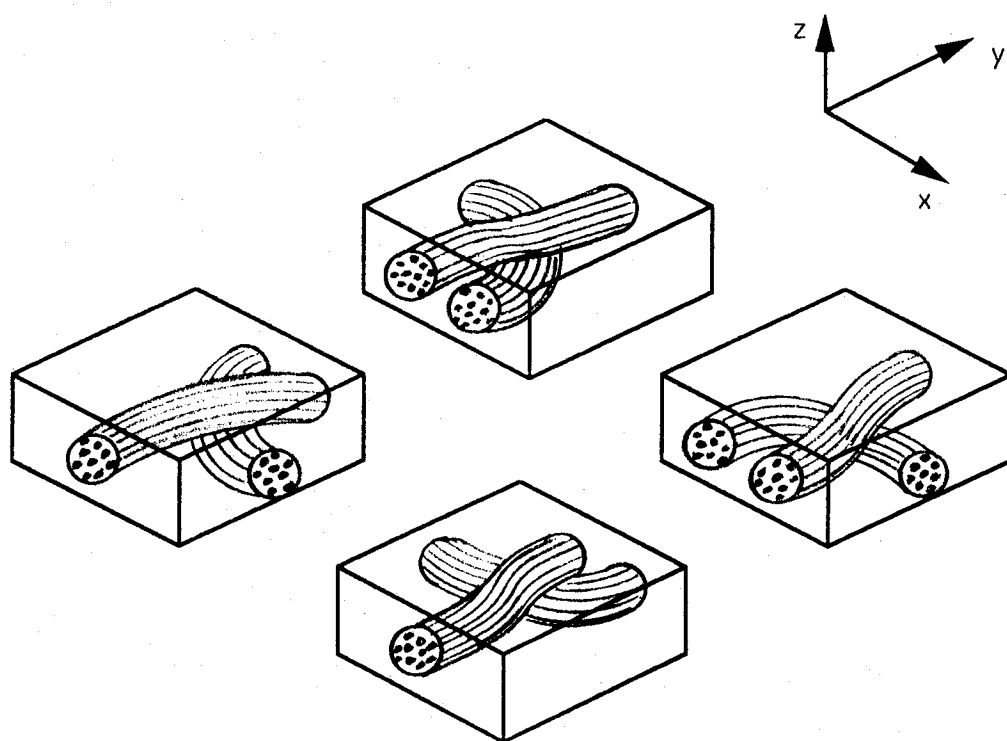
(C) Subcell Assembly

FIGURE 36: JERSEY (PLAIN) KNIT MICROGEOMETRY MODEL

94
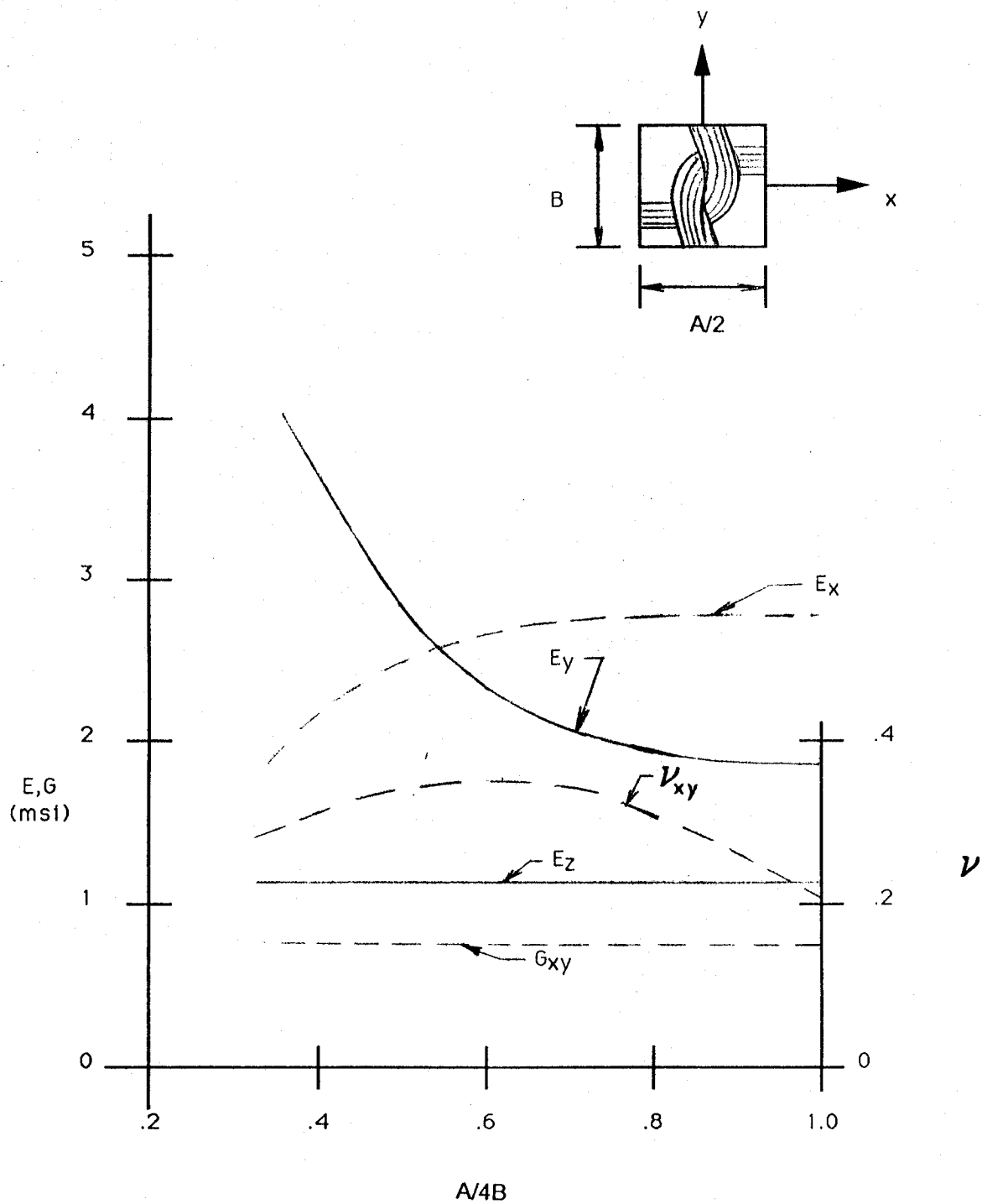
FIGURE 37: EFFECT OF PRESTRAIN ON JERSEY KNIT COMPOSITE STIFFNESS
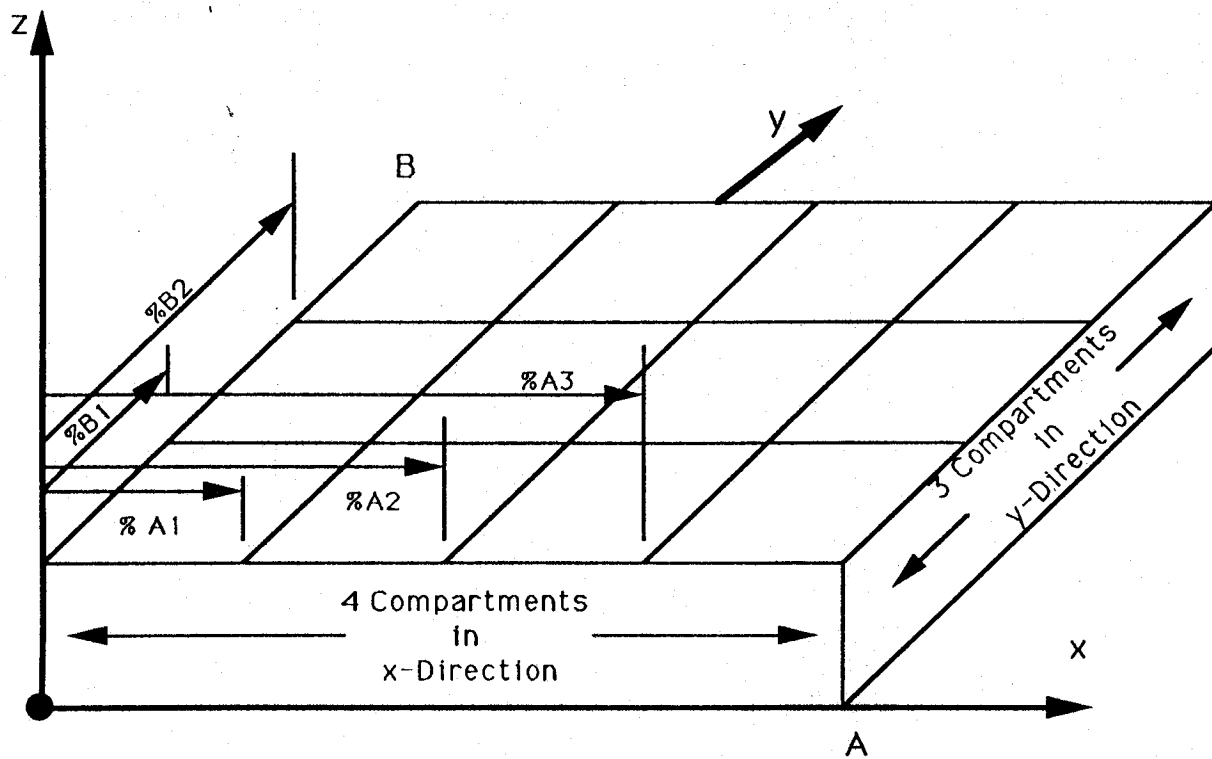
FIGURE 38: SUBCELL COMPARTMENTS OF UNIT CELL CONTAINER
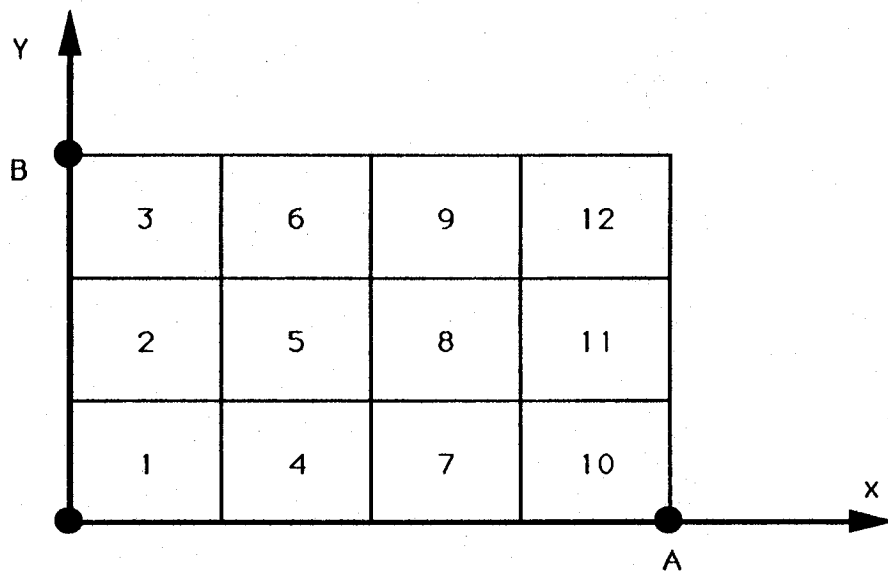
FIGURE 39: SEQUENCE OF FILLING UNIT CELL COMPARTMENTS
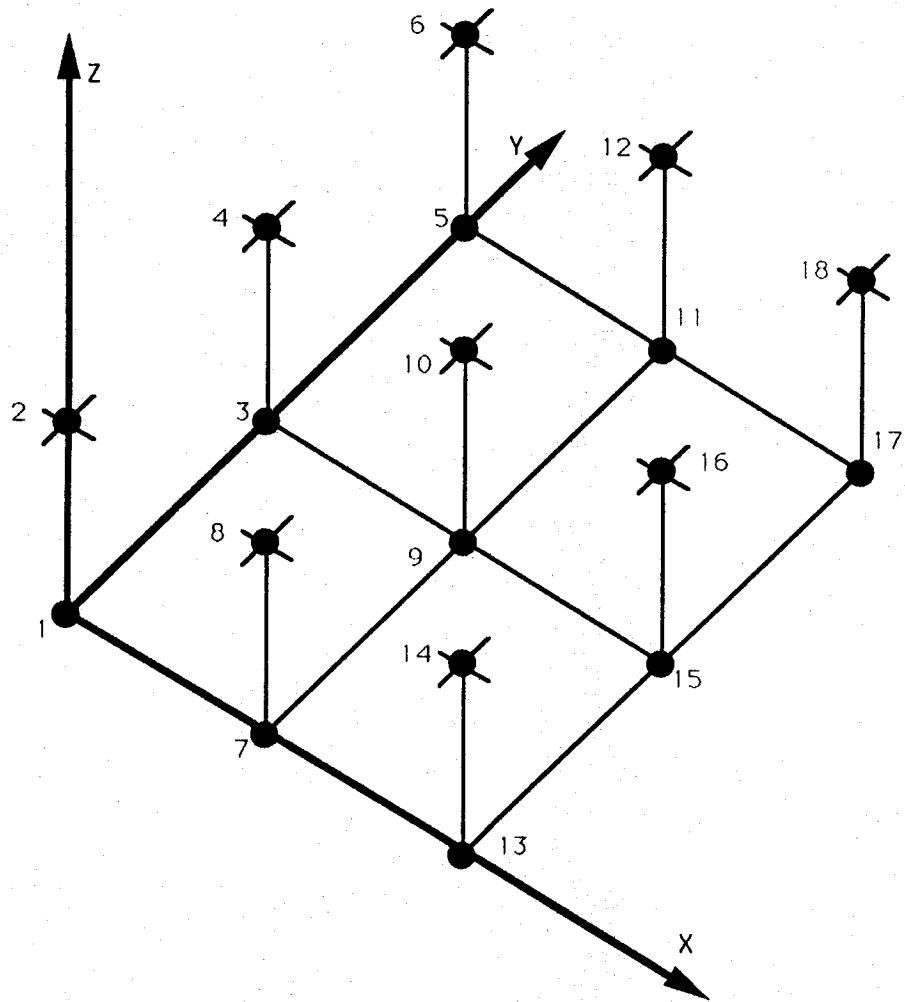
FIGURE 40: INTEGRATION POINT SEQUENCE

Program Listing-Fortran 5

```
      PROGRAM FABNEW (INPUT,OUTPUT,TAPE5=INPUT,TAPE6=OUTPUT)
C
C      CCCCCCCCCCCCCCCCCCCCCCCCCCCCCCCCCCCCCCCCCCCCCCCC
C      CCCCCCCCCCCCCCCCCCCCCCCCCCCCCCCCCCCCCCCCCCCCCCCCCC
C      CC    PROGRAM TO COMPUTE THE 3-D ELASTIC MODULI OF    CC
C      CC     A UNIT CELL OF FIBER REINFORCED COMPOSITE      CC
C      CCCCCCCCCCCCCCCCCCCCCCCCCCCCCCCCCCCCCCCCCCCCCCCCCC
C        CCCCCCCCCCCCCCCCCCCCCCCCCCCCCCCCCCCCCCCCCCCCCC
C
C          SPECIFICATION STATEMENTS
C
      REAL MU,MIXYZ,MIYYZ,MIZYZ,MIXXZ,MIYXZ,MIZXZ
      REAL MIXXY,MIYXY,MIZXY
      REAL MP(6,6),KS(24,24),KMOD(24,24),SK(24,24)
      DIMENSION KA(7),LC(24),VF(8)
      DIMENSION PR(6,6),SS(6,6),T(6,6),BIG(6,6)
      DIMENSION BM(6,24),DB(6,24)
      DIMENSION GM(6,9),DG(6,9),GDG(9,9)
      DIMENSION GB(9,24),BDG(24,9)
      PARAMETER (MM=10,MMM=100,NNN=216)
      DIMENSION PROP(MM,6),DX(MM),DY(MM),DZ(MM)
      DIMENSION NBL(MM,MM),FDX(MM+1),FDY(MM+1)
      DIMENSION FB(NNN,7),FS(MMM,7),FT(6,6),TF(6,6)
      DIMENSION IP(MMM),WK(MMM),UVW(NNN,6)
      REAL KB(NNN,NNN),KM(MMM,NNN),KN(MMM,MMM)
      INTEGER QT,QTR(MM,MM)
      LOGICAL LX,LY
C
C BUILT IN MATERIAL PROPERTY DATA
C
      DATA (MP(1,I),I=1,6)/30.E6,1.5E6,.25,.35,.7E6,.7E6/,
     1     (MP(2,I),I=1,6)/25.E6,1.5E6,.25,.35,.7E6,.7E6/,
     2     (MP(3,I),I=1,6)/20.E6,1.5E6,.3,.45,.7E6,.7E6/,
     3     (MP(4,I),I=1,6)/10.E6,1.E6,.3,.4,2.E5,2.E5/,
     4     (MP(5,I),I=1,6)/ 1.E7,1.E7,.25,.25,4.E6,4.E6/
     5     (MP(6,I),I=1,6)/ .5E6,.5E6,.35,.35,.185E6,.185E6/
      DATA (KA(I),I=1,7)/10,6,6,1,6,0,0/
C
C INITIALIZE VARIABLES
C
      ISYM=0
      DO 10 I=1,MMM
      DO 5 J=1,7
    5 FS(I,J)=0.0
      DO 10 J=1,MMM
   10 KN(I,J)=0.0
      DO 15 I=1,6
      DO 15 J=1,6
      TF(I,J)=0.0
   15 FT(I,J)=0.0
      WRITE(6,9100)
      READ(5,9030) NM
C
C MATERIAL PROPERTY DATA INPUT
C
      DO 18 I=1,NM
      WRITE(6,9180)
```

```fortran
      READ(5,9030) M
      IF(M.GT.6) THEN
      WRITE(6,9120)
      READ(5,9010) PROP(I,1)
      WRITE(6,9130)
      READ(5,9010) PROP(I,2)
      WRITE(6,9140)
      READ(5,9010) PROP(I,3)
      WRITE(6,9150)
      READ(5,9010) PROP(I,4)
      WRITE(6,9160)
      READ(5,9010) PROP(I,5)
      WRITE(6,9170)
      READ(5,9010) PROP(I,6)
      END IF
      IF(M.LE.6) THEN
      DO 17 J=1,6
   17 PROP(I,J)=MP(M,J)
      END IF
   18 CONTINUE
      WRITE(6,9190)
      DO 19 I=1,NM
   19 WRITE(6,9020)   (PROP(I,J),J=1,6)
      WRITE(6,9110)
      READ(5,9030) NB
      WRITE(6,9080)
      READ(5,9030) NBX
      WRITE(6,9090)
      READ(5,9030) NBY
      NP=((NBY+1)*(NBX+1))*6
      IJ=3*(NBX*NBY-1)
      WRITE(6,9470)
      READ(5,9000) C
      WRITE(6,9440)
      READ(5,9000) XL
      FDX(1)=0.0
      FDX(NBX+1)=100.0
      IF(NBX.LE.1) GO TO 25
      DO 22 I=1,NBX-1
      WRITE(6,9460) I+1
   22 READ(5,9000) FDX(I+1)
   25 WRITE(6,9450)
      READ(5,9000) YL
      FDY(1)=0.0
      FDY(NBY+1)=100.0
      IF(NBY.LE.1) GO TO 35
      DO 30 I=1,NBY-1
      WRITE(6,9460) I+1
   30 READ(5,9000) FDY(I+1)
   35 DO 50 I=1,NP
      DO 40 J=1,7
   40 FB(I,J)=0.0
      DO 50 J=1,NP
   50 KB(I,J)=0.0
      DO 70 I=1,NBX
      DO 70 J=1,NBY
      WRITE(6,9060) I,J
      READ(5,9030) NBL(I,J)
      WRITE(6,9070) I,J
      READ(5,9030) QTR(I,J)
```

99

```
   70 CONTINUE
      WRITE(6,9050)
      READ(5,9040) LX
      IF(LX) IJ=IJ+(NBY+1)
      WRITE(6,9055)
      READ(5,9040) LY
      IF(LY) IJ=IJ+(NBX+1)
      ICOUNT=0
  350 CONTINUE
C
CCCCCCCCCCCCCCCCCCCCCCCCCCCCCCCCCCCCCCCCCCCCCCCCCCCCCCCCCC
C OUTER DO LOOP ON NO. OF SUBCELLS IN UNIT CELL BEGINS   C
CCCCCCCCCCCCCCCCCCCCCCCCCCCCCCCCCCCCCCCCCCCCCCCCCCCCCCCCCC
C
C INPUT BLOCK GRID GEOMETRY
C
      WRITE(6,9300)
      WRITE(6,9200) ICOUNT+1
      WRITE(6,9300)
      WRITE(6,9210)
      READ(5,9000) A
      AA=0.5*A
      WRITE(6,9240)
      READ(5,9030) NX
      DX(1)=0.0
      DX(NX)=A
      IF (NX.LE.2) GOTO 460
      DO 450 I=2,NX-1
      WRITE(6,9270) I
      READ(5,9010) DX(I)
  450 DX(I)=DX(I)*A/100.0
  460 CONTINUE
      WRITE(6,9220)
      READ(5,9000) B
      BB=0.5*B
      WRITE(6,9250)
      READ(5,9030) NY
      DY(1)=0.0
      DY(NY)=B
      IF (NY.LE.2) GOTO 510
      DO 500 I=2,NY-1
      WRITE(6,9280) I
      READ(5,9010) DY(I)
  500 DY(I)=DY(I)*B/100.0
  510 CONTINUE
      WRITE(6,9230)
      READ(5,9000) HT
      CC=0.5*C
      IF(.NOT.(HT.EQ.C)) WRITE(6,9330)
      WRITE(6,9260)
      READ(5,9030) NZ
      DZ(1)=0.0
      DZ(NZ)=C
      IF (NZ.LE.2) GOTO 560
      DO 550 I=2,NZ-1
      WRITE(6,9290) I
      READ(5,9010) DZ(I)
  550 DZ(I)=DZ(I)*C/100.0
  560 CONTINUE
C
```

```
C GENERAL MATERIALS INFORMATION FOR THE SUBCELL
C
      WRITE(6,9310) ICOUNT+1
      READ(5,9030) NMAT
      MCOUNT=0
      DO 570 I=1,24
      DO 570 J=1,24
  570 KS(I,J)=0.0
      DO 580 I=1,24
      DO 580 J=1,9
  580 BDG(I,J)=0.0
      DO 590 I=1,9
      DO 590 J=1,9
  590 GDG(I,J)=0.0
CCCCCCCCCCCCCCCCCCCCCCCCCCCCCCCCCCCCCCCCCCCCCCCCCCCCCCCCCCC
C   INNER DO LOOP ON MATLS. WITHIN SUBCELL BEGINS HERE     C
CCCCCCCCCCCCCCCCCCCCCCCCCCCCCCCCCCCCCCCCCCCCCCCCCCCCCCCCCCC
  600 WRITE(6,9320)
      READ(5,9030) MN
C
C INPUT 8 MATL. VOL. FRACTIONS AT EACH INTEGRATION POINT
C
      DO 2000 I=1,NX
      DO 2000 J=1,NY
      DO 2000 K=1,NZ
      DO  800 LL=1,8
  800 VF(LL)=0.0
      WRITE(6,9480)
      READ(5,9000) A1
      WRITE(6,9490)
      READ(5,9000) A2
  850 WRITE(6,9420) I,J,K
      READ(5,9030) L
      IF((L.LT.0).OR.(L.GT.8)) GO TO 860
      WRITE(6,9430) L
      READ(5,9000) VF(L)
      GO TO 850
  860 CONTINUE
      IF(I.EQ.NX) THEN
      XP=0.0
      ELSE
      XP=(DX(I+1)-DX(I))/2.0
      END IF
      IF(I.EQ.1) THEN
      XM=0.0
      ELSE
      XM=(DX(I)-DX(I-1))/2.0
      END IF
      IF(J.EQ.NY) THEN
      YP=0.0
      ELSE
      YP=(DY(J+1)-DY(J))/2.0
      END IF
      IF(J.EQ.1) THEN
      YM=0.0
      ELSE
      YM=(DY(J)-DY(J-1))/2.0
      END IF
      IF(K.EQ.NZ) THEN
      ZP=0.0
```

```fortran
      ELSE
      ZP=(DZ(K+1)-DZ(K))/2.0
      END IF
      IF(K.EQ.1) THEN
      ZM=0.0
      ELSE
      ZM=(DZ(K)-DZ(K-1))/2.0
      END IF
      V1=VF(1)*XP*YP*ZP
      V2=VF(2)*XP*YP*ZM
      V3=VF(3)*XP*YM*ZP
      V4=VF(4)*XP*YM*ZM
      V5=VF(5)*XM*YP*ZP
      V6=VF(6)*XM*YP*ZM
      V7=VF(7)*XM*YM*ZP
      V8=VF(8)*XM*YM*ZM
      VOL=V1+V2+V3+V4+V5+V6+V7+V8
C
C GET THE STRAIN TRANSFORMATION MATRIX (T)
C
      S1=SIND(A1)
      S2=SIND(A2)
      C1=COSD(A1)
      C2=COSD(A2)
      S1S=S1*S1
      S2S=S2*S2
      C1S=C1*C1
      C2S=C2*C2
      SC1=S1*C1
      SC2=S2*C2
      T(1,1)=C1S*C2S
      T(1,2)=S1S*C2S
      T(1,3)=S2S
      T(1,4)=SC1*C2S
      T(1,5)=S1*SC2
      T(1,6)=C1*SC2
      T(2,1)=S1S
      T(2,2)=C1S
      T(2,3)=0.0
      T(2,4)=-SC1
      T(2,5)=0.0
      T(2,6)=0.0
      T(3,1)=C1S*S2S
      T(3,2)=S1S*S2S
      T(3,3)=C2S
      T(3,4)=SC1*S2S
      T(3,5)=-S1*SC2
      T(3,6)=-C1*SC2
      T(4,1)=-2.0*SC1*C2
      T(4,2)=-T(4,1)
      T(4,3)=0.0
      T(4,4)=(C1S-S1S)*C2
      T(4,5)=C1*S2
      T(4,6)=-S1*S2
      T(5,1)=2.0*SC1*S2
      T(5,2)=-T(5,1)
      T(5,3)=0.0
      T(5,4)=-(C1S-S1S)*S2
      T(5,5)=C1*C2
      T(5,6)=-S1*C2
```

```
            T(6,1)=-2.0*C1S*SC2
            T(6,2)=-2.0*S1S*SC2
            T(6,3)=2.0*SC2
            T(6,4)=-SC1*SC2*2.0
            T(6,5)=S1*(C2S-S2S)
            T(6,6)=C1*(C2S-S2S)
C
C GET STRESS-STRAIN MATRIX (SS) IN MATL. COORD. SYSTEM
C
            DO 1100 II=1,6
            DO 1100 JJ=1,6
 1100 SS(II,JJ)=0.0
            MC=MN
            MU=PROP(MC,4)
            R=PROP(MC,3)*PROP(MC,3)*PROP(MC,2)/PROP(MC,1)
            D=(1.0+MU)*(1.0-MU-2.0*R)
            IF(D.LE.0.0) D=1.0
            SS(1,1)=PROP(MC,1)*(1.0-MU*MU)/D
            SS(1,2)=PROP(MC,2)*PROP(MC,3)*(1.0+MU)/D
            SS(1,3)=SS(1,2)
            SS(2,1)=SS(1,2)
            SS(2,2)=PROP(MC,2)*(1.0-R)/D
            SS(2,3)=PROP(MC,2)*(MU+R)/D
            SS(3,1)=SS(1,3)
            SS(3,2)=SS(2,3)
            SS(3,3)=SS(2,2)
            SS(4,4)=PROP(MC,5)
            SS(5,5)=PROP(MC,6)
            SS(6,6)=PROP(MC,5)

C
C GET STRESS-STRAIN MATRIX (SS) IN COORDS. OF THE SUBCELL
C
            DO 1200 II=1,6
            DO 1200 JJ=1,6
            SUM=0.0
            DO 1150 KK=1,6
 1150 SUM=SUM+SS(II,KK)*T(KK,JJ)
 1200 PR(II,JJ)=SUM
            DO 1225 II=1,3
            DO 1225 JJ=4,6
            T(II,JJ)=2.0*T(II,JJ)
 1225 T(JJ,II)=0.5*T(JJ,II)
            CALL MATOPS(KA,T,DET,DDDD)
            DO 1300 II=1,6
            DO 1300 JJ=1,6
            SUM=0.0
            DO 1250 KK=1,6
 1250 SUM=SUM+T(II,KK)*PR(KK,JJ)
 1300 BIG(II,JJ)=SUM*VOL
 1350 CONTINUE
C
C SUBCELL GEOMETRY CALCULATIONS
C
            DO 1400 II=1,6
            DO 1400 JJ=1,9
 1400 GM(II,JJ)=0.0
            DO 1500 II=1,6
            DO 1500 JJ=1,24
 1500 BM(II,JJ)=0.0
```

```
C
C FORM 8 NODE FINITE ELEMENT STIFFNESS MATRIX FOR SUBCELL
C
      X=DX(I)-AA
      Y=DY(J)-BB
      Z=DZ(K)-CC
      X1=-(0.125/AA)*(1.0-Y/BB)*(1.0-Z/CC)
      Y1=-(0.125/BB)*(1.0-X/AA)*(1.0-Z/CC)
      Z1=-(0.125/CC)*(1.0-X/AA)*(1.0-Y/BB)
      X2=-(0.125/AA)*(1.0-Y/BB)*(1.0+Z/CC)
      Y2=-(0.125/BB)*(1.0-X/AA)*(1.0+Z/CC)
      Z2=+(0.125/CC)*(1.0-X/AA)*(1.0-Y/BB)
      X3=-(0.125/AA)*(1.0+Y/BB)*(1.0-Z/CC)
      Y3=+(0.125/BB)*(1.0-X/AA)*(1.0-Z/CC)
      Z3=-(0.125/CC)*(1.0-X/AA)*(1.0+Y/BB)
      X4=-(0.125/AA)*(1.0+Y/BB)*(1.0+Z/CC)
      Y4=+(0.125/BB)*(1.0-X/AA)*(1.0+Z/CC)
      Z4=+(0.125/CC)*(1.0-X/AA)*(1.0+Y/BB)
      X5=+(0.125/AA)*(1.0-Y/BB)*(1.0-Z/CC)
      Y5=-(0.125/BB)*(1.0+X/AA)*(1.0-Z/CC)
      Z5=-(0.125/CC)*(1.0+X/AA)*(1.0-Y/BB)
      X6=+(0.125/AA)*(1.0-Y/BB)*(1.0+Z/CC)
      Y6=-(0.125/BB)*(1.0+X/AA)*(1.0+Z/CC)
      Z6=+(0.125/CC)*(1.0+X/AA)*(1.0-Y/BB)
      X7=+(0.125/AA)*(1.0+Y/BB)*(1.0-Z/CC)
      Y7=+(0.125/BB)*(1.0+X/AA)*(1.0-Z/CC)
      Z7=-(0.125/CC)*(1.0+X/AA)*(1.0+Y/BB)
      X8=+(0.125/AA)*(1.0+Y/BB)*(1.0+Z/CC)
      Y8=+(0.125/BB)*(1.0+X/AA)*(1.0+Z/CC)
      Z8=+(0.125/CC)*(1.0+X/AA)*(1.0+Y/BB)
      XX=-2.0*X/(AA*AA)
      YY=-2.0*Y/(BB*BB)
      ZZ=-2.0*Z/(CC*CC)
      GM(1,1)=XX
      GM(2,5)=YY
      GM(3,9)=ZZ
      GM(4,2)=XX
      GM(4,4)=YY
      GM(5,6)=YY
      GM(5,8)=ZZ
      GM(6,3)=XX
      GM(6,7)=ZZ
      BM(1,1)=X1
      BM(2,2)=Y1
      BM(3,3)=Z1
      BM(1,4)=X2
      BM(2,5)=Y2
      BM(3,6)=Z2
      BM(1,7)=X3
      BM(2,8)=Y3
      BM(3,9)=Z3
      BM(1,10)=X4
      BM(2,11)=Y4
      BM(3,12)=Z4
      BM(1,13)=X5
      BM(2,14)=Y5
      BM(3,15)=Z5
      BM(1,16)=X6
      BM(2,17)=Y6
      BM(3,18)=Z6
```

```
      BM(1,19)=X7
      BM(2,20)=Y7
      BM(3,21)=Z7
      BM(1,22)=X8
      BM(2,23)=Y8
      BM(3,24)=Z8
      BM(4,1)=Y1
      BM(5,2)=Z1
      BM(6,3)=X1
      BM(4,4)=Y2
      BM(5,5)=Z2
      BM(6,6)=X2
      BM(4,7)=Y3
      BM(5,8)=Z3
      BM(6,9)=X3
      BM(4,10)=Y4
      BM(5,11)=Z4
      BM(6,12)=X4
      BM(4,13)=Y5
      BM(5,14)=Z5
      BM(6,15)=X5
      BM(4,16)=Y6
      BM(5,17)=Z6
      BM(6,18)=X6
      BM(4,19)=Y7
      BM(5,20)=Z7
      BM(6,21)=X7
      BM(4,22)=Y8
      BM(5,23)=Z8
      BM(6,24)=X8
      BM(6,1)=Z1
      BM(4,2)=X1
      BM(5,3)=Y1
      BM(6,4)=Z2
      BM(4,5)=X2
      BM(5,6)=Y2
      BM(6,7)=Z3
      BM(4,8)=X3
      BM(5,9)=Y3
      BM(6,10)=Z4
      BM(4,11)=X4
      BM(5,12)=Y4
      BM(6,13)=Z5
      BM(4,14)=X5
      BM(5,15)=Y5
      BM(6,16)=Z6
      BM(4,17)=X6
      BM(5,18)=Y6
      BM(6,19)=Z7
      BM(4,20)=X7
      BM(5,21)=Y7
      BM(6,22)=Z8
      BM(4,23)=X8
      BM(5,24)=Y8
      DO 1600 II=1,6
      DO 1600 JJ=1,24
      DB(II,JJ)=0.0
      DO 1600 KK=1,6
 1600 DB(II,JJ)=DB(II,JJ)+BIG(II,KK)*BM(KK,JJ)
      DO 1700 II=1,6
```

```
              DG(II,1)=XX*BIG(II,1)
              DG(II,2)=XX*BIG(II,4)
              DG(II,3)=XX*BIG(II,6)
              DG(II,4)=YY*BIG(II,4)
              DG(II,5)=YY*BIG(II,2)
              DG(II,6)=YY*BIG(II,5)
              DG(II,7)=ZZ*BIG(II,6)
              DG(II,8)=ZZ*BIG(II,5)
       1700   DG(II,9)=ZZ*BIG(II,3)
              DO 1750 II=1,9
              DO 1750 JJ=1,9
              DO 1750 KK=1,6
       1750   GDG(II,JJ)=GDG(II,JJ)+GM(KK,II)*DG(KK,JJ)
              DO 1800 II=1,24
              DO 1800 JJ=1,9
              DO 1800 KK=1,6
       1800   BDG(II,JJ)=BDG(II,JJ)+BM(KK,II)*DG(KK,JJ)
              DO 1900 II=1,24
              DO 1900 JJ=1,24
              DO 1900 KK=1,6
       1900   KS(II,JJ)=KS(II,JJ)+BM(KK,II)*DB(KK,JJ)
       2000   CONTINUE
              MCOUNT=MCOUNT+1
              IF(MCOUNT.LT.NMAT) GO TO 600
              CALL INV(GDG)
              DO 2020 I=1,9
              DO 2020 J=1,24
              GB(I,J)=0.0
              DO 2020 K=1,9
       2020   GB(I,J)=GB(I,J)+GDG(I,K)*BDG(J,K)
              DO 2030 I=1,24
              DO 2030 J=1,24
              KMOD(I,J)=0.0
              DO 2030 K=1,9
       2030   KMOD(I,J)=KMOD(I,J)+BDG(I,K)*GB(K,J)
              DO 2040 I=1,24
              DO 2040 J=1,24
       2040   KS(I,J)=KS(I,J)-KMOD(I,J)
       C
       C PUT SMALL STIF. MATRIX (KS) INTO BIG STIF. MATRIX (KB)
       C
              ICOUNT=ICOUNT+1
              DO 2400 I=1,NBX
              DO 2400 J=1,NBY
              QT=QTR(I,J)
              NK=NBL(I,J)
              IF(.NOT.(NK.EQ.ICOUNT)) GO TO 2400
              IF(QT.LT.0) GO TO 2400
              DO 2050 II=1,24
              DO 2050 JJ=1,24
       2050   SK(II,JJ)=KS(II,JJ)
              IF(QT.EQ.0) GO TO 2100
              CALL TRNS(QT,SK)
       2100   LC(1)=((NBY+1)*(I-1)+J-1)*6+1
              LC(13)=LC(1)+(NBY+1)*6
              DO 2200 K=2,12
              LC(K)=LC(K-1)+1
       2200   LC(K+12)=LC(K+11)+1
              DO 2300 II=1,24
              DO 2300 JJ=1,24
```

```
          III=LC(II)
          JJJ=LC(JJ)
 2300 KB(III,JJJ)=KB(III,JJJ)+SK(II,JJ)
 2400 CONTINUE
          IF(ICOUNT.LT.NB) GO TO 350
          GO TO 2460
 2440 ISYM=1
          DO 2445 I=1,IJ
          DO 2445 J=1,IJ
 2445 KN(I,J)=0.0
          DO 2447 I=1,IJ
 2447 KN(I,I)=1.0
          IF(LX) IJ=IJ-2*NBY+1
          IF(LY) IJ=IJ-2*NBX+1
          DO 2450 I=1,NP
          DO 2450 J=1,6
 2450 FB(I,J)=0.0
 2460 CONTINUE
C
C CALC. DISP. VECTORS FOR 6 HOMOGENEOUS UNIT STRAIN CASES
C
          DO 2500 I=1,NBX+1
          DO 2500 J=1,NBY+1
          K=((I-1)*(NBY+1)+(J-1))*6+1
          FB(K,1)=FDX(I)*XL/100.0
          FB(K+3,1)=FB(K,1)
          FB(K+1,2)=FDY(J)*YL/100.0
          FB(K+4,2)=FB(K+1,2)
          FB(K+5,3)=C
          FB(K,4)=FB(K+1,2)
          FB(K+3,4)=FB(K,4)
          FB(K+4,5)=C
 2500 FB(K+3,6)=C
          DO 2525 I=1,NP
          DO 2525 J=1,6
 2525 UVW(I,J)=FB(I,J)
C
C USE FORCE B.C.S TO ELIMINATE INTERNAL SURFACE FORCES
C
          IN=0
          IF((NBX.LE.1).OR.(NBY.LE.1))GO TO 2950
          DO 2900 I=2,NBX
          DO 2900 J=2,NBY
          L=((I-1)*(NBY+1)+(J-1))*6
          DO 2850 K=1,NP
          KM(IN+1,K)=KB(L+1,K)+KB(L+4,K)
          KM(IN+2,K)=KB(L+2,K)+KB(L+5,K)
 2850 KM(IN+3,K)=KB(L+3,K)+KB(L+6,K)
          IN=IN+3
 2900 CONTINUE
C
C USE FORCE B.C.S TO ELIMINATE FORCE AT SIDE NODES
C
 2950 IF(NBX.LE.1) GO TO 3150
          DO 3100 I=2,NBX
          L=6*(I-1)*(NBY+1)
          LL=L+NBY*6
          IF(LY) GO TO 3050
          DO 3000 K=1,NP
          KM(IN+1,K)=KB(L+1,K)+KB(L+4,K)+KB(LL+1,K)+KB(LL+4,K)
```

```
      KM(IN+2,K)=KB(L+2,K)+KB(L+5,K)+KB(LL+2,K)+KB(LL+5,K)
3000  KM(IN+3,K)=KB(L+3,K)+KB(L+6,K)+KB(LL+3,K)+KB(LL+6,K)
      IN=IN+3
      GO TO 3100
3050  CONTINUE
      IF(ISYM.EQ.1) GO TO 3080
      DO 3075 K=1,NP
      KM(IN+1,K)=KB(L+1,K)+KB(L+4,K)
      KM(IN+2,K)=KB(L+3,K)+KB(L+6,K)
      KM(IN+3,K)=KB(LL+1,K)+KB(LL+4,K)
3075  KM(IN+4,K)=KB(LL+3,K)+KB(LL+6,K)
      IN=IN+4
      GO TO 3090
3080  CONTINUE
      DO 3085 K=1,NP
      KM(IN+1,K)=KB(L+2,K)+KB(L+5,K)
3085  KM(IN+2,K)=KB(LL+2,K)+KB(LL+5,K)
      IN=IN+2
3090  CONTINUE
3100  CONTINUE
3150  IF(NBY.LE.1) GO TO 3305
      DO 3300 J=2,NBY
      L=6*(J-1)
      LL=L+NBX*(NBY+1)*6
      IF(LX) GO TO 3250
      DO 3200 K=1,NP
      KM(IN+1,K)=KB(L+1,K)+KB(L+4,K)+KB(LL+1,K)+KB(LL+4,K)
      KM(IN+2,K)=KB(L+2,K)+KB(L+5,K)+KB(LL+2,K)+KB(LL+5,K)
3200  KM(IN+3,K)=KB(L+3,K)+KB(L+6,K)+KB(LL+3,K)+KB(LL+6,K)
      IN=IN+3
      GO TO 3300
3250  CONTINUE
      IF(ISYM.EQ.1) GO TO 3280
      DO 3275 K=1,NP
      KM(IN+1,K)=KB(L+2,K)+KB(L+5,K)
      KM(IN+2,K)=KB(L+3,K)+KB(L+6,K)
      KM(IN+3,K)=KB(LL+2,K)+KB(LL+5,K)
3275  KM(IN+4,K)=KB(LL+3,K)+KB(LL+6,K)
      IN=IN+4
      GO TO 3290
3280  CONTINUE
      DO 3285 K=1,NP
      KM(IN+1,K)=KB(L+1,K)+KB(L+4,K)
3285  KM(IN+2,K)=KB(LL+1,K)+KB(LL+4,K)
      IN=IN+2
3290  CONTINUE
3300  CONTINUE
3305  CONTINUE
      IF(.NOT.LY) GO TO 3315
      L=6*NBY
      LL=L+6*NBX*(NBY+1)
      IF(ISYM.EQ.1) GO TO 3311
      DO 3310 K=1,NP
      KM(IN+1,K)=KB(L+1,K)+KB(L+4,K)+KB(LL+1,K)+KB(LL+4,K)
3310  KM(IN+2,K)=KB(L+3,K)+KB(L+6,K)+KB(LL+3,K)+KB(LL+6,K)
      IN=IN+2
      GO TO 3314
3311  CONTINUE
      DO 3312 K=1,NP
3312  KM(IN+1,K)=KB(L+2,K)+KB(L+5,K)+KB(LL+2,K)+KB(LL+5,K)
```

```
      IN=IN+1
3314  CONTINUE
3315  CONTINUE
      IF(.NOT.LX) GO TO 3325
      L=6*NBX*(NBY+1)
      LL=L+6*NBY
      IF(ISYM.EQ.1) GO TO 3321
      DO 3320 K=1,NP
      KM(IN+1,K)=KB(L+2,K)+KB(L+5,K)+KB(LL+2,K)+KB(LL+5,K)
3320  KM(IN+2,K)=KB(L+3,K)+KB(L+6,K)+KB(LL+3,K)+KB(LL+6,K)
      IN=IN+2
      GO TO 3324
3321  CONTINUE
      DO 3322 K=1,NP
3322  KM(IN+1,K)=KB(L+1,K)+KB(L+4,K)+KB(LL+1,K)+KB(LL+4,K)
      IN=IN+1
3324  CONTINUE
3325  CONTINUE
      IF(IJ.LT.1) GO TO 3345
9085  FORMAT(1H ,6F12.0)
      DO 3330 I=1,IJ
      DO 3330 J=1,7
3330  FS(I,J)=0.0
      DO 3340 I=1,6
      DO 3335 J=1,IN
      DO 3335 K=1,NP
3335  FS(J,7)=FS(J,7)+KM(J,K)*UVW(K,I)
      DO 3340 J=1,IJ
      FS(J,I)=FS(J,7)
3340  FS(J,7)=0.0
3345  CONTINUE
C
C USE DISPLACEMENT B.C.S TO ELIMINATE DISPLACEMENTS
C
      INN=IN
      IN=0
      IF(IJ.LT.1) GO TO 3575
      IF((NBX.LE.1).OR.(NBY.LE.1)) GO TO 3400
      DO 3375 I=2,NBX
      DO 3375 J=2,NBY
      L=((I-1)*(NBY+1)+(J-1))*6
       DO 3350 K=1,INN
       KN(K,IN+1)=KM(K,L+1)+KM(K,L+4)
       KN(K,IN+2)=KM(K,L+2)+KM(K,L+5)
3350   KN(K,IN+3)=KM(K,L+3)+KM(K,L+6)
      IN=IN+3
3375  CONTINUE
3400  CONTINUE
      IF(NBX.LE.1) GO TO 3475
      DO 3450 I=2,NBX
      L=6*(I-1)*(NBY+1)
      LL=NBY*6+L
      IF(LY) GO TO 3430
      DO 3425 K=1,INN
      KN(K,IN+1)=KM(K,L+1)+KM(K,L+4)+KM(K,LL+1)+KM(K,LL+4)
      KN(K,IN+2)=KM(K,L+2)+KM(K,L+5)+KM(K,LL+2)+KM(K,LL+5)
3425  KN(K,IN+3)=KM(K,L+3)+KM(K,L+6)+KM(K,LL+3)+KM(K,LL+6)
      IN=IN+3
      GO TO 3450
3430  CONTINUE
```

```fortran
      IF(ISYM.EQ.1) GO TO 3445
      DO 3440 K=1,INN
      KN(K,IN+1)=KM(K,L+1)+KM(K,L+4)
      KN(K,IN+2)=KM(K,L+3)+KM(K,L+6)
      KN(K,IN+3)=KM(K,LL+1)+KM(K,LL+4)
 3440 KN(K,IN+4)=KM(K,LL+3)+KM(K,LL+6)
      IN=IN+4
      GO TO 3449
 3445 CONTINUE
      DO 3447 K=1,INN
      KN(K,IN+1)=KM(K,L+2)+KM(K,L+5)
 3447 KN(K,IN+2)=KM(K,LL+2)+KM(K,LL+5)
      IN=IN+2
 3449 CONTINUE
 3450 CONTINUE
 3475 CONTINUE
      IF(NBY.LE.1) GO TO 3510
      DO 3500 J=2,NBY
      L=6*(J-1)
      LL=6*NBX*(NBY+1)+L
      IF(LX) GO TO 3490
      DO 3480 K=1,INN
      KN(K,IN+1)=KM(K,L+1)+KM(K,L+4)+KM(K,LL+1)+KM(K,LL+4)
      KN(K,IN+2)=KM(K,L+2)+KM(K,L+5)+KM(K,LL+2)+KM(K,LL+5)
 3480 KN(K,IN+3)=KM(K,L+3)+KM(K,L+6)+KM(K,LL+3)+KM(K,LL+6)
      IN=IN+3
      GO TO 3500
 3490 CONTINUE
      IF(ISYM.EQ.1) GO TO 3496
      DO 3495 K=1,INN
      KN(K,IN+1)=KM(K,L+2)+KM(K,L+5)
      KN(K,IN+2)=KM(K,L+3)+KM(K,L+6)
      KN(K,IN+3)=KM(K,LL+2)+KM(K,LL+5)
 3495 KN(K,IN+4)=KM(K,LL+3)+KM(K,LL+6)
      IN=IN+4
      GO TO 3499
 3496 CONTINUE
      DO 3497 K=1,INN
      KN(K,IN+1)=KM(K,L+1)+KM(K,L+4)
 3497 KN(K,IN+2)=KM(K,LL+1)+KM(K,LL+4)
      IN=IN+2
 3499 CONTINUE
 3500 CONTINUE
 3510 CONTINUE
      IF(.NOT.LY) GO TO 3550
      L=6*NBY
      LL=L+6*NBX*(NBY+1)
      IF(ISYM.EQ.1) GO TO 3530
      DO 3520 K=1,INN
      KN(K,IN+1)=KM(K,L+1)+KM(K,L+4)+KM(K,LL+1)+KM(K,LL+4)
 3520 KN(K,IN+2)=KM(K,L+3)+KM(K,L+6)+KM(K,LL+3)+KM(K,LL+6)
      IN=IN+2
      GO TO 3540
 3530 CONTINUE
      DO 3535 K=1,INN
 3535 KN(K,IN+1)=KM(K,L+2)+KM(K,L+5)+KM(K,LL+2)+KM(K,LL+5)
      IN=IN+1
 3540 CONTINUE
 3550 CONTINUE
      IF(.NOT.LX) GO TO 3570
```

```fortran
      L=6*NBX*(NBY+1)
      LL=L+6*NBY
      IF(ISYM.EQ.1) GO TO 3565
      DO 3560 K=1,INN
      KN(K,IN+1)=KM(K,L+2)+KM(K,L+5)+KM(K,LL+2)+KM(K,LL+5)
 3560 KN(K,IN+2)=KM(K,L+3)+KM(K,L+6)+KM(K,LL+3)+KM(K,LL+6)
      IN=IN+2
      GO TO 3569
 3565 CONTINUE
      DO 3566 K=1,INN
 3566 KN(K,IN+1)=KM(K,L+1)+KM(K,L+4)+KM(K,LL+1)+KM(K,LL+4)
      IN=IN+1
 3569 CONTINUE
 3570 CONTINUE
C
C GET UNCONSTRAINED DISPLACEMENTS FOR 6 UNIT STRAIN CASES
C
      IZ=0
      CALL GELIM(MMM,IJ,KN,7,FS,IP,IZ,WK,IERR)
C
C GET A COMPLETE SET OF TOTAL DISPLACEMENTS
C
 3575 IN=0
 3590 IF((NBX.LE.1).OR.(NBY.LE.1)) GO TO 3650
      DO 3625 I=2,NBX
      DO 3625 J=2,NBY
      LL=(I*NBY+I+J-NBY-2)*6
      DO 3600 K=1,3
      KP=K+3
      DO 3600 L=1,6
      UVW(LL+K,L)=UVW(LL+K,L)-FS(IN+K,L)
 3600 UVW(LL+KP,L)=UVW(LL+KP,L)-FS(IN+K,L)
      IN=IN+3
 3625 CONTINUE
 3650 IF(NBX.LE.1) GO TO 3750
      DO 3740 I=2,NBX
      L=6*(I-1)*(NBY+1)
      LL=L+NBY*6
      IF(LY) GO TO 3710
      DO 3700 K=1,3
      KP=K+3
      DO 3700 M=1,6
      UVW(L+K,M) =UVW(L+K,M) -FS(IN+K,M)
      UVW(L+KP,M) =UVW(L+KP,M) -FS(IN+K,M)
      UVW(LL+K,M)=UVW(LL+K,M)-FS(IN+K,M)
 3700 UVW(LL+KP,M)=UVW(LL+KP,M)-FS(IN+K,M)
      IN=IN+3
      GO TO 3740
 3710 CONTINUE
      IF(ISYM.EQ.1) GO TO 3730
      DO 3720 M=1,6
      UVW(L+1,M)=UVW(L+1,M)-FS(IN+1,M)
      UVW(L+3,M)=UVW(L+3,M)-FS(IN+2,M)
      UVW(L+4,M)=UVW(L+4,M)-FS(IN+1,M)
      UVW(L+6,M)=UVW(L+6,M)-FS(IN+2,M)
      UVW(LL+1,M)=UVW(LL+1,M)-FS(IN+3,M)
      UVW(LL+3,M)=UVW(LL+3,M)-FS(IN+4,M)
      UVW(LL+4,M)=UVW(LL+4,M)-FS(IN+3,M)
 3720 UVW(LL+6,M)=UVW(LL+6,M)-FS(IN+4,M)
      IN=IN+4
```

```fortran
      GO TO 3737
 3730 CONTINUE
      DO 3735 M=1,6
      UVW(L+2,M)=UVW(L+2,M)-FS(IN+1,M)
      UVW(L+5,M)=UVW(L+5,M)-FS(IN+1,M)
      UVW(LL+2,M)=UVW(LL+2,M)-FS(IN+2,M)
 3735 UVW(LL+5,M)=UVW(LL+5,M)-FS(IN+2,M)
      IN=IN+2
 3737 CONTINUE
 3740 CONTINUE
 3750 IF(NBY.LE.1) GO TO 3850
      DO 3845 J=2,NBY
      L= 6*(J-1)
      LL=L+ 6*(NBY+1)*NBX
      IF(LX) GO TO 3810
      DO 3800 K=1,3
      KP=K+3
      DO 3800 M=1,6
      UVW(L+K,M) =UVW(L+K,M) -FS(IN+K,M)
      UVW(L+KP,M) =UVW(L+KP,M) -FS(IN+K,M)
      UVW(LL+K,M) =UVW(LL+K,M) -FS(IN+K,M)
 3800 UVW(LL+KP,M) =UVW(LL+KP,M) -FS(IN+K,M)
      IN=IN+3
      GO TO 3845
 3810 CONTINUE
      IF(ISYM.EQ.1) GO TO 3825
      DO 3820 M=1,6
      UVW(L+2,M)=UVW(L+2,M)-FS(IN+1,M)
      UVW(L+3,M)=UVW(L+3,M)-FS(IN+2,M)
      UVW(L+5,M)=UVW(L+5,M)-FS(IN+1,M)
      UVW(L+6,M)=UVW(L+6,M)-FS(IN+2,M)
      UVW(LL+2,M)=UVW(LL+2,M)-FS(IN+3,M)
      UVW(LL+3,M)=UVW(LL+3,M)-FS(IN+4,M)
      UVW(LL+5,M)=UVW(LL+5,M)-FS(IN+3,M)
 3820 UVW(LL+6,M)=UVW(LL+6,M)-FS(IN+4,M)
      IN=IN+4
      GO TO 3835
 3825 CONTINUE
      DO 3830 M=1,6
      UVW(L+1,M)=UVW(L+1,M)-FS(IN+1,M)
      UVW(L+4,M)=UVW(L+4,M)-FS(IN+1,M)
      UVW(LL+1,M)=UVW(LL+1,M)-FS(IN+2,M)
 3830 UVW(LL+4,M)=UVW(LL+4,M)-FS(IN+2,M)
      IN=IN+2
 3835 CONTINUE
 3845 CONTINUE
 3850 CONTINUE
      IF(.NOT.LY) GO TO 3870
      L=6*NBY
      LL=L+6*NBX*(NBY+1)
      IF(ISYM.EQ.1) GO TO 3865
      DO 3860 M=1,6
      UVW(L+1,M)=UVW(L+1,M)-FS(IN+1,M)
      UVW(L+3,M)=UVW(L+3,M)-FS(IN+2,M)
      UVW(L+4,M)=UVW(L+4,M)-FS(IN+1,M)
      UVW(L+6,M)=UVW(L+6,M)-FS(IN+2,M)
      UVW(LL+1,M)=UVW(LL+1,M)-FS(IN+1,M)
      UVW(LL+3,M)=UVW(LL+3,M)-FS(IN+2,M)
      UVW(LL+4,M)=UVW(LL+4,M)-FS(IN+1,M)
 3860 UVW(LL+6,M)=UVW(LL+6,M)-FS(IN+2,M)
```

```
         IN=IN+2
         GO TO 3869
 3865 CONTINUE
         DO 3866 M=1,6
         UVW(L+2,M)=UVW(L+2,M)-FS(IN+1,M)
         UVW(L+5,M)=UVW(L+5,M)-FS(IN+1,M)
         UVW(LL+2,M)=UVW(LL+2,M)-FS(IN+1,M)
 3866 UVW(LL+5,M)=UVW(LL+5,M)-FS(IN+1,M)
         IN=IN+1
 3869 CONTINUE
 3870 CONTINUE
         IF(.NOT.LX) GO TO 3890
         L=6*NBX*(NBY+1)
         LL=L+6*NBY
         IF(ISYM.EQ.1) GO TO 3885
         DO 3880 M=1,6
         UVW(L+2,M)=UVW(L+2,M)-FS(IN+1,M)
         UVW(L+3,M)=UVW(L+3,M)-FS(IN+2,M)
         UVW(L+5,M)=UVW(L+5,M)-FS(IN+1,M)
         UVW(L+6,M)=UVW(L+6,M)-FS(IN+2,M)
         UVW(LL+2,M)=UVW(LL+2,M)-FS(IN+1,M)
         UVW(LL+3,M)=UVW(LL+3,M)-FS(IN+2,M)
         UVW(LL+5,M)=UVW(LL+5,M)-FS(IN+1,M)
 3880 UVW(LL+6,M)=UVW(LL+6,M)-FS(IN+2,M)
         IN=IN+2
         GO TO 3889
 3885 CONTINUE
         DO 3886 M=1,6
         UVW(L+1,M)=UVW(L+1,M)-FS(IN+1,M)
         UVW(L+4,M)=UVW(L+4,M)-FS(IN+1,M)
         UVW(LL+1,M)=UVW(LL+1,M)-FS(IN+1,M)
 3886 UVW(LL+4,M)=UVW(LL+4,M)-FS(IN+1,M)
         IN=IN+1
 3889 CONTINUE
 3890 CONTINUE
C
C COMPUTE NODAL FORCES
C
         IF(NP.LT.1) GO TO 3950
         DO 3900 I=1,NP
         DO 3900 J=1,6
         FB(I,J)=0.0
         DO 3900 K=1,NP
 3900 FB(I,J)=FB(I,J)+KB(I,K)*UVW(K,J)
 3950 CONTINUE
C
C COMPUTE SIDE LOADS FOR EACH OF THE 6 UNIT STRAIN CASES
C
         YLC=YL*C
         XLC=XL*C
         DO 4500 I=1,6
          DO 4200 J=1,NBY+1
          K=(J-1)*6
          FT(1,I)=FT(1,I)+FB(K+1,I)+FB(K+4,I)
          FT(4,I)=FT(4,I)+FB(K+2,I)+FB(K+5,I)
 4200    FT(6,I)=FT(6,I)+FB(K+3,I)+FB(K+6,I)
          FT(1,I)=-FT(1,I)/YLC
          FT(4,I)=-FT(4,I)/YLC
          FT(6,I)=-FT(6,I)/YLC
           DO 4300 J=1,NBX+1
```

```
              K=(NBY+1)*(J-1)*6
                FT(2,I)=FT(2,I)+FB(K+2,I)+FB(K+5,I)
  4300        FT(5,I)=FT(5,I)+FB(K+3,I)+FB(K+6,I)
              FT(2,I)=-FT(2,I)/XLC
              FT(5,I)=-FT(5,I)/XLC
                DO 4400 J=1,NBX+1
                DO 4400 K=1,NBY+1
                L=((NBY+1)*(J-1)+(K-1))*6
  4400        FT(3,I)=FT(3,I)+FB(L+3,I)
              FT(3,I)=-FT(3,I)/(XL*YL)
  4500 CONTINUE
        IF(ISYM.EQ.0) THEN
        DO 4600 I=1,6
        DO 4600 J=1,6
        TF(I,J)=FT(I,J)
  4600 FT(I,J)=0.0
        END IF
        IF((LX.OR.LY).AND.(ISYM.EQ.0)) GO TO 2440
        IF(ISYM.EQ.1) THEN
        DO 4700 I=1,6
        TF(I,4)=FT(I,4)
        IF(LY) TF(I,5)=FT(I,5)
  4700 IF(LX) TF(I,6)=FT(I,6)
        END IF
        DO 4800 I=1,6
        DO 4800 J=1,6
  4800 FT(I,J)=TF(I,J)
C
C CALCULATE THE ELASTIC CONSTANTS OF THE UNIT CELL
C
        CALL MATOPS(KA,FT,DET,HH)
        EX=1.0/FT(1,1)
        EY=1.0/FT(2,2)
        EZ=1.0/FT(3,3)
        GXY=1.0/FT(4,4)
        GYZ=1.0/FT(5,5)
        GXZ=1.0/FT(6,6)
        PRXY=-FT(1,2)/FT(2,2)
        PRXZ=-FT(1,3)/FT(3,3)
        PRYZ=-FT(2,3)/FT(3,3)
        MIXXY=FT(4,1)/FT(1,1)
        MIXXZ=FT(6,1)/FT(1,1)
        MIXYZ=FT(5,1)/FT(1,1)
        MIYXY=FT(4,2)/FT(2,2)
        MIYXZ=FT(6,2)/FT(2,2)
        MIYYZ=FT(5,2)/FT(2,2)
        MIZXY=FT(4,3)/FT(3,3)
        MIZXZ=FT(6,3)/FT(3,3)
        MIZYZ=FT(5,3)/FT(3,3)
        CXYXZ=FT(4,5)/FT(5,5)
        CXYYZ=FT(4,6)/FT(6,6)
        CXZYZ=FT(5,6)/FT(6,6)
        WRITE(6,9560)
        WRITE(6,9560)
        WRITE(6,9600)
        WRITE(6,9560)
        WRITE(6,9500) EX,EY,EZ
        WRITE(6,9510) GYZ,GXZ,GXY
        WRITE(6,9520) PRYZ,PRXZ,PRXY
        WRITE(6,9530) MIXYZ,MIYYZ,MIZYZ
```

```
      WRITE(6,9540) MIXXZ,MIYXZ,MIZXZ
      WRITE(6,9550) MIXXY,MIYXY,MIZXY
      WRITE(6,9550) MIXXY,MIYXY,MIZXY
      WRITE(6,9560)
      WRITE(6,9560)
 9000 FORMAT(F12.5)
 9005 FORMAT(1H ,8F9.3)
 9010 FORMAT(F12.2)
 9020 FORMAT(6F12.2)
 9030 FORMAT(I5)
 9031 FORMAT(3I5)
 9040 FORMAT(L5)
 9050 FORMAT(1H ,'SYMMETRY ABOUT YZ PLANE (T OR F)')
 9055 FORMAT(1H ,'SYMMETRY ABOUT XZ PLANE (T OR F)')
 9060 FORMAT(1H ,'INPUT SUBCELL ID. NO. AT LOCATION',2I4)
 9070 FORMAT(1H ,'INPUT SUBCELL ROTATION CODE NO. AT',2I4)
 9080 FORMAT(1H ,'INPUT NO. SUBCELLS (X DIR.) IN UNIT CELL')
 9090 FORMAT(1H ,'INPUT NO. SUBCELLS (Y DIR.) IN UNIT CELL')
 9100 FORMAT(1H ,'INPUT NO. COMPOSITE MATERIALS NEEDED,NM')
 9110 FORMAT(1H ,'INPUT NO. OF MASTER SUBCELLS NEEDED,NB')
 9120 FORMAT(1H ,'INPUT E IN FIBER DIRECTION')
 9130 FORMAT(1H ,'INPUT E NORMAL TO FIBER DIRECTION')
 9140 FORMAT(1H ,'INPUT MAJOR POISSONS RATIO IN LT PLANE')
 9150 FORMAT(1H ,'INPUT POISSONS RATIO IN TT PLANE')
 9160 FORMAT(1H ,'INPUT SHEAR MODULUS G IN LT PLANE')
 9170 FORMAT(1H ,'INPUT SHEAR MODULUS G IN TT PLANE')
 9180 FORMAT(1H ,'SELECT A MATERIAL NUMBER FROM ONE TO TEN')
 9190 FORMAT(1H ,'MATERIAL PROPERTY DATA ECHO')
 9200 FORMAT(1H ,'GRID GEOMETRY FOR SUBCELL NUMBER ',I5)
 9210 FORMAT(1H ,'INPUT SIDE LENGTH OF SUBCELL (X DIR.)')
 9220 FORMAT(1H ,'INPUT SIDE LENGTH OF SUBCELL (Y DIR.)')
 9230 FORMAT(1H ,'INPUT HEIGHT OF SUBCELL (Z DIR.)')
 9240 FORMAT(1H ,'INPUT NO. INTEG/PTS. ON SUBCELL (X DIR.)')
 9250 FORMAT(1H ,'INPUT NO. INTEG/PTS. ON SUBCELL (Y DIR.)')
 9260 FORMAT(1H ,'INPUT NO. INTEG/PTS. ON SUBCELL (Z DIR.)')
 9270 FORMAT(1H ,'INPUT DELTA X IN % FOR INTERVAL NO. ',I5)
 9280 FORMAT(1H ,'INPUT DELTA Y IN % FOR INTERVAL NO. ',I5)
 9290 FORMAT(1H ,'INPUT DELTA Z IN % FOR INTERVAL NO. ',I5)
 9300 FORMAT(1H ,'***')
 9310 FORMAT(1H ,'INPUT NO. OF MATLS.IN SUBCELL NO.',I5)
 9320 FORMAT(1H ,'SPECIFY THE CURRENT MATL. ID. NO.')
 9330 FORMAT(1H ,'SUBCELL HT. NOT EQUAL UNIT CELL HT.')
 9390 FORMAT(1H ,'INPUT 1ST SPH. FIBER ANG. AT GRID PT.',3I4)
 9400 FORMAT(1H ,'INPUT 2ND SPH. FIBER ANG. AT GRID PT.',3I4)
 9420 FORMAT(1H ,'INPUT OCTANT NO. AT GRID NO.',3I4)
 9430 FORMAT(1H ,'INPUT MATL. VOL/FR. AT OCTANT NO.',I5)
 9440 FORMAT(1H ,'INPUT SIDE LENGTH OF UNIT CELL IN X DIR.')
 9450 FORMAT(1H ,'INPUT SIDE LENGTH OF UNIT CELL IN Y DIR.')
 9460 FORMAT(1H ,'INPUT DIST.(%) ORIGIN TO UNIT CELL NODE',I3)
 9470 FORMAT(1H ,'INPUT THICKNESS OF UNIT CELL IN INCHES')
 9480 FORMAT(1H ,'INPUT 1ST FIBER SPHERICAL ANGLE')
 9490 FORMAT(1H ,'INPUT 2ND FIBER SPHERICAL ANGLE')
 9500 FORMAT(1H ,'EX,EY,EZ = ',3F12.2)
 9510 FORMAT(1H ,'GYZ,GXZ,GXY = ',3F12.2)
 9520 FORMAT(1H ,'MUZY,MUZY,MUYX = ',3F12.4)
 9530 FORMAT(1H ,'NUYZ,X ; NUYZ,Y ; NUYZ,Z = ',3F12.4)
 9540 FORMAT(1H ,'NUXZ,X ; NUXZ,Y ; NUXZ,Z = ',3F12.4)
 9550 FORMAT(1H ,'NUXY,X ; NUXY,Y ; NUXY,Z = ',3F12.4)
 9560 FORMAT(1H )
 9600 FORMAT(1H ,13X,'ELASTIC CONSTANTS OF THE COMPOSITE ')
```

```
 5000 END
C
C SUBROUTINE TO TRANSFORM THE SUBCELL STIFFNESS MATRIX
C
      SUBROUTINE TRNS(QT,KS)
      DIMENSION SK(24,24)
      REAL KS(24,24)
      INTEGER QT
 7117 FORMAT(1H ,'IN SUB TRNS, QT=',I3)
      IF(QT.GE.100) THEN
      DO 10 I=1,3
       SN=1.0
      IF (I.EQ.3) SN=-1.0
      DO 10 J=1,24
      SK(I,J)=KS(I+3,J)*SN
      SK(I+3,J)=KS(I,J)*SN
      SK(I+6,J)=KS(I+9,J)*SN
      SK(I+9,J)=KS(I+6,J)*SN
      SK(I+12,J)=KS(I+15,J)*SN
      SK(I+15,J)=KS(I+12,J)*SN
      SK(I+18,J)=KS(I+21,J)*SN
   10 SK(I+21,J)=KS(I+18,J)*SN
      DO 20 J=1,3
      SN=1.0
      IF(J.EQ.3) SN=-1.0
      DO 20 I=1,24
      KS(I,J)=SK(I,J+3)*SN
      KS(I,J+3)=SK(I,J)*SN
      KS(I,J+6)=SK(I,J+9)*SN
      KS(I,J+9)=SK(I,J+6)*SN
      KS(I,J+12)=SK(I,J+15)*SN
      KS(I,J+15)=SK(I,J+12)*SN
      KS(I,J+18)=SK(I,J+21)*SN
   20 KS(I,J+21)=SK(I,J+18)*SN
      QT=QT-100
      END IF
      IF(QT.GE.10) THEN
      DO 100 I=1,3
      SN=-1.0
      IF(I.EQ.1) SN=1.0
      DO 100 J=1,24
      SK(I,J)=KS(I+9,J)*SN
      SK(I+3,J)=KS(I+6,J)*SN
      SK(I+6,J)=KS(I+3,J)*SN
      SK(I+9,J)=KS(I,J)*SN
      SK(I+12,J)=KS(I+21,J)*SN
      SK(I+15,J)=KS(I+18,J)*SN
      SK(I+18,J)=KS(I+15,J)*SN
  100 SK(I+21,J)=KS(I+12,J)*SN
      DO 200 J=1,3
      SN=-1.0
      IF(J.EQ.1) SN=1.0
      DO 200 I=1,24
      KS(I,J)=SK(I,J+9)*SN
      KS(I,J+3)=SK(I,J+6)*SN
      KS(I,J+6)=SK(I,J+3)*SN
      KS(I,J+9)=SK(I,J)*SN
      KS(I,J+12)=SK(I,J+21)*SN
      KS(I,J+15)=SK(I,J+18)*SN
      KS(I,J+18)=SK(I,J+15)*SN
```

116

```
  200 KS(I,J+21)=SK(I,J+12)*SN
      QT=QT-10
      END IF
      IF((QT.EQ.1).OR.(QT.EQ.3)) THEN
      DO 300 I=1,3
      SN=1.0
      IF(I.EQ.2) SN=-1.0
      IF(I.EQ.1) II=I+1
      IF(I.EQ.2) II=I-1
      IF(I.EQ.3) II=I
      DO 300 J=1,24
      SK(I    ,J)=KS(II+12,J)*SN
      SK(I+3 ,J)=KS(II+15,J)*SN
      SK(I+6 ,J)=KS(II    ,J)*SN
      SK(I+9 ,J)=KS(II+3 ,J)*SN
      SK(I+12,J)=KS(II+18,J)*SN
      SK(I+15,J)=KS(II+21,J)*SN
      SK(I+18,J)=KS(II+6 ,J)*SN
  300 SK(I+21,J)=KS(II+9 ,J)*SN
      DO 400 J=1,3
      SN=1.0
      IF(J.EQ.2) SN=-1.0
      IF(J.EQ.1) JJ=J+1
      IF(J.EQ.2) JJ=J-1
      IF(J.EQ.3) JJ=J
      DO 400 I=1,24
      KS(I,J    )=SK(I,JJ+12)*SN
      KS(I,J+3 )=SK(I,JJ+15)*SN
      KS(I,J+6 )=SK(I,JJ    )*SN
      KS(I,J+9 )=SK(I,JJ+3 )*SN
      KS(I,J+12)=SK(I,JJ+18)*SN
      KS(I,J+15)=SK(I,JJ+21)*SN
      KS(I,J+18)=SK(I,JJ+6 )*SN
  400 KS(I,J+21)=SK(I,JJ+9 )*SN
      END IF
      IF((QT.EQ.2).OR.(QT.EQ.3)) THEN
      DO 500 I=1,3
      SN=-1.0
      IF(I.EQ.3) SN=1.0
      DO 500 J=1,24
      SK(I,J)=KS(I+18,J)*SN
      SK(I+3,J)=KS(I+21,J)*SN
      SK(I+6,J)=KS(I+12,J)*SN
      SK(I+9,J)=KS(I+15,J)*SN
      SK(I+12,J)=KS(I+6,J)*SN
      SK(I+15,J)=KS(I+9,J)*SN
      SK(I+18,J)=KS(I,J)*SN
  500 SK(I+21,J)=KS(I+3,J)*SN
      DO 600 J=1,3
      SN=-1.0
      IF(J.EQ.3) SN=1.0
      DO 600 I=1,24
      KS(I,J)=SK(I,J+18)*SN
      KS(I,J+3)=SK(I,J+21)*SN
      KS(I,J+6)=SK(I,J+12)*SN
      KS(I,J+9)=SK(I,J+15)*SN
      KS(I,J+12)=SK(I,J+6)*SN
      KS(I,J+15)=SK(I,J+9)*SN
      KS(I,J+18)=SK(I,J)*SN
  600 KS(I,J+21)=SK(I,J+3)*SN
```

```
          END IF
  900 RETURN
          END
C
C MATRIX INVERSION
C
          SUBROUTINE INV(AK)
          DIMENSION KA(7),AK(9,9)
          KA(1)=10
          KA(2)=9
          KA(3)=9
          KA(4)=1
          KA(5)=9
          KA(6)=0
          KA(7)=0
          CALL MATOPS(KA,AK,DET,DUMMY)
          RETURN
          END
/
```

APPENDIX II - INPUT DATA FORMAT

This program operates interactively and is largely self-explanatory. The first block of input data establishes a 2-D array containing principal elastic constants for each different material needed in the run. Each material is assumed to be orthotropic with a principal plane of isotropy. Therefore, only six elastic constants (per material) must be specified. The first input is an integer between one and ten quantifying the number of materials needed for the run. This number sizes the array that contains the elastic constants of each material. For convenience six sets of elastic constants reside in the program in the form of data statements:

1. High Modulus Graphite/Epoxy (E_1 = 30 msi)
2. Intermediate Modulus Graphite/Epoxy (E_1 = 25 msi)
3. Low Modulus Graphite/Epoxy (E_1 = 20 msi)
4. Fiberglass/Epoxy (E_1 = 10 msi)
5. Aluminum (E = 10 msi)
6. Bulk Epoxy (E = .5 msi)

When called for, by integer 1-6, the corresponding set of elastic constants is inserted into the next empty row of the material property array. The material calling sequence establishes a new material numbering sequence for subsequent use. Any material may be requested more than once. If a material number between 7 and 10, inclusive, is requested the program immediately asks for six elastic constants to be input. Young's modulus in the reinforcement direction is requested first, followed by Young's modulus in the plane of isotropy. Then the program requests two Poisson's ratios: first, that which specifies contraction normal to fiber direction (per unit strain in the fiber direction); second, that which relates to the plane of isotropy. Finally, two shear moduli are requested: first, in a plane

containing the fiber principal axis; second, in the plane of isotropy. The material sequencing then resumes. The number of materials listed must equal the initial input integer specifying the number of materials to be used.

The next number requested (an integer from one to ten) establishes the total number of master subcells needed to build the unit cell.

The next block of input data establishes size, subcell division, and subcell content of the unit cell model. This data describes the unit cell as a 2-D compartmented container for subcells. The first number (an integer from one to ten) specifies the number of subcell compartments in the unit cell, as the cell is traversed in the x-direction (Figure 38). The second integer specifies the number of subcell compartments in the y direction. The program assumes single subcell thickness in the z-direction of the unit cell. (Other versions of this program allow more than one subcell in the thickness direction.)

The next series of real numbers establish dimensions of all unit cell compartments. The first number sets unit cell height, i.e., ply thickness and subcell height. The second real number sets the x-parallel side length of the unit cell. This number is followd by a sequence of percentages (0.0 to 100.0) specifying the fractions of x-parallel side length from the origin to the largest x-dimension within each subcell (Figure 38).

The next set of real numbers establishes the same dimensions along a y-parallel side of the unit cell. Numbers and sizes of all unit cell compartments are now fixed. The next pair of integers specifies both the type of master subcell associated with the first compartment of the unit cell and the type of coordinate transformation to be performed on that master subcell (prior to placement in that unit cell compartment). The first integer (specifying subcell type) also tacitly establishes the sequence of master subcell descriptions that follow. The second

integer selects the desired subcell coordinate transformation according to the following code:

Integer	Transformation (When viewed from the subcell origin, looking in the + direction along a coordinate axis)
-1	No subcell inserted
0	No subcell transformation necessary
1	Rotation of 90° CCW about z axis
2	Rotation of 180° CCW about z axis
3	Rotation of 270° CCW about z axis
1X	Rotation of 270° CCW about x axis (plus whichever one of the previous transformations is specified by X)
1XX	Reversal of the z axis (plus whichever one of the previous transformations is specified by XX)

CW   Indicates clockwise transformation
CCW Indicates counterclockwise transformation

Subsequent pairs of integers are coded in the order shown in Figure 39 until all the compartments of the unit cell are filled with transformed subcells. There is no way to put more than one subcell in a compartment. This completes the description of the unit cell.

It remains to describe the details of material placement within each master subcell. To facilitate this task an outer do-loop is established over the number of master subcells. Each master subcell stiffness matrix is then formed by an inner do-loop ranging over the number of materials in that subcell. The volume integration associated with $\iiint [B]^T [D] [B] \, d(vol)$ is performed separately for each material. The same integration scheme and 3-D integration network is used for each material in the subcell. However, different integration networks can be used

121

for different master subcells. What follows pertains to the integration grid dimensions for the first master subcell.

The next real number input is the integration grids dimension in the x-direction, followed by an integer that specifies the number of integration points on the x-axis. This is followed by a sequence of percentages (0.0 to 100.00) specifying the fraction of the overall grid dimension represented by the distance of each x-axis integration point from the origin (except for the first and last values which are assumed to be 0.0% and 100.0%).

The next two batches of input data repeat this same information for the integration grid points along the y-axis and along the z-axis. Subsequently, an integer is specified establishing the number of materials in the first master subcell. This sets the upper limit on the inner do-loop that begins at this point.

The first integer related to the inner do-loop is a material number. This selects a set of material properties from that row of the material property matrix. The program is now ready for detailed information on fiber orientation and amount of material at each integration point. First, two spherical angles (ϕ_1,ϕ_2 in degrees) specifying fiber direction (Figure 11) at the first integration point, are input, followed by the volume fraction of each octant of volume surrounding that integration point that contains the material of interest. These volume fractions are determined by examining photomicrographs of the actual composite and unit cell models constructed from the same photomicrographs. To save time each octant volume fraction is read in by means of a two number code. The first number specifies which of the eight octants is being referenced. Octant one is the +++ octant, octant two the ++- one, octant three the +-+ one, octant four the +-- one, octant five the -++ one, octant six the -+- one, octant seven the --+ one, and

octant eight the --- one (Figure 12). A negative octant reference means skip to the next integration point. Any octant reference number between one and eight must be followed by a real number (between 0.0 and 1.0) specifying the volume fraction of current material occupying that octant of that integration point.

The sequence of points over which the intregration ranges is fixed. The first point is always the origin. The path then runs along the plus z-axis, returns to the next integration point along the y-axis, and moves in the plus z-direction again, etc. (Figure 40). When the farthest integration point from the origin is reached the program returns to the start of the inner do loop for the inclusion of the next material within that master subcell. When all materials in the master subcell have been allotted to the various integration points, the program returns to the outer do loop to repeat the same input data pattern for the next master subcell. When all the master subcells have been described the program proceeds to calculate the unit cell moduli.

Sample Problem

As an example of data input/output consider the previous model of the plain weave microgeometry based on diamond shaped tow cross-sections (Figure 24). Only one master subcell is required. The unit cell consists of 16 inhomogeneous finite elements. Their eight-node stiffness matrices are all transformations of the master subcell stiffness matrix. For simplicity the master subcell may be considered to be a unit cube containing 50% bulk matrix material and 50% unidirectional composite tow material.

The unit cell, before the subcells are inserted, may be considered to be an empty, four by four, compartmented container (Figure 24). The first subcell is placed in the first compartment bounded by the planes x=0, x=1, y=0, y=1. The first subcells is the untransformed master subcell. The second subcell is placed in the second compartment bounded by the planes x=0, x=1, y=1, y=2. It is a transformed master subcell. The transformation consists of a rotation of 90° about an axis normal to the middle plane of the fabric plus a reflections about the middle plane. The third subcell is placed in compartment x=0, x=1, y=2, y=3. It is a master subcell reflected about the fabric middle plane; etc.

The following sequence of prompts and inputs leads to the composite moduli predictions that follow. All input values are enclosed in double brackets. Most of the master subcell inputs come from Table 2.

```
INPUT NO. COMPOSITE MATERIALS NEEDED, NM
       ((3))
SELECT A MATERIAL NUMBER FROM ONE TO TEN
       ((3))
SELECT A MATERIAL NUMBER FROM ONE TO TEN
       ((3))
SELECT A MATERIAL NUMBER FROM ONE TO TEN
       ((6))
MATERIAL PROPERTY DATA ECHO
20000000.00   1500000.00      .30      .45    700000.00    700000.00
20000000.00   1500000.00      .30      .45    700000.00    700000.00
  500000.00    500000.00      .35      .35    185000.00    185000.00
INPUT NO. OF MASTER SUBCELLS NEEDED, NB
       ((1))
INPUT NO. SUBCELLS (X DIR.) IN UNIT CELL
       ((4))
INPUT NO. SUBCELLS (Y DIR.) IN UNIT CELL
       ((4))
INPUT THICKNESS OF UNIT CELL IN INCHES
       ((1.0))
INPUT THICKNESS OF UNIT CELL IN X DIRECTION
       ((4.0))
INPUT DIST. (%) ORIGIN TO UNIT CELL NODE    2
       ((25.0))
INPUT DIST. (%) ORIGIN TO UNIT CELL NODE    3
       ((50.0))
INPUT DIST. (%) ORIGIN TO UNIT CELL NODE    4
       ((75.0))
INPUT SIDE LENGTH OF UNIT CELL IN Y DIRECTION
       ((4.0))
INPUT DIST. (%) ORIGIN TO UNIT CELL NODE    2
       ((25.0))
INPUT DIST. (%) ORIGIN TO UNIT CELL NODE    3
       ((50.0))
INPUT DIST. (%) ORIGIN TO UNIT CELL NODE    4
       ((75.0))
INPUT SUBCELL ID. NO. AT LOCATION    1    1
       ((1))
INPUT SUBCELL ROTATION CODE NO. AT    1    1
       ((0))
INPUT SUBCELL ID. NO. AT LOCATION    1    2
       ((1))
INPUT SUBCELL ROTATION CODE NO. AT  1    2
       ((101))
INPUT SUBCELL ID. NO. AT LOCATION    1    3
       ((1))
INPUT SUBCELL ROTATION CODE NO. AT  1    3
       ((100))
INPUT SUBCELL ID. NO. AT LOCATION    1    4
       ((1))
INPUT SUBCELL ROTATION CODE NO. AT  1    4
       ((1))
INPUT SUBCELL ID. NO. AT LOCATION    2    1
       ((1))
```

```
INPUT SUBCELL ROTATION CODE NO. AT   2   1
     ((103))
INPUT SUBCELL ID. NO. AT LOCATION    2   2
     ((1))
INPUT SUBCELL ROTATION CODE NO. AT   2   2
     ((2))
INPUT SUBCELL ID. NO. AT LOCATION    2   3
     ((1))
INPUT SUBCELL ROTATION CODE NO. AT   2   3
     ((3))
INPUT SUBCELL ID. NO. AT LOCATION    2   4
     ((1))
INPUT SUBCELL ROTATION CODE NO. AT   2   4
     ((102))
INPUT SUBCELL ID. NO. AT LOCATION    3   1
     ((1))
INPUT SUBCELL ROTATION CODE NO. AT   3   1
     ((100))
INPUT SUBCELL ID. NO. AT LOCATION    3   2
     ((1))
INPUT SUBCELL ROTATION CODE NO. AT   3   2
     ((1))
INPUT SUBCELL ID. NO. AT LOCATION    3   3
     ((1))
INPUT SUBCELL ROTATION CODE NO. AT   3   3
     ((0))
INPUT SUBCELL ID. NO. AT LOCATION    3   4
     ((1))
INPUT SUBCELL ROTATION CODE NO. AT   3   4
     ((101))
INPUT SUBCELL ID. NO. AT LOCATION    4   1
     ((1))
INPUT SUBCELL ROTATION CODE NO. AT   4   1
     ((3))
INPUT SUBCELL ID. NO. AT LOCATION    4   2
     ((1))
INPUT SUBCELL ROTATION CODE NO. AT   4   2
     ((102))
INPUT SUBCELL ID. NO. AT LOCATION    4   3
     ((1))
INPUT SUBCELL ROTATION CODE NO. AT   4   3
     ((103))
INPUT SUBCELL ID. NO. AT LOCATION    4   4
     ((1))
INPUT SUBCELL ROTATION CODE NO. AT   4   4
     ((2))
SYMMETRY ABOUT YZ PLANE (T OR F)
     ((F))
SYMMETRY ABOUT XZ PLANE (T OR F)
     ((F))
```

```
***
GRID GEOMETRY FOR SUBCELL NUMBER      1
***
INPUT SIDE LENGTH OF SUBCELL (X DIR.)
      ((1.0))
INPUT NO. INTEG/PTS. OF SUBCELL (X DIR.)
      ((2))
INPUT SIDE LENGTH OF SUBCELL (Y DIR)
      ((1.0))
INPUT NO INTEG/PTS. ON SUBCELL (Y DIR.)
      ((2))
INPUT HEIGHT OF SUBCELL (Z DIR.)
      ((1.0))
INPUT NO INTEG/PTS. ON SUBCELL (Z DIR.)
      ((2))
INPUT NO. OF MATLS. IN SUBCELL NO.    1
      ((3))
SPECIFY THE CURRENT MATL. ID. NO.
      ((1))
INPUT 1ST FIBER SPHERICAL ANGLE
      ((90.0))
INPUT 2ND FIBER SPHERICAL ANGLE
      ((10.0))
INPUT OCTANT NO. AT GRID NO.    1  1  1
      ((1))
INPUT MATL. VOL/FR AT OCTANT NO.   1  1  1
      ((0.04))
INPUT OCTANT NO. AT GRID NO.    1  1  1
      ((-1))
INPUT 1ST FIBER SPHERICAL ANGLE
      ((90.0))
INPUT 2ND FIBER SPHERICAL ANGLE
      ((10.0))
INPUT OCTANT NO. AT GRID NO.    1  1  2
      ((2))
INPUT MATL. VOL/FR AT OCTANT NO.   1  1  2
      ((0.21))
INPUT OCTANT NO. AT GRID NO.    1  1  2
      ((-1))
INPUT 1ST FIBER SPHERICAL ANGLE
      ((90.0))
INPUT 2ND FIBER SPHERICAL ANGLE
      ((10.0))
INPUT OCTANT NO. AT GRID NO.    1  2  1
      ((-1))
INPUT 1ST FIBER SPHERICAL ANGLE
      ((90.0))
INPUT 2ND FIBER SPHERICAL ANGLE
      ((10.0))
INPUT OCTANT NO. AT GRID NO.    1  2  2
      ((4))
INPUT MATL. VOL/FR AT OCTANT NO.      4
      ((0.25))
INPUT OCTANT NO. AT GRID NO.    1  2  2
```

127

```
                ((-1))
INPUT 1ST FIBER SPHERICAL ANGLE
                ((90.0))
INPUT 2ND FIBER SPHERICAL ANGLE
                ((10.0))
INPUT OCTANT NO. AT GRID NO.    2  1  1
                ((5))
INPUT MATL. VOL/FR AT OCTANT NO.     5
                ((0.25))
INPUT OCTANT NO. AT GRID NO.    2  1  1
                ((-1))
INPUT 1ST FIBER SPHERICAL ANGLE
                ((90.0))
INPUT 2ND FIBER SPHERICAL ANGLE
                ((10.0))
INPUT OCTANT NO. AT GRID NO.    2  1  2
                ((6))
INPUT MATL. VOL/FR AT OCTANT NO.     6
                ((0.50))
INPUT OCTANT NO. AT GRID NO.    2  1  2
                ((-1))
INPUT 1ST FIBER SPHERICAL ANGLE
                ((90.0))
INPUT 2ND FIBER SPHERICAL ANGLE
                ((10.0))
INPUT OCTANT NO. AT GRID NO.    2  2  1
                ((7))
INPUT MATL. VOL/FR AT OCTANT NO.     7
                ((0.04))
INPUT OCTANT NO. AT GRID NO.    2  2  1
                ((-1))
INPUT 1ST FIBER SPHERICAL ANGLE
                ((90.0))
INPUT 2ND FIBER SPHERICAL ANGLE
                ((10.0))
INPUT OCTANT NO. AT GRID NO.    2  2  2
                ((8))
INPUT MATL. VOL/FR AT OCTANT NO.     8
                ((0.71))
INPUT OCTANT NO. AT GRID NO.    2  2  2
                ((-1))
SPECIFY THE CURRENT MATL ID. NO.
                ((2))
INPUT 1ST FIBER SPHERICAL ANGLE
                ((0.0))
INPUT 2ND FIBER SPHERICAL ANGLE
                ((-10.0))
INPUT OCTANT NO. AT GRID NO.    1  1  1
                ((1))
INPUT MATL. VOL/FR AT OCTANT NO.     1
                ((0.21))
INPUT OCTANT NO. AT GRID NO.    1  1  1
                ((-1))
INPUT 1ST FIBER SPHERICAL ANGLE
```

```
        ((0.0))
INPUT 2ND FIBER SPHERICAL ANGLE
        ((-10.0))
INPUT OCTANT NO. AT GRID NO.    1   1   2
        ((2))
INPUT MATL. VOL/FR AT OCTANT NO.    2
        ((0.04))
INPUT OCTANT NO. AT GRID NO.    1   1   2
        ((-1))
INPUT 1ST FIBER SPHERICAL ANGLE
        ((0.0))
INPUT 2ND FIBER SPHERICAL ANGLE
        ((-10.0))
INPUT OCTANT NO. AT GRID NO.    1   2   1
        ((3)
INPUT MATL. VOL/FR AT OCTANT NO.    3
        ((0.50))
INPUT OCTANT NO. AT GRID NO.    1   2   1
        ((-1))
INPUT 1ST FIBER SPHERICAL ANGLE
        ((0.0))
INPUT 2ND FIBER SPHERICAL ANGLE
        ((-10.0))
INPUT OCTANT NO. AT GRID NO.    1   2   2
        ((4))
INPUT MATL. VOL/FR AT OCTANT NO.    4
        ((0.25))
INPUT OCTANT NO. AT GRID NO.    1   2   2
        ((-1))
INPUT 1ST FIBER SPHERICAL ANGLE
        ((0.0))
INPUT 2ND FIBER SPHERICAL ANGLE
        ((-10.0))
INPUT OCTANT NO. AT GRID NO.    2   1   1
        ((5))
INPUT MATL. VOL/FR AT OCTANT NO.    5
        ((0.25))
INPUT OCTANT NO. AT GRID NO.    2   1   1
        ((-1))
INPUT 1ST FIBER SPHERICAL ANGLE
        ((0.0))
INPUT 2ND FIBER SPHERICAL ANGLE
        ((-10.0))
INPUT OCTANT NO. AT GRID NO.    2   1   2
        ((-1))
INPUT 1ST FIBER SPHERICAL ANGLE
        ((0.0))
INPUT 2ND FIBER SPHERICAL ANGLE
        ((-10.0))
INPUT OCTANT NO. AT GRID NO.    2   2   1
        ((7)
INPUT MATL. VOL/FR AT OCTANT NO.    7
        ((0.71))
INPUT OCTANT NO. AT GRID NO.    2   2   1
```

```
                 ((-1))
INPUT 1ST FIBER SPHERICAL ANGLE
        ((0.0))
INPUT 2ND FIBER SPHERICAL ANGLE
        ((-10.0))
INPUT OCTANT NO. AT GRID NO.    2  2  2
        ((8))
INPUT MATL. VOL/FR AT OCTANT NO.    8
        ((0.04))
INPUT OCTANT NO. AT GRID NO.    2  2  2
        ((-1))
SPECIFY THE CURRENT MATL. ID. NO.
        ((3))
INPUT 1ST FIBER SPHERICAL ANGLE
        ((0.0))
INPUT 2ND FIBER SPHERICAL ANGLE
        ((0.0))
INPUT OCTANT NO. AT GRID NO.    1  1  1
        ((1))
INPUT MATL. VOL/FR AT OCTANT NO.    1
        ((0.75))
INPUT OCTANT NO. AT GRID NO.    1  1  1
        ((-1))
INPUT 1ST FIBER SPHERICAL ANGLE
        ((0.0))
INPUT 2ND FIBER SPHERICAL ANGLE
        ((0.0))
INPUT OCTANT NO. AT GRID NO.    1  1  2
        ((2))
INPUT MATL. VOL/FR AT OCTANT NO.    2
        ((0.75))
INPUT OCTANT NO. AT GRID NO.    1  1  2
        ((-1))
INPUT 1ST FIBER SPHERICAL ANGLE
        ((0.0))
INPUT 2ND FIBER SPHERICAL ANGLE
        ((0.0))
INPUT OCTANT NO. AT GRID NO.    1  2  1
        ((3))
INPUT MATL. VOL/FR AT OCTANT NO.    3
        ((0.50))
INPUT OCTANT NO. AT GRID NO.    1  2  1
        ((-1))
INPUT 1ST FIBER SPHERICAL ANGLE
        ((0.0))
INPUT 2ND FIBER SPHERICAL ANGLE
        ((0.0))
INPUT OCTANT NO. AT GRID NO.    1  2  2
        ((4))
INPUT MATL. VOL/FR AT OCTANT NO.    4
        ((0.50))
INPUT OCTANT NO. AT GRID NO.    1  2  2
        ((-1))
INPUT 1ST FIBER SPHERICAL ANGLE
```

```
      ((0.0))
INPUT 2ND FIBER SPHERICAL ANGLE
      ((0.0))
INPUT OCTANT NO. AT GRID NO.    2  1  1
      ((5))
INPUT MATL. VOL/FR AT OCTANT NO.    5
      ((0.50))
INPUT OCTANT NO. AT GRID NO.    2  1  1
      ((-1))
INPUT 1ST FIBER SPHERICAL ANGLE
      ((0.0))
INPUT 2ND FIBER SPHERICAL ANGLE
      ((0.0))
INPUT OCTANT NO. AT GRID NO.    2  1  2
      ((6))
INPUT MATL. VOL/FR AT OCTANT NO.    6
      ((0.50))
INPUT OCTANT NO. AT GRID NO.    2  1  2
      ((-1))
INPUT 1ST FIBER SPHERICAL ANGLE
      ((0.0))
INPUT 2ND FIBER SPHERICAL ANGLE
      ((0.0))
INPUT OCTANT NO. AT GRID NO.    2  2  1
      ((7))
INPUT MATL. VOL/FR AT OCTANT NO.    7
      ((0.25))
INPUT OCTANT NO. AT GRID NO.    2  2  1
      ((-1))
INPUT 1ST FIBER SPHERICAL ANGLE
      ((0.0))
INPUT 2ND FIBER SPHERICAL ANGLE
      ((0.0))
INPUT OCTANT NO. AT GRID NO.    2  2  2
      ((8))
INPUT MATL. VOL/FR AT OCTANT NO.    8
      ((0.25))
INPUT OCTANT NO. AT GRID NO.    2  2  2
      ((-1))
```

ELASTIC CONSTANTS OF THE COMPOSITE

```
EX, EY, EZ =     4395007.97     4395007.97     1181426.56
GYZ,GXZ,GXY =     482009.43      482009.43      423769.42
MUYZ,MUXZ,MUXY =   .1274         .1274      .1370
NUYZ,X ;  NUYZ,Y ;  NUYZ,Z =    .0000        .0000       .0000
NUXZ,X ;  NUXZ,Y ;  NUXZ,Z =    .0000        .0000       .0000
NUXY,X ;  NUXY,Y ;  NUXY,Z =    .0000        .0000       .0000
```

REPORT DOCUMENTATION PAGE

1. AGENCY USE ONLY (Leave blank)	2. REPORT DATE	3. REPORT TYPE AND DATES COVERED
	February 1992	Contractor Report

4. TITLE AND SUBTITLE

Finite Element Analysis of the Stiffness of Fabric Reinforced Composites

5. FUNDING NUMBERS

C NAS1-19000
505-63-50-04

6. AUTHOR(S)

R. L. Foye

7. PERFORMING ORGANIZATION NAME(S) AND ADDRESS(ES)

Lockheed Engineering and Sciences Company
144 Research Drive
Hampton, VA 23666

8. PERFORMING ORGANIZATION REPORT NUMBER

9. SPONSORING / MONITORING AGENCY NAME(S) AND ADDRESS(ES)

National Aeronautics and Space Administration
Langley Research Center
Hampton, VA 23665-5225

10. SPONSORING / MONITORING AGENCY REPORT NUMBER

NASA CR-189597

11. SUPPLEMENTARY NOTES

Langley Technical Monitor: H. Benson Dexter/C. C. Poe

12a. DISTRIBUTION / AVAILABILITY STATEMENT

Unclassified-Unlimited

Subject Category 24

12b. DISTRIBUTION CODE

13. ABSTRACT (Maximum 200 words)

The objective of this work is the prediction of all 3-D elastic moduli of textile fabric reinforced composites. The analysis is general enough for use with complex reinforcing geometries and capable of subsequent improvements. It places no restrictions on fabric microgeometry except that the unit cell be determinate and rectangular. The unit cell is divided into rectangular subcells in which the reinforcing geometries are easier to define and analyze. The analysis, based on inhomogeneous finite elements, is applied to a variety of weave, braid, and knit reinforced composites. Some of these predictions are correlated to test data.

14. SUBJECT TERMS

Fabrics; Elastic properties; Finite element analysis

15. NUMBER OF PAGES

137

16. PRICE CODE

A07

17. SECURITY CLASSIFICATION OF REPORT	18. SECURITY CLASSIFICATION OF THIS PAGE	19. SECURITY CLASSIFICATION OF ABSTRACT	20. LIMITATION OF ABSTRACT
Unclassified	Unclassified		